National University of Lesotho

The Impact of Intermittent Renewable Energy Generators on Lesotho National Electricity Grid

Sebota Mokeke

A dissertation submitted in partial fulfilment
of the requirements for the degree of

Master of Science in Sustainable Energy

Offered by the

Energy Research Centre
Faculty of Science & Technology

August 2020

Abstract

Lesotho is confronted with huge challenge of low electricity access, with 63.9 % of the population lacking access to electricity. Lack of electricity impedes both economic and social development. However, Lesotho has abundant renewable energy resources that can be exploited through large integration of renewable energy sources. The inherent variability and uncertainty of renewable energy sources (solar-PV and wind) creates both operational and planning challenges for the power system. This results in the reluctance of the power system operators integrating large-scale renewables to the national grid due to the power system stability problems. The characteristics of the intermittent renewable energy generators mandates that careful grid impact studies be performed in ensuring that the power grid is operated stably.

The thesis focuses on the impact of the Intermittent Renewable Energy Generators (IREGs) on the power stability of Lesotho electrical grid considering both solar photovoltaic (PV) and wind generation at Ha-Ramarothole and Letseng respectively. The integration of IREGs involves both steady state and dynamic analysis of the electrical network. To this aim, the thesis assesses the impact of the IREGs on the stability of Lesotho electrical network at transmission level. In addition, maximum allowable penetration levels were determined at the point of interconnection.

Load flow simulations were performed to assess the steady state performance of the electrical network. Furthermore, the transient analysis was performed by applying the 3-phase short circuit at the critical points of the network and observing how voltage, frequency and rotor angle stability were affected and evaluated against grid code of Lesotho. The simulations were performed using DigSILENT PowerFactory software, which was used to model the electrical network of Lesotho. The maximum allowable penetrations for solar was about 19 % at substation at Ramarothole while for the wind it was found to be 27 % at Letseng substation. The simulations revealed that increased penetration of the IREGs led to grid instability. For all the simulations, frequency stability was observed except for the penetration of 36 MW for solar farm. The voltage

violations at the Tlokoeng substation of 1.051 p.u. resulted from penetration limit of 52 MW capacity of the wind farm at Letseng. The solar penetration limit resulted from the rotor angle instability as increased penetration resulted in large rotor angle oscillations.

Acknowledgements

I would like to give my sincere thanks to my supervisor Ass. Prof. Thamae for guidance, encouragement and the support he has given me throughout the research project. His insightful comments and criticism, not only made me develop better understanding of the subject but also the better researcher. I also pass my gratitude to the ERC staff in equipping me with the necessary skills to carry out the research project.

I appreciate the support I got from the Lesotho Electricity Company (LEC) in providing me with the necessary data carry out the research. My special thanks goes to my family (father, brother and sister) who had unconditionally supported me through my study project. It's a blessing to have the family like them.

I dedicate this work to my late Mother who sacrificed a lot in ensuring I am the person I am today. Finally, and above all, I thank GOD for his grace, protection, guidance and granting me wisdom and courage to carry out this research project.

List of Figures

List of Tables

Table of Contents

1 Introduction

1.1 Background

Advocacy for sustainable economic development coupled with the need for environmental conservation has resulted in accelerated integration of renewable energy resources to the power grids. Amongst the renewable energy resources solar and wind generation has taken the lead with the world wide capacity of 398 GW for solar photovoltaic (PV) and 546 GW of wind in 2017 [1]. Improved technology and mass deployment of both solar and wind plants has brought their per unit cost down, making them to be competitive with conventional power plants [1], [2]. Increased and successful integration of both wind and solar energy poses an inevitable challenge to power system operators and planners.

The power generated by Intermittent Renewable Energy Generators (IREGs (solar or wind)) is variable and not deterministic over the range of timescales. This makes IREGs different from the conventional power (fossil fuels) which are dispatchable. Successful integration of IREGs studies and experiences into the electrical grid reveals that there is the need for fast balancing generators, accurate short and long term weather forecasting and flexible markets [3], [4]. These changes require comprehensive analysis since the issues relating to IREGs integration into the grid could be multifaceted and span different disciplines. The European Union (EU) has pledged to reach 20 % renewable energy penetration by 2020 and 27 % by 2030 while Denmark pledged 50 % penetration by 2020 and 100% by 2050 [5]–[7]. United States of America (USA) has set a target of 27 % renewable energy by 2030 while states like New Jersey and California set the target of renewable penetration of 50 % by 2030 [8]. Continual integration of renewable energy sources (RES) will displace conventional power plants and impose both technical and economic challenges to the power grids.

Firstly, for successful integration of IREGs the transmission network needs to be upgraded as the solar/wind farms are usually in remote areas or at places with low population density. The

construction of long transmission lines could be costly and take long time to construct hence investment in transmission expansion. In addition, poor policy framework makes it hard to provide decisive direction on transmission network expansions and capacity.

The second challenge relating to the integration of IREGs is the flexibility of the power grid to maintain the load-generation balance under different generation conditions [9]. The variability and uncertainty of the RES pose the main challenge to flexibility of the power grid as RES are constantly changing hence variable power generation. The variable power generation may result in load-generation imbalance, which may compromise the stability of power grid. The load generation imbalance might be mitigated by fast spinning and balancing reserves.

Thirdly, IREGs affect power grid dynamics differently from the conventional power plants when subjected to disturbances (electrical faults) as they exhibit different electrical characteristics. The use of power electronics converters results in acceptable grid connection using the low voltage ride through capability. Studies revealed that IREGs penetration level of more than 30 % is possible without compromising the transient stability of the power system [3], [10]. But IREGs (wind and solar) have low short circuit ratio and contribute minimally to the power system synchronous inertia as they are build using power electronics [4]. Under high IREGs, low short circuit ratio could result in both frequency and voltage instability, which may cause large generators to trip, hence lead to complete system shutdown.

Lastly, the issue of integrating IREGs relates to the power market context. The new power market needs to be designed such that it ensures optimum scheduling of the IREGs and conventional power plants [11]. Optimum scheduling results in improved market efficiency and increased power system reliability. Integral to the new power market is accurate renewable energy forecasting as it provides efficient commitment and dispatching of the conventional power plants. In addition, accurate forecasting of renewable energy generation improves the economics of the power system.

1.2 Problem Statement

The peak load demand of Lesotho has been continually increasing yet its generation capacity has remained stagnant. In 2015-2016 the peak load demand was 153 MW, 2016-2017 was 161.91 MW and the 2017-2018 was 166.91 MW [12]–[14]. The generation capacity of Lesotho has remained stagnant at 74.46 MW of which 72 MW is generated from Muela Hydro Power Station and the rest is generated from the small hydropower plants across the country [15], [16]. The vast majority of the electricity is imported from South Africa and Mozambique. Most of the households (64 % in 2014) rely on the biomass, as the source of energy for the daily energy needs [6]. Biomass is considered unhealthy and environmentally hazardous [17]. The electrification rate in rural areas of Lesotho was 5.5 % while for the urban areas was 72 % in 2015 [18].

Lesotho has abundant Renewable Energy Sources (RES) that can be exploited to meet its energy needs. Lesotho has unexploited wind energy capacity of 758 MW, 70 MW solar energy at Ha-Ramarothole, 1334 MW pumped storage at Monontsa and 361 MW of hydro resource [19]. Further studies done by Mplolo et al suggest that the wind resource at Letseng-La-Terae and Masitise are 5.97 m/s and 4.93 m/s at 10 m above ground [20], [21]. Taele et al also argues that Lesotho has an average horizontal global radiation of 5.5 – 7.2 kWh/m^2 which he claims to be good for the erection of solar farm power plants [22].

In order for Lesotho to exploit its renewable resources, it has launched some grid-connected and off-grid solutions. In the Grid Development Plan (2017-2036) Lesotho has allocated M 150 million per annum of which 80 % of it was budgeted for the grid expansion and 20 % of it would be allocated for off-grid solutions [23]. Figure 1.1 displays the present and the future electricity transmission and distribution for Lesotho under the state-owned Lesotho Electricity Company (LEC).

Figure 1.1 : Present and Future Transmission and Distribution LEC Network

Also, the Lesotho Country Action Agenda stipulated that Lesotho is aiming to have 375 MW of renewables by 2030 [24]. For the off-grid solutions Lesotho had finished the feasibility study on mini-grids and energy centers for the districts of Thaba-Tseka, Mokhotlong and Qacha's Nek [25]. These mini-grids will serve as the pilot projects for the further development of the min-grids in Lesotho. In January 2019 Government of Lesotho (GoL) had launched the call for consultancy on the Renewable Energy Grid Integration Study to investigate the impact of Intermittent Renewables Energy Generators (IREGs) resources on the national grid [26]. The African Development Bank (AfDB) funds the initiative.

Electricity access on Lesotho is around 36.1 % of which more than 50 % of it is imported[27] [28]. The low electrification rate restrains the social and the economic development. The increasing demand is met with the increased imported electricity, which compromises the energy security of Lesotho and result in the uncontrolled costly energy tariffs. Electricity access in Lesotho is mainly achieved through grid extension, which calls for more power plants to be build. Exploitation of the renewable energy sources remains the only option for Lesotho to increase its electricity access as Lesotho lacks fossil fuels. The vast majority of the imported electricity is generated from coal in South Africa, which is environmentally hazardous and not sustainable.

Lack of technical awareness and relevant renewable energy grid impact studies inhibit the employed of large-scale integration of renewable energy sources (wind and solar-PV). Utility scale integration of the renewables has been the success for most countries where relevant rigorous grid impact studies are conducted [29], [30]. The impact of utility scale renewables (wind and solar) have not been investigated in Lesotho.

In response to the electricity challenges of Lesotho, the research project aims to assess the technical impact of the IREGs on the Lesotho National grid. The emphasis will be on dynamic voltage, frequency, and rotor angle stability as the penetrations of the renewables increase. In addition, the steady-state voltage response of the will be analyzed. The study also acts as both informative research document on system operators and the policy makers in accelerating the electricity access. The research presents the practical and easy methodology, which effectively demonstrate the dynamical behavior of Lesotho National grid due to the integration of the utility scale solar and wind power plants. The methodology used has the advantage over the energy methods that use the energy functions that require the detailed mathematical system definitions and associated operating conditions [31].

1.3 Goals

The government of Lesotho has embarked on some initiatives to promote and integrate IREGs into the main grid. This initiative will result in increased access to electricity and reduce the dependence of Lesotho on imported electricity. The possible downside of the initiative is that the IREGs results in grid instability and may require new network configurations for them to be accommodated. Based on this context the report analyses grid impact of IREGs on Lesotho electricity transmission network. The objectives of the project are to:

- Simulate the power system performance and stability due to IREGs integration to the national grid.
- Assess the maximum allowable IREGs penetrations to Lesotho national electricity grid
- Assess the impacts of IREGs on grid stability and security of supply

1.4 Structure of the Thesis

The thesis had been structured into five chapters. Chapter 1 discussed the background information pertaining the integration IREGs. It briefly discussed the challenges that results from the integration of IREGs into the grid. Then the energy status of Lesotho was briefly explained, from which the problem statement is formulated and clear objectives of the thesis outline. The next chapter deals the literature review. In chapter 2, the overview of power stability is detailed providing the necessary definitions of power system stability and major causes of power system stability were discussed. In addition, the stability assessment methods were briefly discussed. The following sections in chapter 2 explained the solar PV and the wind generation technologies focusing on how they generate electricity and the underlying fundamental equations for both technologies were explained. Having defined power system stability fundamentals and the generating technology for the IREGs, the methodology for carrying grid impact studies was formulated and the results obtained discussed and major conclusions drawn.

2 Literature Review

2.1 Overview of Power System Stability

Since the invention of the electric power system by Thomas Edison, power systems have continually evolved into complex and essential drivers of society development. The primary task of the power system is to deliver the electric energy to the customers reliably, within the acceptable quality (voltage and frequency) and in an economic manner [32]. Power systems are operated over the interconnected transmission network, which links generators to the loads over the vast geographical area spanning countries and regions in form of power pools. The power systems operators are faced with challenge to constantly know how the security (*defines the potential of the power system to survive disturbances without compromising customer service*) of electrical power network varies. The power security problem is exacerbated by the integration of variable renewable energy sources, which are preferred sources to meet the growing load

demand globally. To ensure secure operation of the power system the electrical network must be continually evaluated such that [33]:

i.   the security of the present state of the power system is known

ii. how the security is affected if the power system is operated under different operating conditions and configurations.

iii. what remedial actions need to be conducted to ensure the power system is operated within acceptable limits.

To ensure security, the power system must be operated under stable conditions. Power system stability is defined by IEE/CIGRE Task Force on stability as "*the ability of the electric power for the given operating condition, to regain a state of operating equilibrium after being subjected to the physical disturbance, with the system variables being bounded such that the entire system remain intact*" [34]. As depicted in Figure 2.1, the power system stability can be classified into rotor angle stability, frequency stability and voltage stability.

Figure 2.1 Classification of Power System Stability. Adopted from [29]
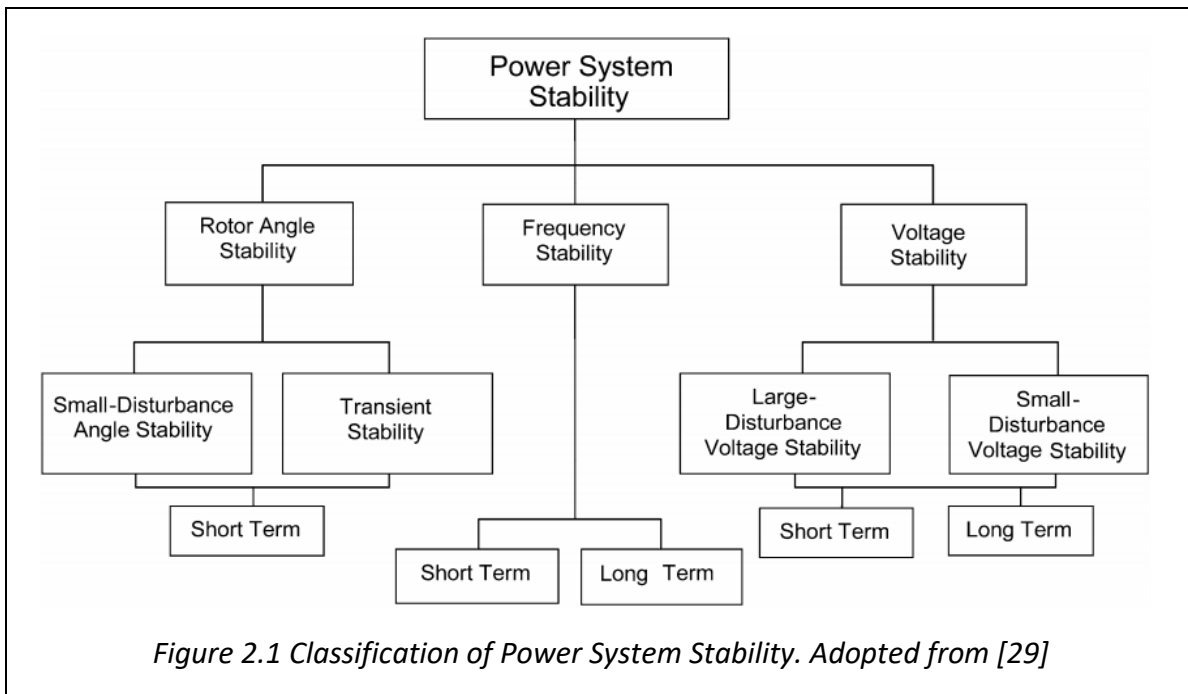
2.1.1 Rotor angle stability

The rotor angle stability analysis focuses on the ability of the synchronous machine within the power system network to remain synchronized under normal operating conditions and after being subjected to the perturbation [34], [35]. The rotor angle stability depends on the balance between the electromagnetic torque and mechanical torque of the power system. If the electromagnetic and mechanical torques are not equal, instability may occur due to the angular swings of some of the generators which may result in loss of synchronism with other generators [36]. Under steady state, the synchronous speed and the rotor speed of the machines are equal and the power system is operated at the nominal frequency.

When there is no load connected to the output terminals of the generator, the stator and the rotor magnetic fields are aligned and there is no power delivered from the generator. If the load is gradually increased, the angular separation of the stator and rotor field's results in the angular torque and the electrical power is delivered to the load. The power transferred to the power system (load) P_e by the generator is given by:

$$P_e = \frac{E_g V_2}{X_g + X_{eq}} \sin \delta \tag{1}$$

where δ is the rotor angle, E_g is the electromagnetic force (emf) developed from the synchronous machine, X_g is generator reactance, X_{eq} is the equivalent reactance of the transmission line and V_2 and V_1 are the voltages at the power system and generator terminals respectively. The single line diagram for the equivalent network and a plot of how the power varies with rotor angle is given in Figure 2.2 and Figure 2.3 respectively.

Figure 2.2 Equivalent Network of Single Machine Infinite Bus System. Adopted from [31]

Figure 2.3 Power angle relation to real power adopted from [31]
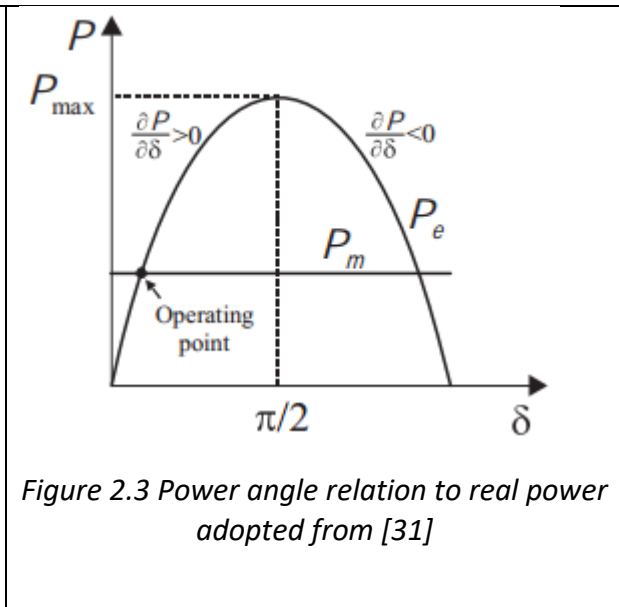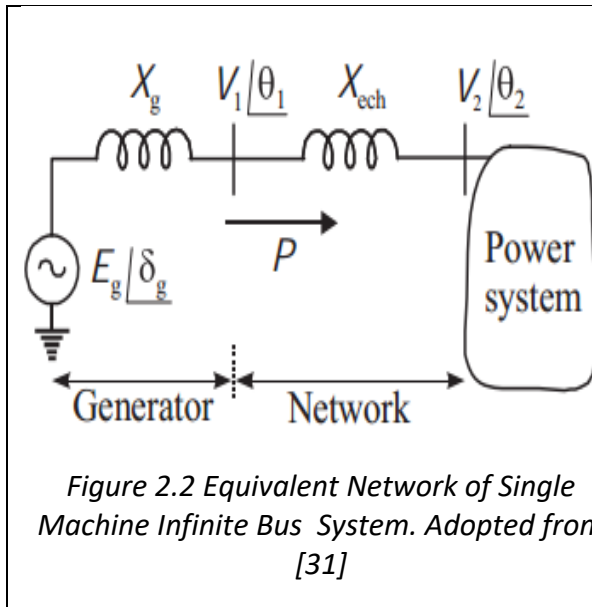
From equation 1 and Figure 2.3 it is shown that as δ is increased so does the power delivered to the load up to the point where the $\delta = \frac{\pi}{2}$, where maximum P_e is reached. As δ is increased beyond $\frac{\pi}{2}$ the power delivered to the load decreases and this leads to instability [37]. In addition, from equation 1, if X_{eq} is high the power delivered to the power system is reduced. High X_{eq} results from long or weakly connected transmission lines.

The rotor angle can be used to characterize the stability of the power system such that the steady state stability of the power system is attained for $\partial P/_{\partial\delta} > 0$ and unstable for $\partial P/_{\partial\delta} < 0$ [35], [38]. As depicted in Figure 2.3 small increase in P is met by the increase in the rotor angle. On the other hand, if the increase in load results in the decrease in generator power the electrical network experiences some instability. If the network is operated such that $\partial P/_{\partial\delta} < 0$ the power flows in the electrical network are altered. The alteration of the over flow in the electrical network may lead to loss of generation or line disconnection resulting in voltage variations which may cause the system blackouts and damage the power system equipment.

Long transmission lines in weakly connected electrical networks between the generating units and loads cause rotor angle instability. Also poorly coordinated voltage regulators, loss of major

loads or generators results in rotor angle oscillations that needs to be damped quickly to avoid instability. The change in electromechanical torque ΔC_e due to the disturbance is given as [35]:

$$\Delta C_e = C_s\Delta\delta + C_D\Delta\omega \qquad (2)$$

such that $C_s\Delta\delta$ defines the synchronizing torque while $C_D\Delta\omega$ represent damping torque where C_s and C_D are the synchronizing torque and damping torque coefficient respectively.

The change in rotor angle and speed are represented by $\Delta\delta$ and $\Delta\omega$ respectively. Lack of synchronizing torque results in aperiodic or nonoscillatory instability while lack of damping torque results in oscillatory instability. Figure 2.4 shows how the rotor angle stability is affected by different combinations of C_s and C_D.

Figure 2.4 Power system response to small disturbance. Adopted from [31]
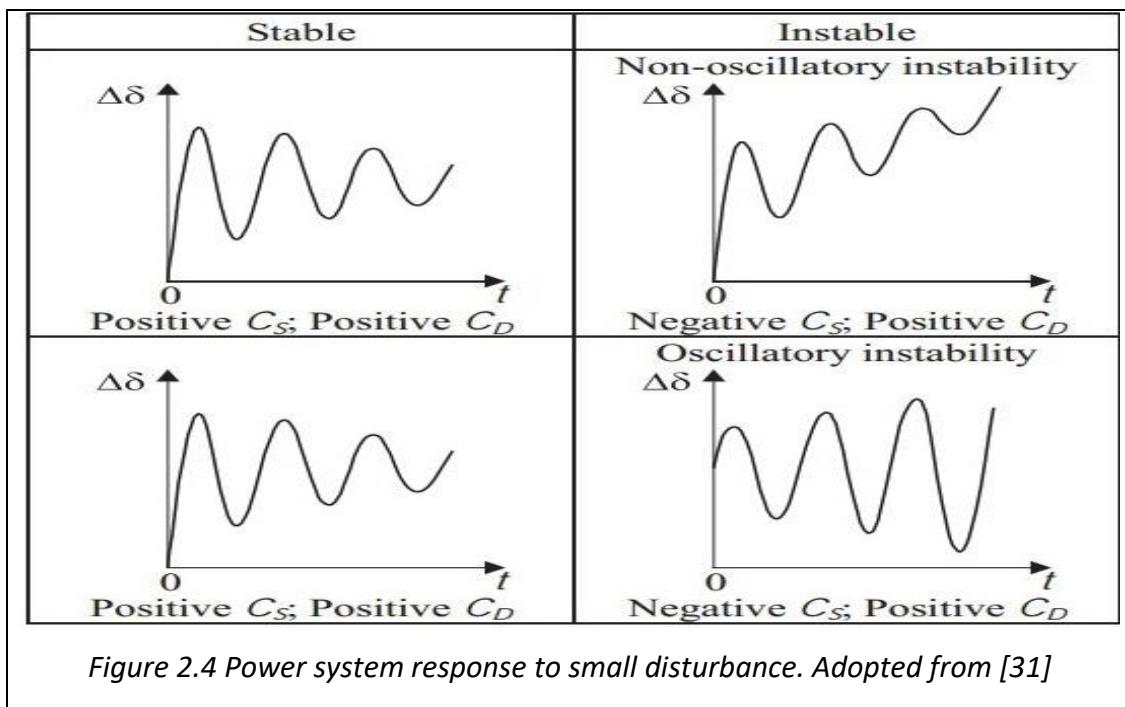
The synchronizing torque ensures that the rotor speed is maintained to the nominal speed by applying torque on the shaft of the synchronous machine [35], [39]. The rotor torque is maintained by the excitation system, speed governor system and some generator control loops. The damping torque reduces the oscillations of the rotor by providing damping through the damping winding of the generator which is relatively small [36]. For meaningful details, the rotor

angle stability is classified as small-disturbance (small-signal stability) and large-disturbance rotor angle stability (transient stability).

2.1.1.1 Small-Disturbance rotor angle stability

Small angle rotor angle stability focuses on the ability of the power system to maintain synchronism after small perturbations resulting from load and generation imbalance [34]. Small-signal stability deals with the electromechanical dynamic effects of the power system under which the system equations can be linearized around equilibrium point without significant errors after being subjected to small disturbances [35], [36]. The small disturbance stability occurs due to lack of damping oscillations. Accurate evaluation of the small disturbance depends on the initial conditions prior to the disturbance, electrical network configuration and control systems of the power system (excitation, power system stabilizers and voltage and frequency control systems).

To solve stability problems relating to small signal particularly damping oscillations, modal analysis is performed on the power system of interest. The modal analysis involves:

i.   Formulation of the dynamic matrix for the power system linearized near operating point of the power system.

ii.   eigenvalues determination of the dynamic matrix (stable conditions are indicated by negative real parts of the eigenvalues otherwise the system is unstable)

iii. characterization of the power system based on the eigenvalues [40], [41].

The main instability problems encountered by power systems in relation to the small-signal stability are summarized in Table 1 below

Table 1: Small-signal stability issues	
Instability problem	Description
Local Plant Oscillations	Results from some group of the generating units oscillating against the rest of the power system. The automatic voltage regulators (AVR) in weakly

	connected networks could be the cause of such oscillations. Power system stabilizers (PSS) are employed to provide adequate damping to eliminate local plant oscillations.
Inter area mode oscillations	Mainly results from geographically isolated generators swinging against each other in an interconnected power system.
Control mode oscillations	Results from poorly configured control systems within the power system (speed governors, Static VAr Compensators (SVC) or the field exciters).
Torsional mode oscillations	Results from abrupt changes from changes either the power grid or the mechanical machinery within the power plants.

2.1.1.2 Large Disturbance Rotor Angle Stability (Transient Stability)

Transient stability refers to the potential of the power system to maintain synchronism after being subjected to large disturbances [34]. Under large disturbance, the power system equations can no longer be linearized. The power system analysis for the large disturbance of the rotor is carried out using the Differential Algebraic Equations (DAE). Large rotor angle instability results from loss of major load, generators or transmission line. Figure 2.5 typifies rotor angle stability after the major disturbance experienced by the generator.
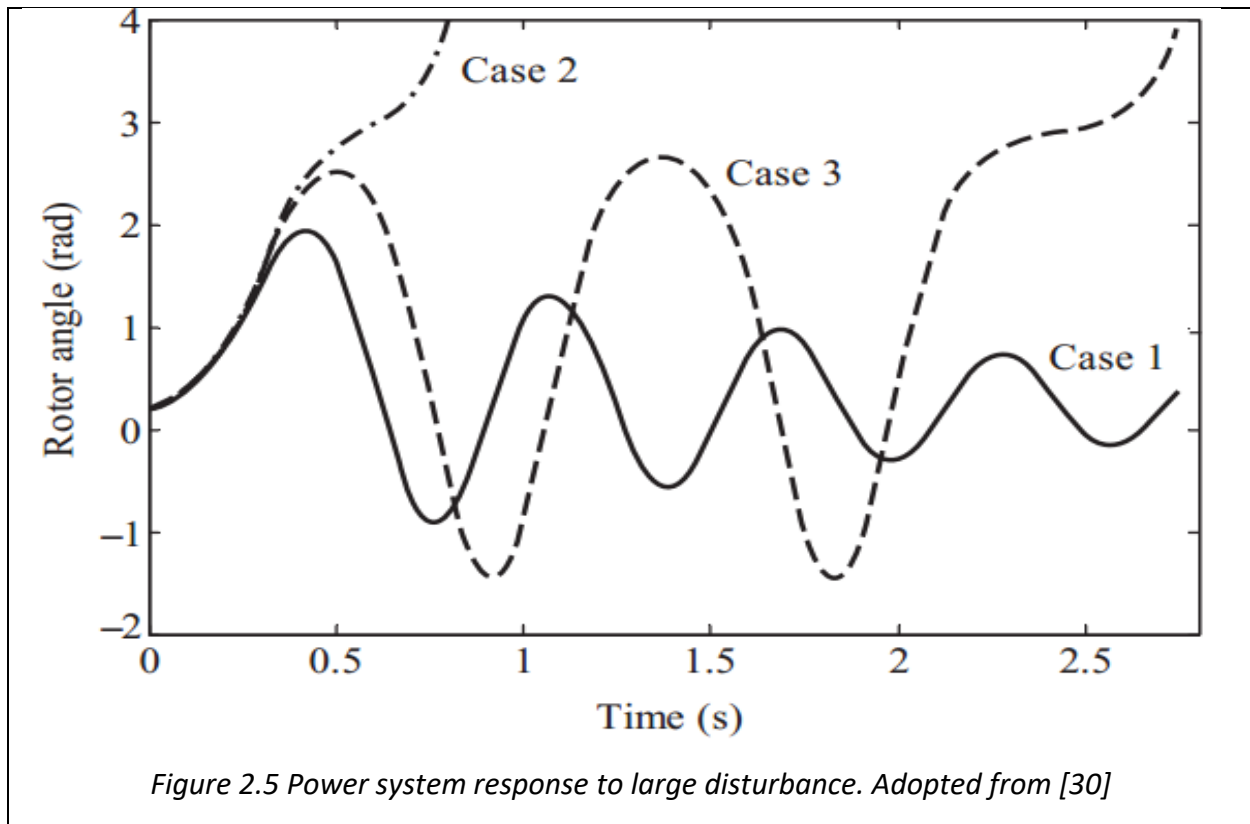
Figure 2.5 Power system response to large disturbance. Adopted from [30]

Case 1 indicates the stable condition after the major disturbance where the rotor angle oscillations reduce to stable state as the time progresses. Both cases 2 and 3 indicate the unstable case after the perturbation where case 2 shows the first swing instability while case 3 shows the sustained critical stability and finally some instability after some few oscillations. The cause of the instability could be the loss of damping or synchronizing torque.

2.1.2 Voltage Stability

Voltage stability defines the power system's ability to maintain bus voltages within the acceptable operational limits after being subjected to disturbance and in normal operation [34], [39]. Power system experiences voltage instability due to the sudden increase in the load, long weakly connected transmission lines, or low generation capacity but the main cause of voltage instability is the lack of the power system to supply reactive power [42]–[44]. Voltage instability could be mitigated by employing reactive power compensating devices such as shunt capacitors,

13

SVC, and under load tap changing (ULTC) transformer.   Voltage stability is mainly classified as large-disturbance and small-disturbance voltage stability.

Small-disturbance voltage stability deals with power system potential to maintain voltage buses at nominal value due to small changes such as gradual increase or decrease of the load demand [45]. On the other hand, large-disturbance stability deals with ability of the power system to maintain voltage buses after being subjected to system faults such as loss of major generator, major load, or transmission line. In addition, voltage stability could be classified in terms of the time duration as short-term and long-term voltage stability. Short-term voltage instability results from inductive loads such as motors and air conditioners while long-term voltage stability results from voltage control equipment such as generator over-excitation limiters and tap changing transformers while close to the loads [46].

Figure 2.6 SMIB representation of the power system. Adopted from [31]

Figure 2.7 Current, Voltage and Power relation at the load. Adopted from [31]
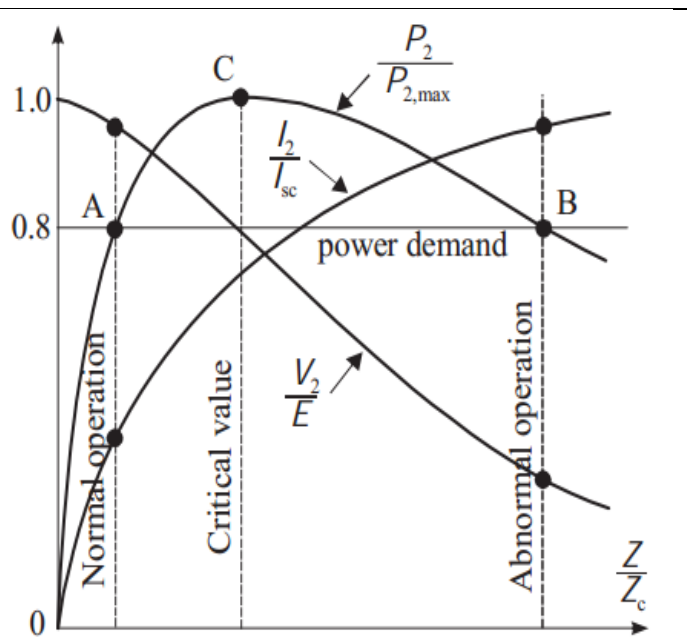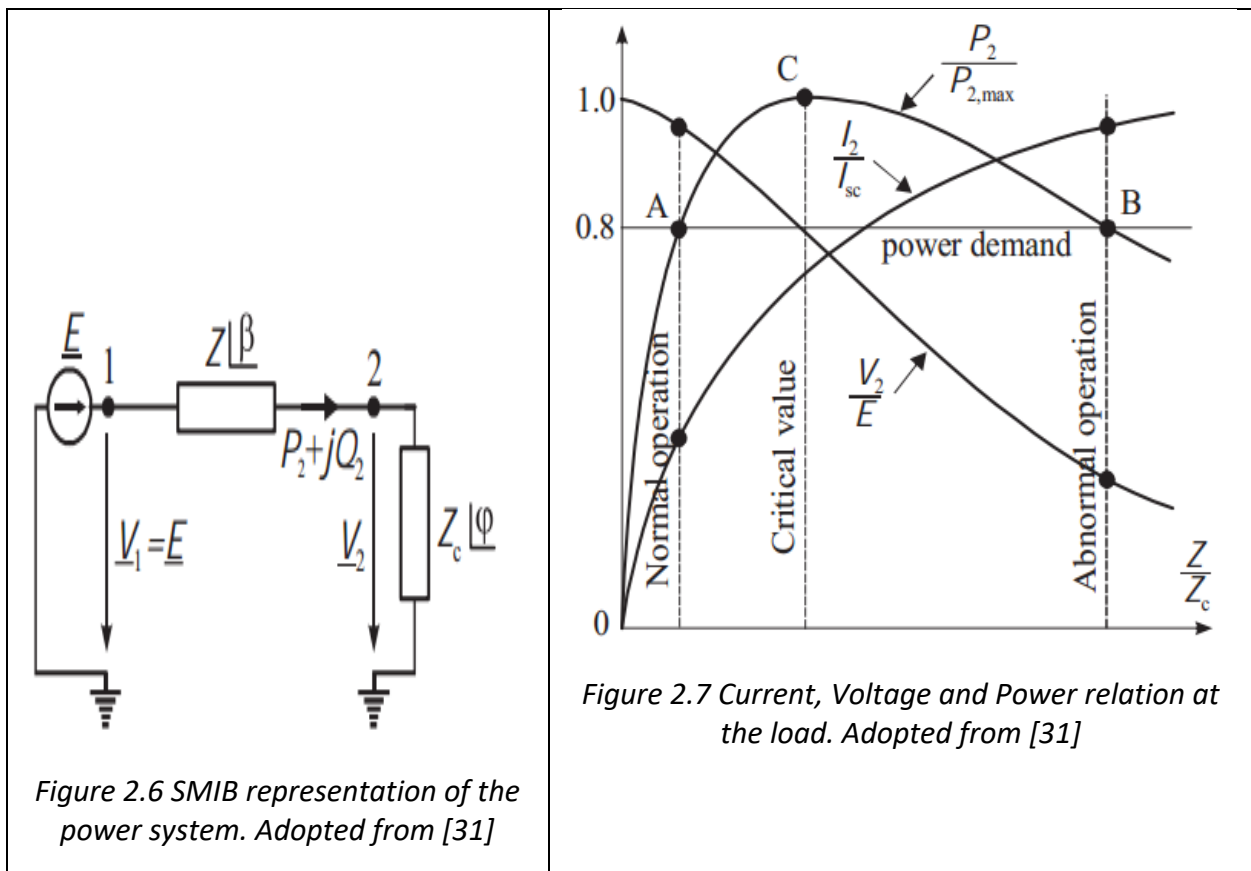
To gain comprehensive insight into the voltage stability problem, Figure 2.6 shows the power system consisting of the single generator, transmission line and a load, which is normally Single Machine Infinite Bus System (SMIB). Figure 2.7 shows the plot relating received real power (P_2) and reactive power (Q_2), and voltage across the load (V_2). From Figure 2.6 the current, voltage, power and maximum power at the load terminal are given by the following equations:

$$I = \frac{E}{Z\sqrt{1 + 2\left(Z_c/Z\right)\cos(\beta - \varphi) + \left(Z_c/Z\right)^2}} \tag{3}$$

$$V_2 = |Z_c I| = \frac{E Z_c}{Z\sqrt{1 + 2\left(Z_c/Z\right)\cos(\beta - \varphi) + \left(Z_c/Z\right)^2}} \tag{4}$$

$$P_2 = V_2 I \cos\varphi = \frac{E^2 Z_c}{z^2(1 + 2\left(Z_c/Z\right)\cos(\beta - \varphi) + \left(Z_c/Z\right)^2)}\cos\varphi \tag{5}$$

$$P_{2max} = \frac{V_1^2 \cos\varphi}{2Z[1 + \cos(\beta - \varphi)]} = \frac{V_1^2 \cos\varphi}{4Z\,\cos^2[(\beta - \varphi)/2]} \tag{6}$$

If $Z_c = \infty$, $V_1 = V_2$ and there is no current flowing through the circuit but as Z_c decreases P_2 increases rapidly and slows down as it approaches the maximum value at P_{2max}. On the other hand I approaches the maximum value which is the short circuit (I_{sc}) while V_2 decreases exponentially. For the given value of P_2 there exist two operating points on either side of the P_{2max}. The left side operating zone corresponds to the high voltage value and low current and is considered stable operating zone while the right zone is characterized by high current and low voltage and is considered unstable [35], [42].

Assuming the reactance of the transmission line (X>>R) where R is the resistance of the transmission then V_2 could be written as:

15

$$\overline{V_2} = \overline{E} - jX\overline{I} \tag{7}$$

Such that complex power (S) absorbed by the load is given as

$$S = P_2 + jQ_2 = \overline{V_2}\overline{I}^* = \overline{V}\left(\frac{\overline{E}^* - \overline{V_2}^*}{-jX}\right)$$

$$= \frac{j}{X}(EV_2\cos(\varphi) + jEV_2\sin(\varphi) - V^2) \tag{8}$$

From equation 8

$$P_2 = \frac{EV_2}{X}\sin(\varphi) \tag{9a}$$

$$Q_2 = \frac{V_2^2}{X} + \frac{EV_2}{X}\cos(\varphi) \tag{9b}$$

Equations 9a and 9b define the power flow equations of the lossless transmission network and provide the good approximation for the real network as R << X for the transmission cables [42]. Eliminating φ from the 9a and 9b leads to:

$$V_2^4 + (2Q_2X - E^2)V_2^2 + X^2(P_2^2 + Q_2^2) = 0 \tag{10}$$

Solving equation 10 for V_2 indicates how the reactive power and active power relates to voltage stability at the terminal connected to the load. Plotting (V_2, P_2, and Q_2) in (V, P, Q space) results in the graph depicted in Figure 2.8.

Figure 2.8 P, Q and V plot for SMIB power system. Adopted from [37]
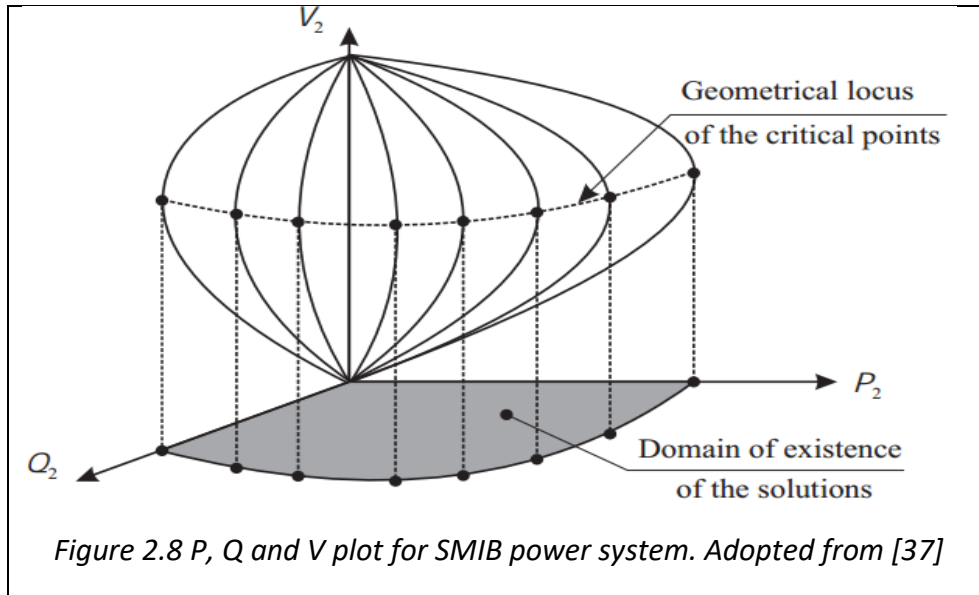
From the plot in Figure 2.8 the locus of (critical points) of the marks the maximum permissible complex power (S_{max}) that could be transferred between the generator and the load without losing stability. Equally so, projecting the critical points to the P-Q plane gives permissible and maximum reactive and active power that could be sustained by the power system without losing voltage stability.

From Figure 2.9 and Figure 2.10 two famous curves namely V-P curves and the Q-V curves can be constructed and play pivotal role in voltage stability analysis. Figure 8a depicts the voltage stability limits and the maximum active power that could be transferred by the power system. In addition, figure 8b shows the Q-V curve indicating the minimum reactive power requirement to maintain voltage stability. For the Q-V curve stability is realized when $\partial Q / \partial V > 0$; critically stable when $\partial Q / \partial V = 0$ and unstable when $\partial Q / \partial V < 0$ [36], [47].
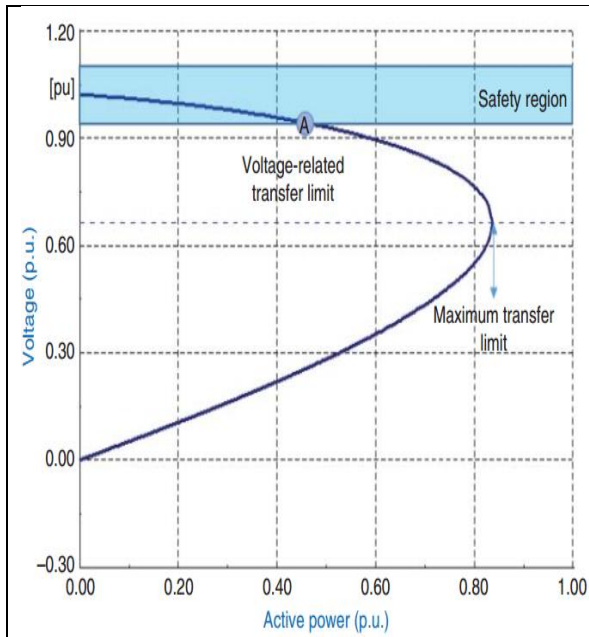
Figure 2.9 P-V Curve illustrating maximum active power limits if voltage stability is observed
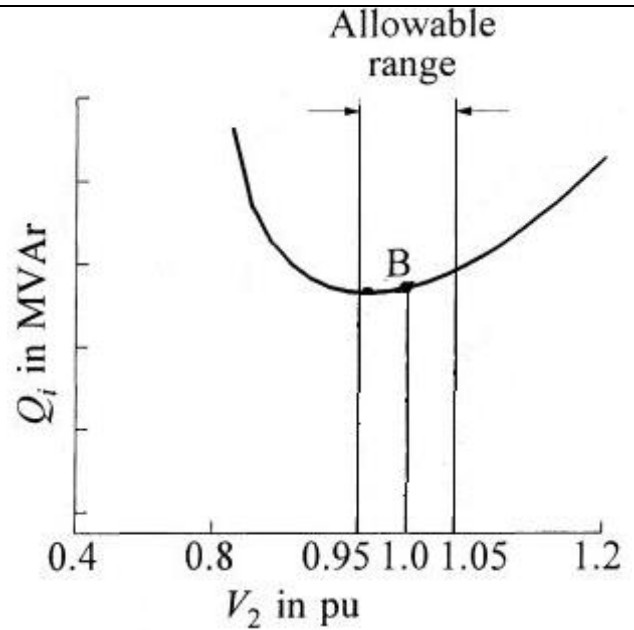
Figure 2.10 Q-V Curve illustrating maximum reactive power limits if voltage stability is observed

2.1.2.1 Assessment method for the voltage stability

Voltage stability assessment methods are generally classified into static (steady-state) methods and dynamic methods. Static methods are based on load flow equations and assess voltage stability based on the capacity of the power system to transfer the power under nominal conditions and faulted operating conditions [44]. Static methods provide the good results and are less computationally intensive than the dynamic methods. Dynamic methods are based on the Algebraic Differential Equations (ADE) and can capture both linear and nonlinear dynamics of the power system. Dynamic methods need detailed models of the electrical network elements to assess voltage stability hence they are more computationally intensive than the static methods [48], [49]. In addition, dynamic methods are not normally used in voltage stability assessment, as they do not reveal stability level. Figure 2.11 shows the voltage stability methods and their subdivisions.

Figure 2.11 Voltage Stability Assessment Methods
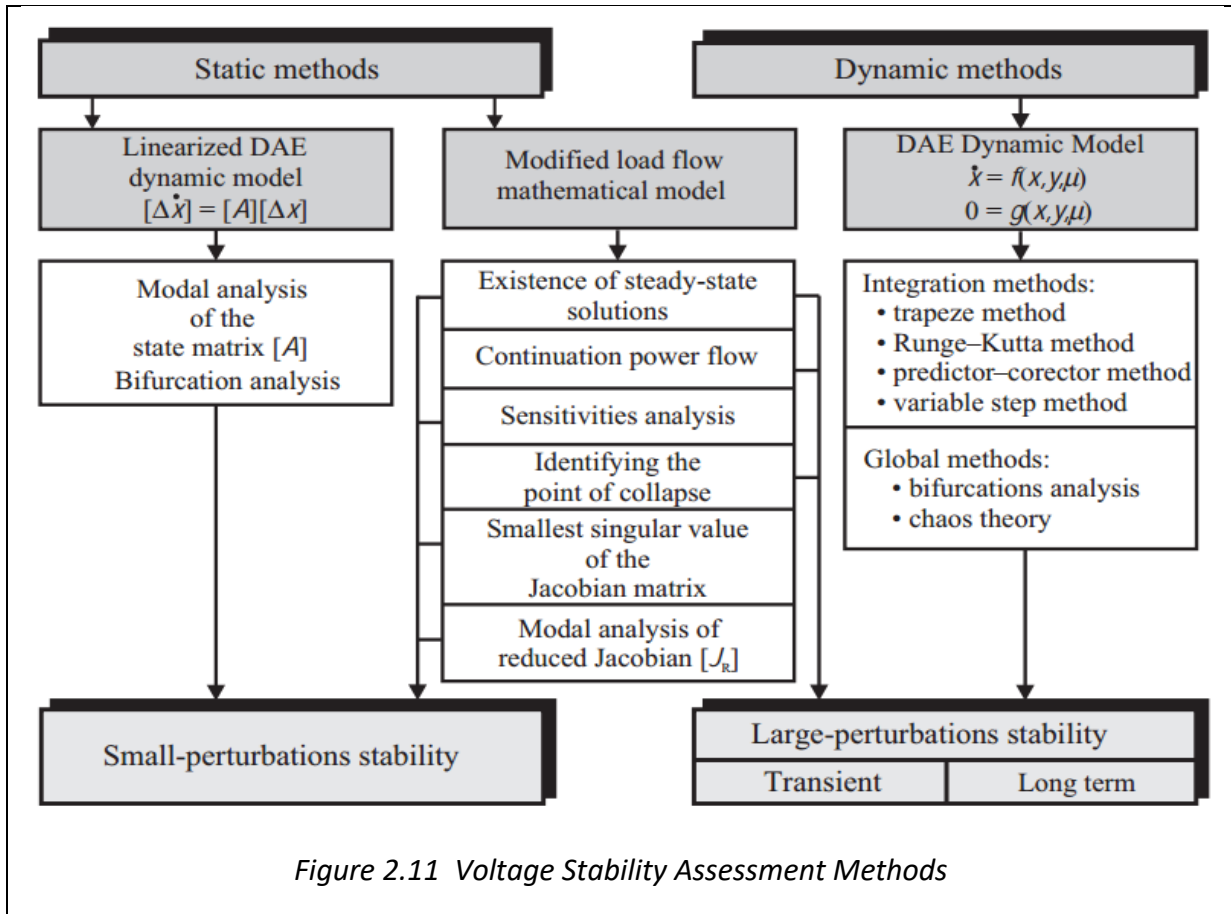
Amongst the static methods, P-V and Q-V curves are the most common voltage stability methods. The static methods can further be classified into the load flow methods and steady-state methods. The load flow methods evaluate the maximum real and reactive power capacity of the power system under converging load flow conditions [36]. The load flow methods assess performance index (PI) of the power system such that the power system is voltage stable when PI is less or equal to the threshold value (TH) and unstable otherwise. The steady state stability evaluates the stability of the power system by assessing the steady-state dynamic equations around equilibrium. Fundamental to the steady-state stability analysis is the sensitivity matrix (S) which is formed from the linearized equations or the Jacobian matrix [50]–[52]. The sensitivity matrix reveals certain properties of the power system such that:

$$[S] \in M^P \Rightarrow (power\ system\ is\ voltage\ stable)$$

$$[S] \notin M^P \Rightarrow (power\ system\ is\ not\ voltage\ stable)$$

where M^P is the group of matrixes with property P (determinant of the S, positive matrix, diagonal matrix).

2.1.3 Frequency Stability

Frequency stability defines ability of the power system to maintain the nominal operating frequency after the system is subjected to the severe unbalance between generation and load [34]. The imbalance between the generation and load results in frequency deviation, which could cause the synchronous generator angular speed variations rotor angle instability. The change in angular frequency causes the imbalance between the electromechanical torque and mechanical torque. Frequency instability can be classified into frequency disturbances that results from the mid-term and long-term situations. Mid-term frequency instability could be caused by lack of generating resources and may result in the islanded electrical power systems [53]. The long-term frequency instability may result from synchronous machine control systems (turbine governing system, failure of the protection system) malfunctioning [53]. If the frequency instability occurs it can be controlled under different levels namely the primary control, secondary control and tertiary control. Primary control stabilizes the frequency within seconds while the secondary control automatically stabilizes frequency by balancing the generation and consumption. The third level frequency controls the power system by providing some reserves or load shedding.

2.1.3.1 Frequency Response of the power system

To gain better grasp of the frequency stability the simplified model for the swing equation with governor droop is developed and can be extended to multiple interconnected area. The electromechanical generator model could be represented by [35]:

$$2H\frac{d\omega}{dt} + D\omega = C_m - C_e \approx P_m - P_e$$

$$\frac{d\delta}{dt} = \omega_0\omega \qquad\qquad (11)$$

such that H is the inertia of the machine, C_m and C_e represent the mechanical and electric torque respectively. D is the damping of the machine, ω and δ are angular speed and rotor angle respectively. The governors droop (R) defines the frequency change of the generator from no load to full load and is given by:

$$R = \frac{\Delta f}{\Delta P} \qquad (12)$$

such that Δf is the change in frequency and ΔP is the change in active power. For generators with different drooping governors connected to the power system, they respond differently to the change in load. The change in real power for two connected generators can be given as:

$$\Delta P_1 = \frac{\Delta f}{R_1} \qquad (13a)$$

$$\Delta P_2 = \frac{\Delta f}{R_2} \qquad (13b)$$

If the generators are operated in the isochronous governor's mode, the generators will oscillate against each other in trying to control the system frequency [54]. For multiple generators that participate in frequency control connected to the power system automatic generation control (AGC) is employed to ensure that frequency stability is maintained.

For the two area network shown in Figure 2.12 the change in frequency due to the load increase can be written as:

Figure 2.12 Load effect on two area network

21
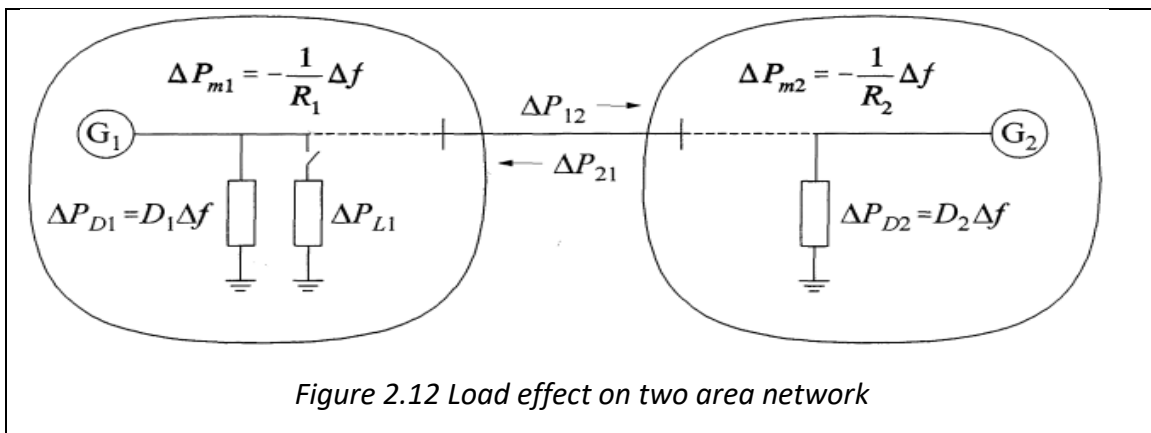
For the load increase ΔP_{L1} in area 1, the change in power could be written as:

$$\Delta P_{m1} - \Delta P_{12} - \Delta P_{L1} = \Delta f D_1 \qquad (14a)$$

and in area 2

$$\Delta P_{m2} - \Delta P_{12} = \Delta f D_2 \qquad (14b)$$

The change in mechanical power can be written as:

$$\Delta P_{m1} = -\frac{\Delta f}{R_1} \qquad (15a)$$

$$\Delta P_{m2} = -\frac{\Delta f}{R_2} \qquad (15b)$$

Eliminating ΔP_{m1} and ΔP_{m2} from 14 using 15 results

$$\Delta f \left(\frac{1}{R_1} + D_1\right) = -\Delta P_{12} - \Delta P_{L1} \qquad (16a)$$

And

$$\Delta f \left(\frac{1}{R_2} + D_2\right) = \Delta P_{12} \qquad (16b)$$

From 16 the change in frequency is given

$$\Delta f = \frac{-\Delta P_{L1}}{\left(1/R_1 + D_1\right) + \left(1/R_2 + D_2\right)} = \frac{-\Delta P_{L1}}{\beta_1 + \beta_2} \qquad (17)$$

also

$$\Delta P_{12} = \frac{-\Delta P_{L1}\left(1/R_2 + D_2\right)}{\left(1/R_1 + D_1\right) + \left(1/R_2 + D_2\right)} = \frac{-\Delta P_{L1}\beta_2}{\beta_1 + \beta_2} \qquad (18)$$

where β_1 and β_2 represent the frequency composite of area 1 and area 2 respectively. From equations (14 -18) [35] the increase in load results in the drop in frequency. For large systems with large number of synchronous machines, their inertia is high and they need substantial change in active power for the frequency to change.

For utility scale integration of solar-PV and wind, the conventional power plants play the pivotal role in maintaining operational limits and stability of the power system as the renewables generation power varies. The impact of solar and wind farms on the power systems stability have been largely investigated. Anaya-Lara et al investigated the interaction of windfarms with the power system comparing Fixed Speed Induction Generators wind turbines and the Doubly Fed Induction Generators wind turbines [55]. The study was done on the simplified United Kingdom (UK) electrical network. Anaya-Lara et al found the integration of FSIGs comprise the power system transient stability more compared to the DFIGs following the system faults. The transient stability of the Danish electrical network due to increased utility scale wind power generation was performed by the Liu et al [56]. Liu et al found that the increasing penetrations of the wind power in the Danish network results in reduced Critical Clearing Time (CCT) thus compromising the transient stability of the Danish electrical grid [56]. This study further concluded that the Danish electrical network can accommodate about 60 % of the wind power with the Nordic countries disconnected [56]. Munkhchuluum et al performed the transient stability on the Reliability and Voltage Stability Test (RVS) system due to high penetration of solar-PV power plants and argues that increased penetration of the solar PV system results in reduced transient stability [57]. In [57] the authors also pointed that the when faults are applied at less critical buses the transient stability of the system was improved.

The impact of the solar-PV on the voltage stability for the Canadian electrical network was conducted by Tamimi et al where they showed the voltage stability of the network was reduced due to the increased penetrations of solar-PV power plants [58]. Further impact studies for the solar-PV on voltage stability were performed by were performed in [59], [60] indicating that displacement of synchronous generators with the solar-PV plants leads to reduced voltage stability. The impact of multi-terminal High Voltage Direct Current (HVDC) windfarms on voltage stability on the Netherlands electrical grid was performed by Ndreko et al indicating that the voltage stability is dependent on the fault location [61]. Further studies on the 118-bus test system revealed that increased penetrations of the wind farms worsens the voltage stability [62]. On the other hand, Vittel et al demonstrated that integration of wind power improved the

voltage stability [63], while Sajadi et al found that it reduces the line loadings hence improving the transient voltage stability [64].

The intrinsic variability of the IREGs results in continual generation load imbalance, which poses some frequency stability challenges in the electrical network. The frequency response due to faults on the Western Interconnection [65] and Eastern Interconnection [66] suggest that the integration of the wind power generation improves the transient frequency stability of the network. Similar studies performed on the New England test system for the wind penetration of 40 % reveal that the frequency stability is dependent on the fault location [67]. This study further suggests that the areas with low inertia were affected most following the fault. However, Vittel et al argues that the increased penetration of the DFIGs wind farms worsen the transient frequency stability if the conventional power plants are displayed [68]. The research work performed by Alquthami et al on the 39-bus test system point out that the solar-PV generation of around 20 % results in frequency instability when the network is faulted and due to the temperature and irradiance variations [69]. The South Australia's frequency response due the increased solar-PV integration demonstrated that the trip from solar-PV plants renders network into frequency instability [70]. For the power, system with high penetration of RES the power system inertia is low and load fluctuations may lead to the frequency instability [71], [72]. Several studies [73]–[75] suggest that the use of energy storage systems reduce frequency fluctuations. Furthermore, Morren et al argues that the blades of the wind turbine could be used to increase the inertia of the wind turbine hence improve the wind power plant inertia.

The studies reviewed in the above literature are mostly done in the developed countries where electricity access in already high. As such the integration of the renewables in this countries aims to displace the conventional power plants (mainly coal) [58], [68]. In the case of Lesotho, the study wishes to assess the impact of the both solar and wind to the existing generation capacity. Also some of the studies were conducted on the test systems or reduced the reduced electrical models which may not accurately capture the dynamic behavior of the system [57], [67], [69]. For this research work, the impact of the renewables was done on the detailed electrical Lesotho network. Unlike the studies in [56], [58] where they considered either voltage or frequency or rotor angle stability, this study examines the all stability phenomenon considering their relations

as the penetrations are levels are increased. Additionally, the study considers the steady state voltage as the renewables vary.

Despite Lesotho having the low electricity access of 36.1 % and good renewable energy resources in form of solar-PV and wind power generation, the impact of their integration to the grid has not been investigated rigorously. As the first step towards the integration of the wind power to Lesotho grid Mathaba et al performed the resource assessment at Letseng [20]. From the research work, it was demonstrated that the bi-annual availability wind power generation would be 82.8 ± 6.7 %. The study also revealed that the wind power is mostly available during the August and lowest in March [20]. The comparative study done by Mpholo et al found that the availability of wind power for Masitise was 80 ± 10 % while that for Sani was 75 ± 14 % [21]. From both studies it was found that Letseng and Sani fall under class 4 and class 3 category respectively which make them suitable for grid integration [20], [21]. Masitise falls under class 2 category and is suitable for the stand alone systems [21]. The grid impact studies for both Letseng and Sani had not been done. For this research work, Letseng was chosen for the grid impact studies due to its close proximity to the grid. Taele et al state that Lesotho has good solar resource averaging daily radiation of 5 – 7 kWh/m^2 and the sunshine hours of 10.2 – 13.8 hours which is good for the large integration of solar-PV plants [22]. Further studies done by Taele et al suggest that the use of solar energy technologies in the rural areas will increase the energy access in Lesotho [76]. Though the deployment of standalone solar energy technologies will definitely increase electricity access, the study does not cater for the fact that the electricity access in Lesotho is mostly done through grid extension and more than 50 % of the electricity is imported. Hence this study focuses on the impact of utility scale solar-PV on the stability of Lesotho National grid. Understanding both solar and wind technology remain crucial in the integration studies.

2.2 Solar PV Technology

Among the solar-based renewables the solar PV ranks the first due to its simplicity, low maintenance and high reliability [77]. In addition to these advantages, the improvement in technology and economics of scale had reduced the cost of PV systems. One of the reasons that

has led to the massive utilization of the PV systems is the climate change as the PV systems are pollution free and renewable. These advantages had resulted into PV systems being employed in large grid-connected systems making PV systems play the pivotal role in the power generation as opposed to the traditional stand-alone systems. The large-scale integration of grid-connected PV systems results in new challenges in management and operation of the power systems due to the intermittence and variability PV power plants [78]. Hence, for successful integration of the PV systems accurate modeling of the PV systems and its power conditioning systems needs to be fully understood in order to design and assess performance of PV systems on the grid. Failure to successful assessment of the PV systems may led to grid instability hence compromising the power system reliability, security of supply and the power quality of the utility grid.

2.2.1 Photovoltaic Generator Model

At the heart of the PV generator is the solar cell build from the P-N junction, which uses the photovoltaic effect to convert the solar radiation into DC current. The solar cell is usually modelled based on the single diode lumped circuit model which predicts and characterizes the power production from the solar cells. The single diode model is depicted in Figure 2.13 and consists of current source (converts light to current), diode representing the P-N junction, and series and parallel resistors that represent the resistive loses [79].

Figure 2.13 PV cell generator equivalent circuit
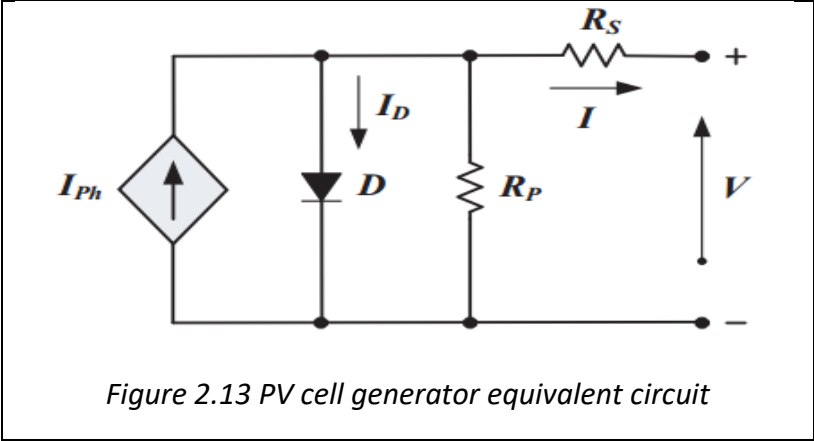
The photovoltaic solar cells are connected together to form modules, and the modules are connected together to form the PV arrays, which are connected together to provide the required power output of the PV system. The equivalent circuit for the solar module is constructed by connecting a number of solar cells in parallel ($N_{p)}$ and in series (N_p) as displayed in Figure 2.14 below.

Figure 2.14 Generalized PV cell generator equivalent circuit
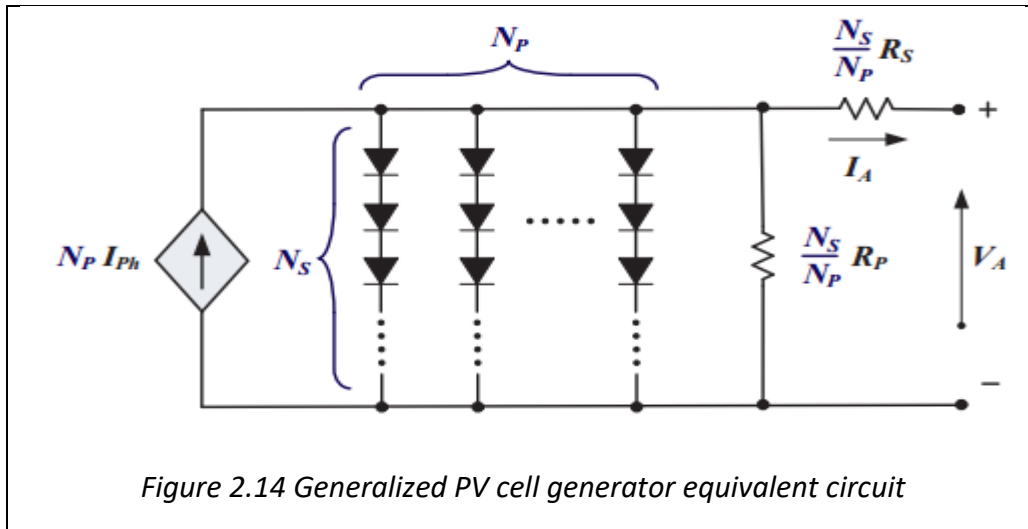
Mathematically the power from the solar cells can be derived using equation 19.

$$I_A = N_P I_{Ph} - N_p I_{RS} \left\{ exp \left[\frac{1}{AV_{Th}} \left(\frac{V_A}{N_S} + \frac{I_A R_S}{N_P} \right) \right] - 1 \right\} - \frac{N_P}{R_P} \left(\frac{V_A}{N_S} + \frac{I_A R_S}{N_P} \right) \quad (19)$$

where:

Table 2 PV model parameters

Parameter	Description
I_A	Current Output from PV array (A)
V_A	Voltage Output from PV array (V)
I_{Ph}	Solar cell photovoltaic current (A)
I_{RS}	Reverse current of the solar cell (A)
A	Ideality factor of the solar cell
R_S	Series Intrinsic Resistance (Ω)
R_P	Parallel Intrinsic Resistance (Ω)

V_{Th}	Thermal cell Voltage ($V_{Th} = kT_C/q$)
k	Boltzmann Constant (1.380658e-23 J/K)
T_C	Solar Cell Operation Temperature (K)
q	Electron Charge (1.6022e-19 Cb)

To find the output power from the equation 19 I_{Ph}, I_{RS}, R_S, R_P, and A must be known and referred to as "five parameters" hence "five-parameter PV generator model". In addition to the five parameters, the solar isolation and temperature conditions largely influence the electrical performance of the PV generator. PV module manufactures normally provide the five parameters under the known test conditions such as the Standard Test Conditions (STC) (solar radiation of 1000 W/m^2, solar cell temperature of 25 °C, and air mass of 1.5) and under Nominal Operating Cell Temperature (NOCT) (solar radiation of 800 W/m^2, solar cell temperature of 20 °C and wind speed of 1 m/s) [80]–[82]. However, the operating conditions under which the PV generators operate are different from the STC hence real performance of the PV system under real conditions remain an interest.

Under the real operating conditions, the photocurrent is related to the incident radiation (G) and solar cell temperature (T_c) by equation 20:

$$I_{Ph} = f_{AM}f_{IA}[I_{sc} + \alpha_{Isc}(T_C - T_R)] \, {}^{G}\!/_{G_R} \qquad (20)$$

Such that:

Table 3 Parameters for I_{ph} Equation

Parameter	Description
f_{AM}	Air mass which describes the solar radiation path through the atmosphere to the absorbing array
f_{IA}	Angle of incidence of the solar radiation on the absorbing array
I_{SC}	Short circuit current at of the solar cell at STC
α_{Isc}	Solar cell temperature coefficient
G_R	Solar Radiation at STC (1000 W/m^2)

The air mass describes the path taken by the radiation beam before reaching the earth as it passes through the atmosphere relative to the direct path length [83]. The air mass accounts for the solar radiation that attenuated through the atmosphere by scattering and atmospheric absorption. The air mass can be computed from zenith angle which dependent on the location of the place and time. The angle of incident function (f_{IA}) accounts for the optical effects of the solar radiation as absorbed and reflected by the PV array in generation electrical energy. The reflected and absorbed radiation largely depend on the angle of incident, which defines the angle between solar radiation beam and the normal to the PV array surface. Detailed mathematical equations describing the incident angle on PV array surface at any given orientation and time can be found in references [84], [85].

In addition to the incident angle and air mass, the performance the PV generator is distinguished by the I-V characteristics, which are dependent on the cell temperature and the incident radiation. The open-circuit voltage (V_{OC}) of the solar cell varies with temperature and solar radiation according equation 21.

$$V_{OC} = V_{OCS}(1 + \beta_T(T_C - T_R))v_T \tag{21}$$

where V_{OCS} is open circuit voltage at STC; β_T and v_T are the temperature and voltage correction factors that are determined empirically.

Based on instantaneous values V_{OCS} and I_{Ph} the solar cell current and voltage can be known hence the output power of the module or PV array. The I-V curves showing how PV power varies with irradiance and temperature are shown in Figure 2.15 and Figure 2.16 respectively.
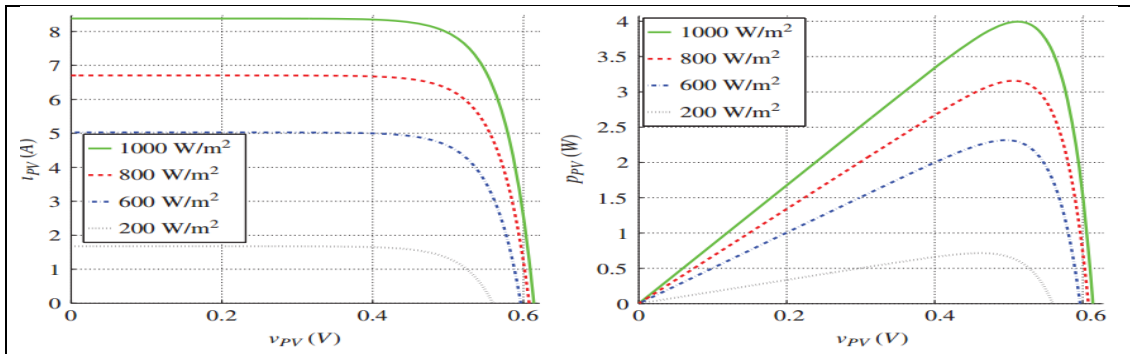
Figure 2.15 I-V indicating how V_{pv}, i_{pv} and P_{pv} vary with irradiance under constant temperature [86]
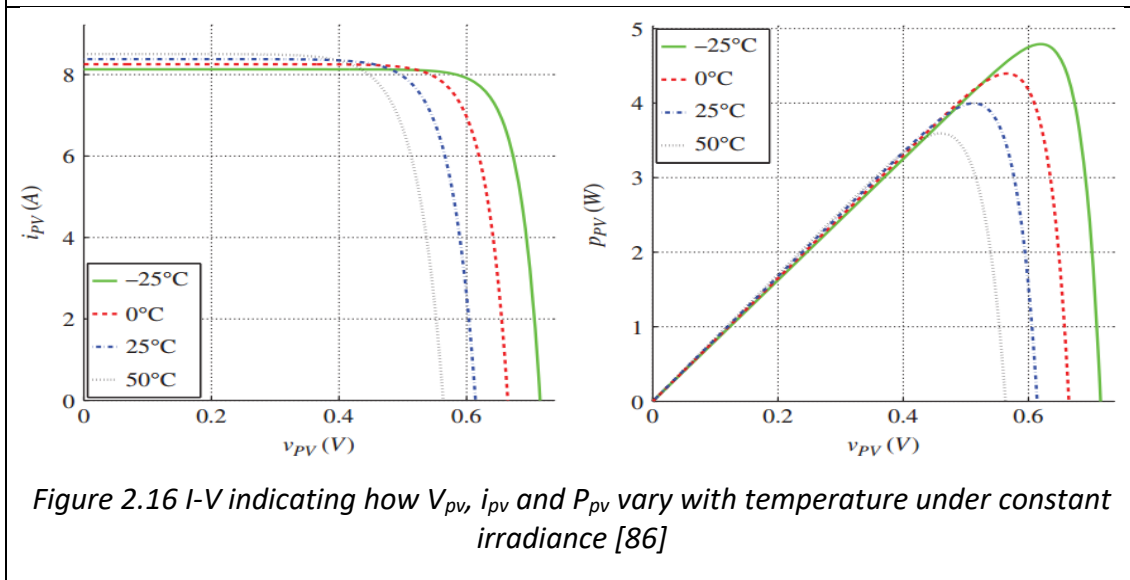
Figure 2.16 I-V indicating how V_{pv}, i_{pv} and P_{pv} vary with temperature under constant irradiance [86]

2.2.2 PV Power Conditioning

The power from the PV array is not compatible with the grid power since the PV array produces the DC voltage. For the PV array power, to be compatible with the grid electricity, additional circuitry is required so that the PV power synchronizes with the utility grid. Additionally, the PV power depends on the atmospheric conditions that are constantly changing hence some conditioning circuitry. To reduce the power variability to the grid from the PV system, maximum power point tracking (MPPT) technique is employed and integrated into the power conditioning system. The main function of the power conditioning system is to inject the power to the utility without violating the power quality standards and grid code.

The power conditioning circuitry can be classified into three categories depending on the number of power stages employed. Figure 2.17, Figure 2.18, and Figure 2.19 display three different power conditioning configurations namely single stage, dual stage and multistage topologies [87].

Figure 2.17 Single Stage Inverter Topology [87]

Figure 2.18 Dual Stage Inverter Topology [87]

Figure 2.19 Multi Stage Inverter Topology [87]
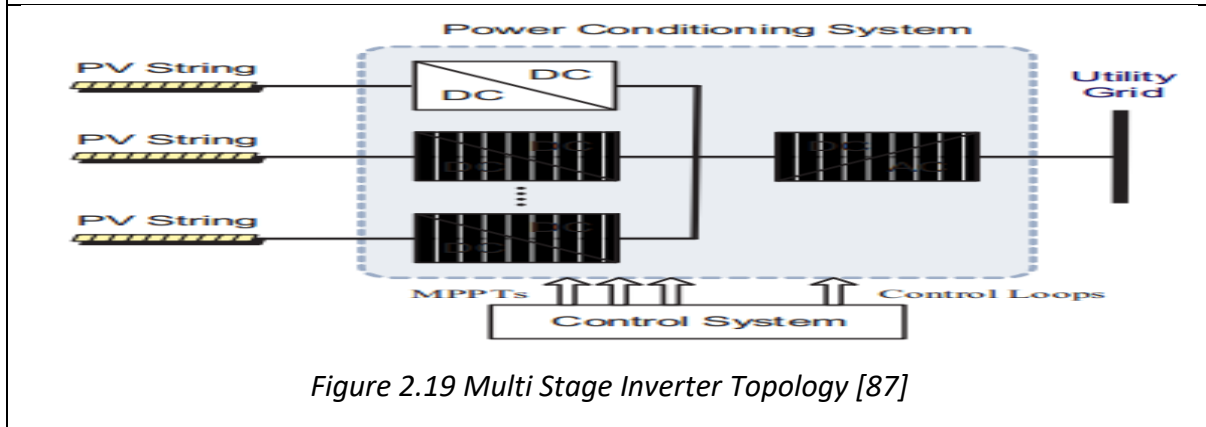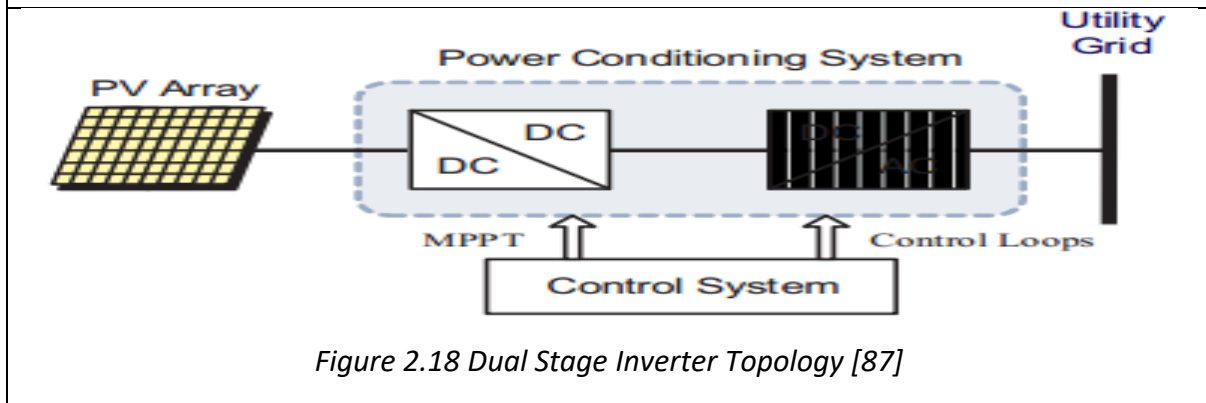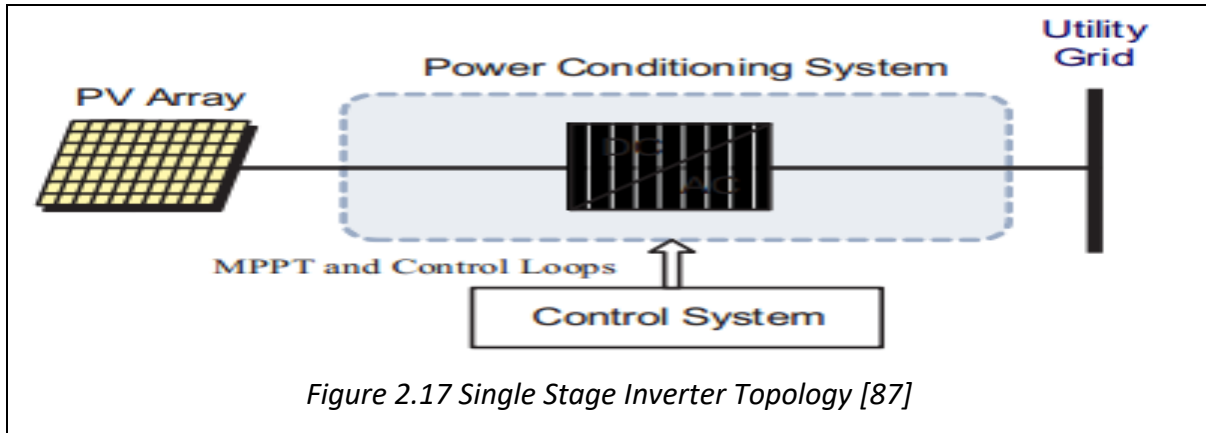
For the single stage topology both MPPT and inverter loops are performed in single stage, while the dual stage configuration utilizes the DC-DC converter which acts as the interface between the

PV array and the inverter. For the dual stage topology, the DC-DC handles the MMPT while the inverter deals DC/AC conversion. Lastly for the multistage topology the DC-DC converter implements MPPT for each PV array string and the DC-AC converter handles the DC-AC conversion. The dual-stage and multi stage topologies are normally employed in grid-connected PV systems as they provide better control strategies of both voltage, reactive and damping oscillations.

Figure 2.20 depicts the detailed model for the grid-connected PV system showing the details of major block components [79]. The PV panels are connected in series and in parallel to produce the DC voltage that is feed DC-DC converter then to the utility grid through the step-up transformer.
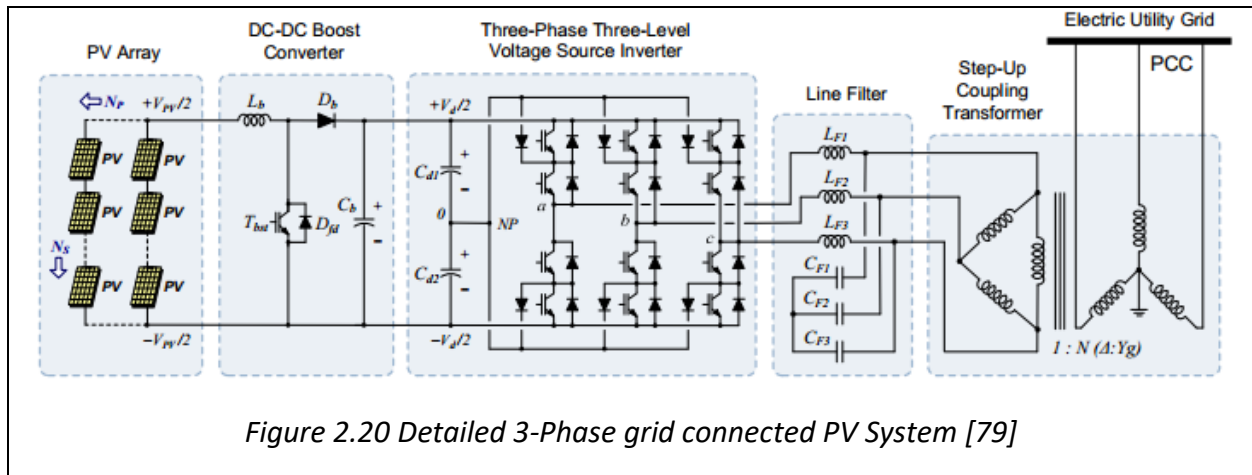
Figure 2.20 Detailed 3-Phase grid connected PV System [79]

The DC-DC power conditioning (PV-Side Converter (PVSC)) is commonly implemented by DC-DC topologies such as the buck, boost, buck-boost and the full-bridge DC-DC converters. The PVSC keeps the input voltage to the DC-AC inverter constant as the PV array voltage varies with the atmospheric conditions. The voltage at the DC-AC inverter is kept constant by the switching power devices (a rectifier diode and the power transistor) and the smoothing devices in form of the capacitor (C_b) and the inductor (L_b). The duty circle of the switching devices is continually varied such that the input voltage to the inverter is kept near the MPPT under different loading and atmospheric conditions.

32

The DC-AC inverter (Grid Side Converter (GSC)) transforms the DC power from PVSC to the AC grid compatible power. GSC is normally implemented using H-bridge for the single-phase grid connected to the PV systems and voltage source inverter for the three-phase connections. The GSC is built using power transistors and switched diodes. Using the sinusoidal pulse width modulation (SPWM) the GSC synthesis the sinusoidal voltage from different input voltages levels [88]. The output of the GSC is filtered to eliminate harmonics from the SPWM and then stepped-up through the transformer to the point of common coupling (PCC). The filtering circuitry must be designed such that the total harmonic distortion is less than 5 %. The governing mathematical equations for the inverter are described in references [89], [90].

2.2.3 PV Generator Controls

The controls employed on large-scale grid-connected PV systems are classified into three control levels namely external, middle and the internal control as shown in Figure 2.21. The external control determines both reactive and active power injected into the utility grid by the PV system [87]. The control is achieved through voltage and active power control loops. The voltage control loop employs the voltage-droop strategy, which modulates the reactive component of the voltage, source inverter (VSI) using i_{qr} in maintaining the voltage at the point of common coupling (PCC) [88]. For the stable and fast response of the reactive power loop the proportional-integral, (PI) controller is used. The active power control loop matches the active power injected to the grid with the active power extracted from the PV array. This is accomplished by the MPPT strategy, which controls the input voltage of the inverter by adjusting the duty circle of the DC-DC converter. The MPPT can be implemented using the fuzzy or neural networks algorithms, but perturb and observe algorithm is normally employed.

Figure 2.21 Control Levels of 3-Phase grid connected PV System [87]
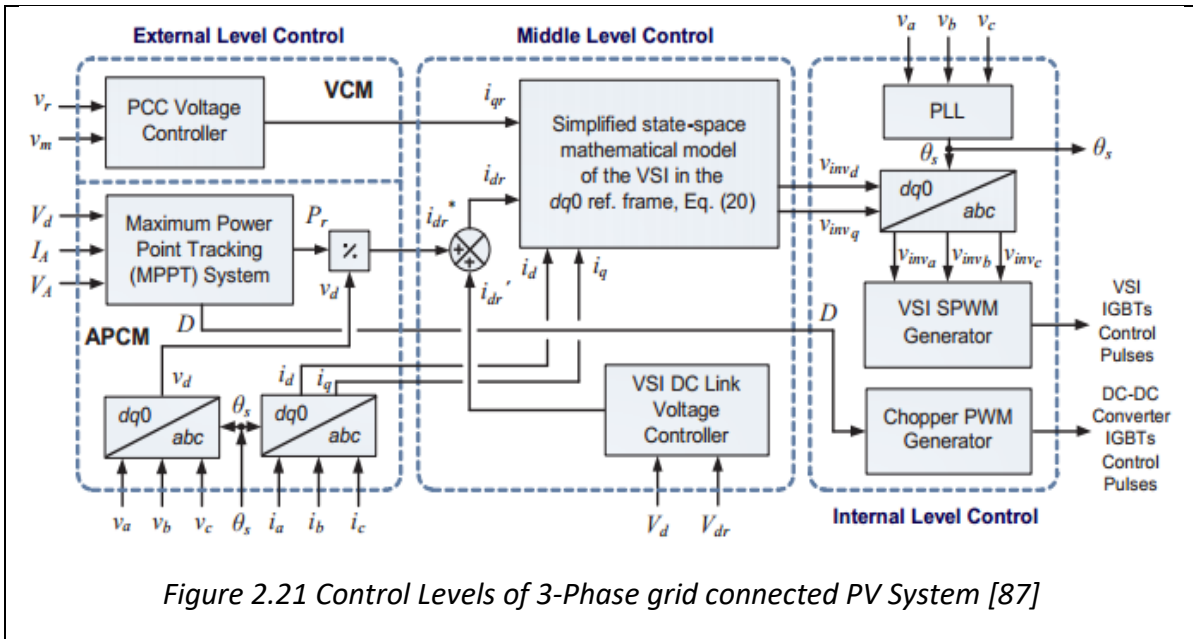
The middle level control dynamically tracks the output reference values (i_{qr} and i_{dr}) from the external level control [87]. The reference values are tracked by employing the current control of the inverter in synchronous-rotating dq frame [91]. The PI controllers are used to decouple the DC-side of the inverter and the AC-side if the inverter such that there is some power balance from the AC and DC side of the inverter. The internal level control generates the switching signals for the voltage source inverter insulated-gate bipolar transistor (IGBT) based on the pulse width modulation. The output of the VSI produces the 3-phase voltage, which is synchronized to the utility grid power by the Phase Locked Loop (PLL).

2.3 Wind Technology

Increased power generation from wind resource necessitates accurate modelling of the wind variability for evaluation of the power systems performance analysis. The kinetic energy from blowing wind is captured by the rotor blades and then converted to mechanical energy through the rotating blades. The rotor blades drive the rotor of the generator, which converts the mechanical energy to the electrical energy, which is fed to the electrical grid. Figure 2.22 briefly

illustrates the conversion process of how the wind turbine converts the energy from wind to electrical energy.

Figure 2.22 Main Components of wind turbine and their components
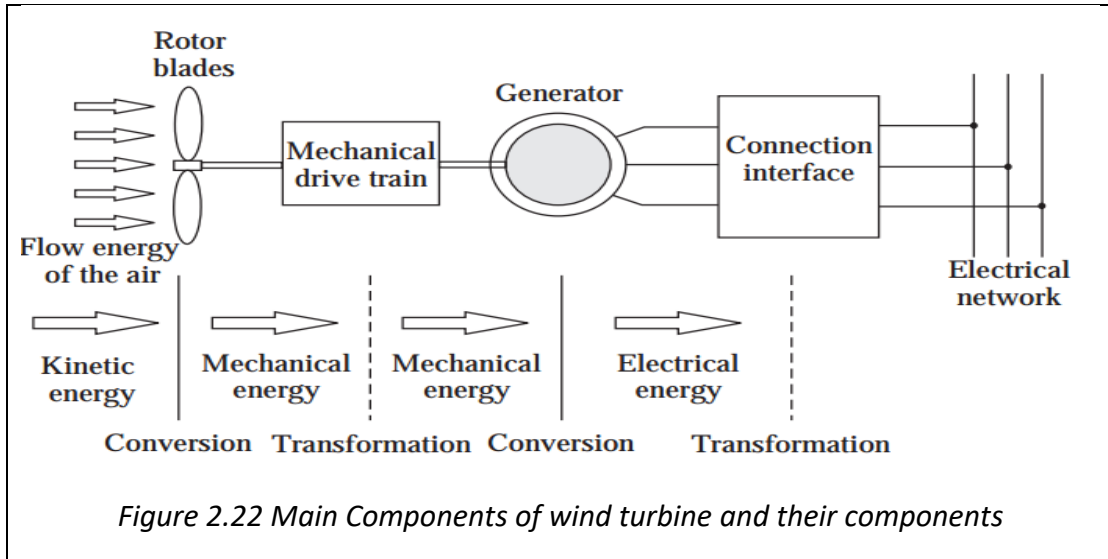
The power of the blowing air passing through the perpendicular area A (swept by the rotor blades) is expressed by equation 22 while the power captured by the rotor blades of the wind turbine is given by equation 23 [92].

$$P_w = \frac{1}{2} \rho A V_w^3 \tag{22}$$

$$P_w = C_p(\lambda, \beta) \frac{1}{2} \rho A V_w^3 \tag{23}$$

From equation 22, ρ represents the air density, V_w represent the wind speed and C_p is the performance coefficient, which is the function of both tip speed ratio λ and blade pitch angle β. The power curve relates the output power of the turbine to wind speed as depicted in Figure 2.23.
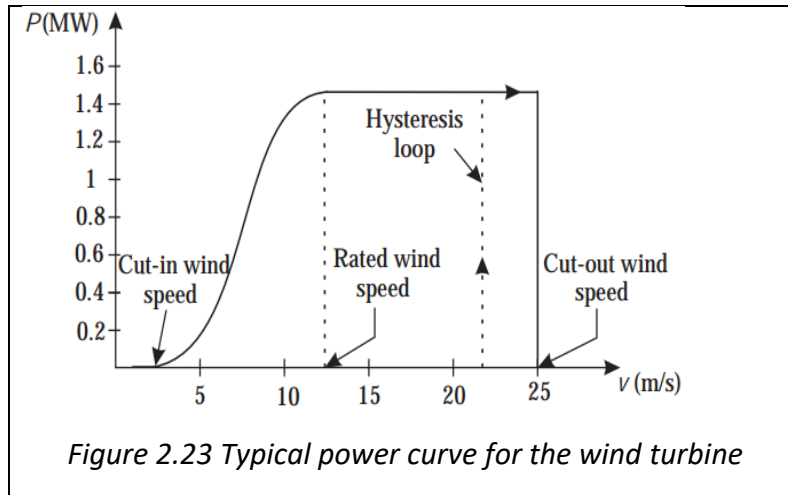
Figure 2.23 Typical power curve for the wind turbine

At low wind speeds beneath cut-in, wind turbine does not generate power but as the wind speed increases above cut-in, the generated power sharply increases up to the rated power where the output levels remain constant as the wind speed increases. At cut-out, the generated power shuts down to protect the wind turbine from distraction. Furthermore, the wind turbine power output could be controlled by adjusting the rotor blades pitch angle. The output power regulation of the fixed speed wind turbine is attained using the stall mechanism to control the output power and the variable-speed wind turbines use dynamic pitching mechanism to control the output power.

2.3.1 Fixed-Speed Wind Turbines

Fixed wind-speed wind turbines represents early technology of the wind turbines that are based on the fixed speed generators. The induction generator (Squirrel cage or Wound rotor) is normally used for the fixed wind speed turbines where the rotor speed is constant in spite of the wind speed. For the fixed wind-speed turbines, the power grid frequency determines the rotor speed and the stator side of the generator is directly connected to the electrical power network. This configuration results in simple, robust and cheap wind turbines but causes increased power system instability as the variation in the wind speed results in rotor speed fluctuations, which causes active power, reactive power and voltage fluctuations at the point of interconnection of

the wind farm [93], [94]. Furthermore, the increased active power production results in huge reactive power absorption from the electrical grid, which further results in increased voltage instability [36]. In addition, the induction generator requires some external reactive power to start running [36]. Due to these problems, the fixed-speed wind turbines are no longer used in wind farms and the variable wind speed turbines were constructed to overcome the disadvantages of the fixed-speed wind.

2.3.2 Variable-Speed Wind Turbines

The improved technology in generator and power electronics interfacing circuits had led to the establishment of the variable-speed wind turbines. Variable-speed wind turbines are designed to capture maximum power from a wide range of the wind speed using the improved aerodynamics mechanisms. The main converter technology employed for variable-speed wind turbines is the partial-scale converter based on doubly fed induction generator (DFIG) and the full-scale wind turbine converter (FSWT) based on either induction or synchronous generator [93]. As opposed to the fixed-speed wind turbine, the rotational speed of the rotor varies relative to the wind speed and rotor speed is decoupled from the grid frequency through the partial-scale converter for DFIGs [95]. The decoupled rotor speed and grid frequency results in almost constant torque hence reduced fluctuations of active, reactive power and frequency of the electrical network employing variable-speed wind turbines [94]. For the FSWT, both the rotor and stator speed are decoupled from the grid frequency through the back-to-back converter resulting in full control on the active, reactive and voltage control. In addition, FSWTs are less susceptible to the grid faults and can provide reactive power to the grid. For the FSWTs, depending on the generator type employed, the gearbox might be eliminated hence reduce size of the wind turbine. Nonetheless, the use of power electronic converters results in increased power losses and induces some harmonics to the power grid. Moreover, cost of the full converter wind turbines remains the challenge for their full adaptation. The wind turbines configurations can further be based on the control speed and power control strategies based on the generator type.

2.3.3 Wind Turbines Configurations

The wind turbines configurations can be classified mainly into four categories, namely Type I, Type II, Type III, and Type IV. Figure 2.24 displays the schematics of the generator technologies for the main wind turbine configurations.

Type I: Fixed-Speed

Type II : Finite variable Speed

Type III: Limited Variable with DFIG

Type IV: Variable Speed with full convertor

Figure 2.24 : Wind turbine generator systems[96]
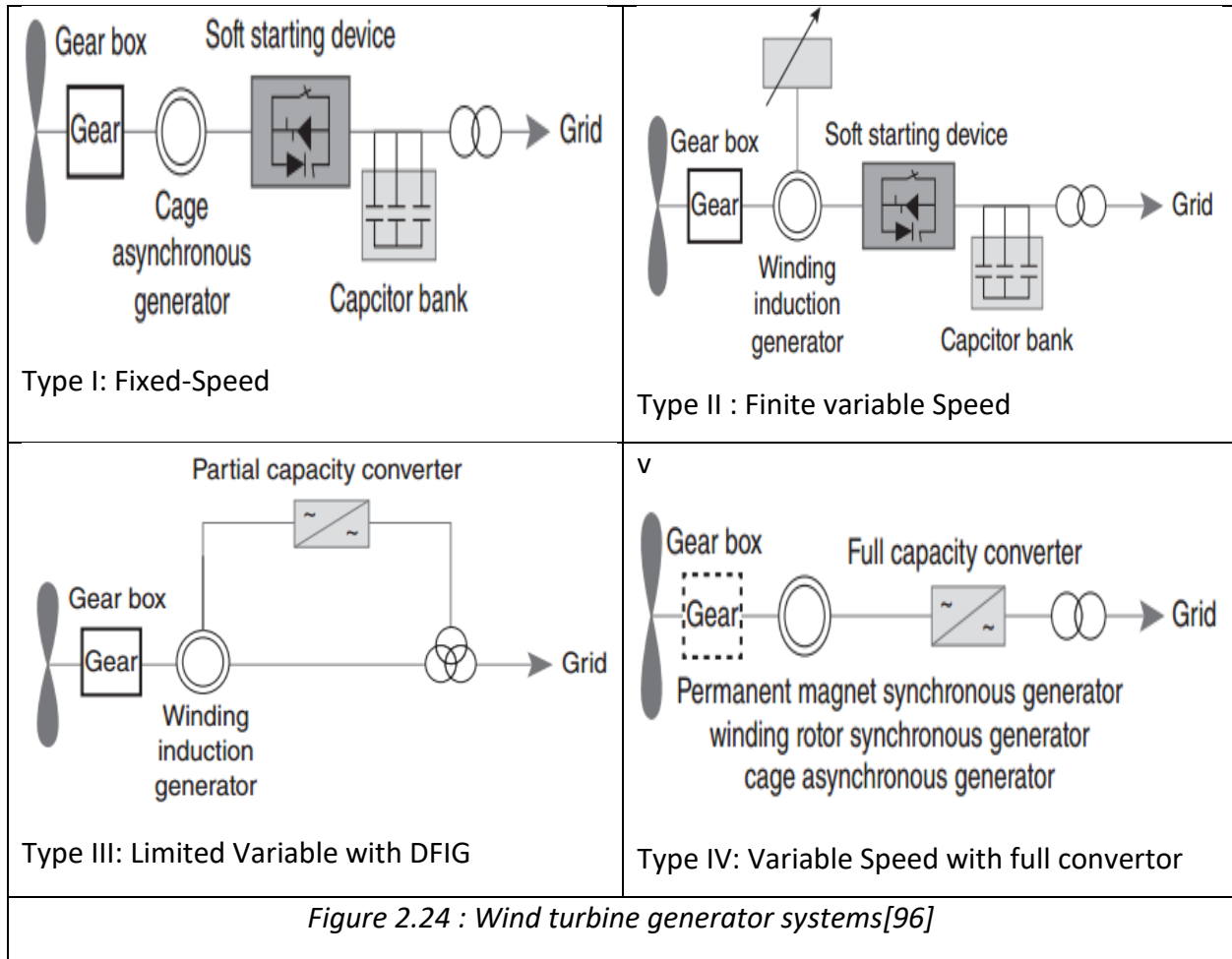
Type I (Fixed speed): is based on the squirrel cage or wound rotor induction generator, which is connected to the grid via the step-up transformer. For the smooth connection to the grid, Type I utilizes the soft-starter and the capacitor bank for reactive power compensation. This exhibits the same disadvantages as the fixed-speed wind turbines.

Type II (Limited Variable Speed with Variable Resistance): uses the wound rotor induction generator and controls the rotor speed using the variable resistor known as the OptiSlip or

FlexiSlip [93]. Same as the Type I wind turbine, Type II still uses the soft-starter to suppress the inrush currents and uses the capacitor bank for reactive power compensation. The use of OptiSlip or FlexiSlip allows the variation of the rotor speed to about 10 % and 16 % respectively [36]. Type II generators still have poor active and reactive power control with limited rotor speed range.

Type III (Variable Speed with Partial-Scale Frequency Converter): utilizes the wound rotor induction generator based on the doubly fed induction generator (DFIG) principles. Contrary to Type I and Type II, wind turbines which use soft-starter and capacitor banks for smooth connection to the grid and reactive power compensation, Type III is equipped with partial frequency converter capable of better reactive compensation and smooth connection to the grid [97]. The use of the partial frequency converter results in better synchronous speed range of -40 % to 30 % [93]. The downside of the Type III is some additional protection needed to isolate grid faults. In addition, the use of slip rings between the generator and the rotor results in increased maintenance due to wear and tear.

Type IV (Variable Speed and Full-Scale Frequency Converter): is based on the wound rotor synchronous generator (WRSG) or the permanent magnet synchronous generator (PMSG). For Type IV, the generator is connected to the electrical grid using the full-scale frequency converter. This results in the better control of the synchronous speed (compared to Type III) hence full control of active, reactive and voltage on the point of common coupling. For Type IV, the gearbox is not a must as the generator could be driven directly from drive train. Increased use of power electronics implies increased power losses and complex designed with high cost.

2.3.4 Wind Turbine Generator Modelling

To further gain, fundamental understanding of the wind turbines, both mathematical models of the electrical and mechanical wind turbine needs to be understood for effective grid integration studies. Wasynczuk et al and Anderson et al pioneered the modelling of the wind turbines in trying to understand behavior of the wind generators due to wind variations and their stability [98], [99]. Figure 2.25 displays the basic components on the wind turbine model.

Figure 2.25 Block diagram for the wind turbine model [31]
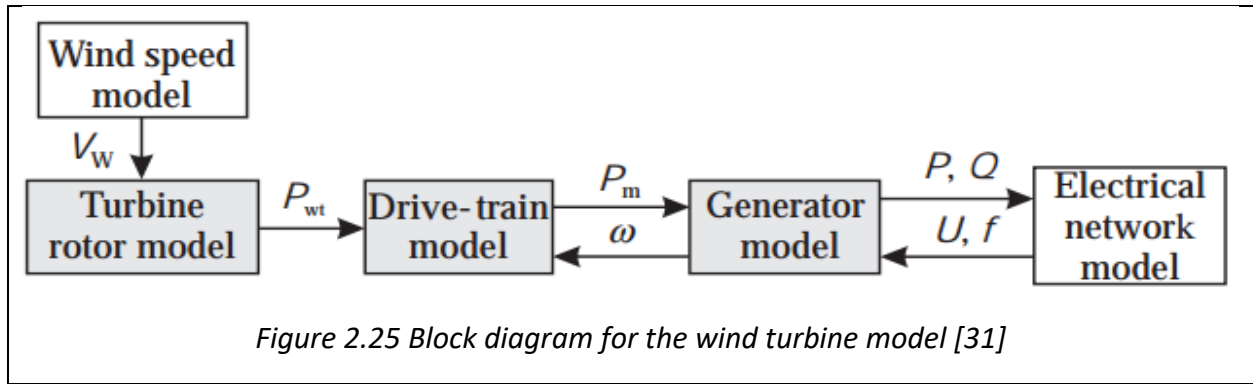
The Wind Speed Model: represents the wind speed based on the historical measurements for the proposed wind farm site. The wind speed historical data simulations are limited to the historical recorded wind speed, hence analytical methods are employed to model the wind speed [100]. Commonly used equation for the analytical wind model is given in equation 24 where V_W (t) is the wind speed at particular time and $V_{wa}(t)$, V_{wr} (t), V_{wg} (t), V_{wt} (t) are average wind speed, ramp component of the wind speed, gust component of the wind speed, and turbulence component of the wind speed respectively [99].

$$V_w(t) = V_{wa}(t) + V_{wr}(t) + V_{wg}(t) + V_{wt}(t) \tag{24}$$

The Wind Turbine Rotor Model: represents the power that can be extracted from the kinetic energy of the wind through the rotor blades. The output from the rotor blades is given as in equation 23. The air density ρ and area swept by the rotor blades are considered constant while the performance coefficient varies and is dependent on pitch angle β and the tip speed ratio λ.

Wind Turbine Drive Train Model: is modelled by the multi-mass system described by the angular position, angular velocity and the inertia of the rotating bodies. The mass objects are connected to each other through the damping coefficient and some spring constants as depicted by the two mass system in Figure 2.26.

Figure 2.26 Two-Mass Drive Train [36]
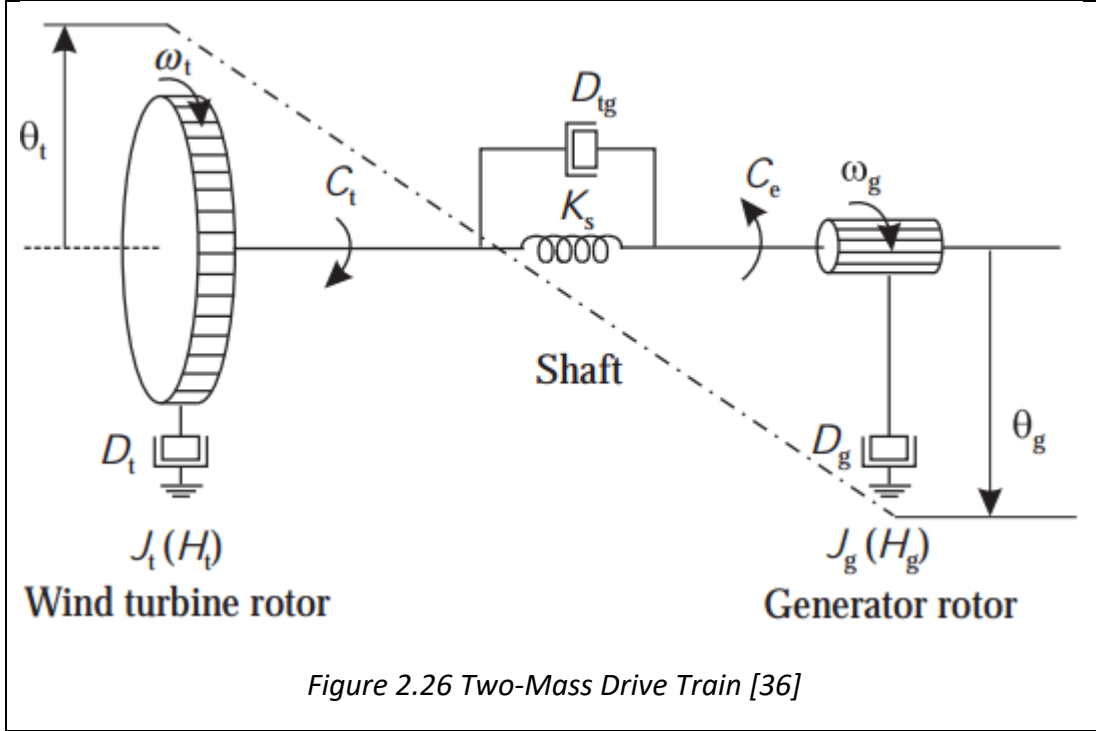
J_t represents the inertia for the rotating blades due to pitch and the drive train (hub, low speed shaft, and rotating parts of the gearbox connected to low-speed shaft) while the inertia for the generator rotor, high-speed shaft and the gearbox parts connected to high speed shaft are represented by the J_g. In addition, the ω_t and ω_g represent the angular velocities for the turbine and the generator respectively, while θ_t and θ_g denote turbine and generator rotor. D_{tg} and K_s give the mutual damping and the shaft stiffness respectively. The self-damping for the aerodynamic of the turbine blades is given as D_t and the self-damping for the generator is given as D_g. The equation describing the two-mass model of the wind turbine can be given as [36], [94], [101]:

$$2H_t \frac{d\omega_t}{dt} = C_t - K_s(\theta_t - \theta_g) - D_{tg}(\omega_t - \omega_g)$$

$$2H_g \frac{d\omega_g}{dt} = -C_e + K_s(\theta_t - \theta_g) + D_{tg}(\omega_t - \omega_g)$$

$$\frac{d\theta_t}{dt} = \omega_t; \frac{d\theta_g}{dt} = \omega_g \tag{25}$$

where C_t and C_e denote aerodynamic torque developed from the turbine blade and electromagnetic torque developed from the generator. The inertia constants for wind turbine and the generator are represented as H$_t$ and H$_g$ respectively. Under the assumption that velocities of the generator rotor and turbine speeds are equal, the two-mass equations of motion could be reduced to:

$$2(H_t + H_g)\frac{d\omega_m}{dt} = C_t - C_e \qquad (26)$$

The Generator Model: is modelled depending on the type of the generator being used. The generator model follows the typical model of the induction generator for Type I – III and synchronous generator for the Type IV wind turbines. For the sake of space the detailed models and equations describing the generator models are not discussed but can be found in references [35], [93], [102], [103].

The Electrical Network Model: represents the electrical components to which the wind turbine or wind farm is connected. These components range from the transmission lines, transformers, other generators and the electrical loads served with some electrical energy.

2.3.5 Wind Power Plant Model

The wind power plant model remains pivotal in grid studies for wind farms. Several studies discussed the early aggregation of the constant wind turbines [104]–[106]. Castro et al discussed the singular perturbation approach in reducing the wind farm model, which only simplifies the individual wind turbines based on power systems dynamics. Furthermore, in studies performed by Castro et al and Akhmatov et al the wind farm was aggregated based on the individual summation of wind turbines such that the total rated power (S_{eq}), total compensating capacitance (C_{eq}) and the total mechanical power are given as [105], [106]:

$$S_{eq} = \sum_{i=1}^{n} S_i \,;\, C_{eq} = \sum_{i=1}^{n} C_i \,;\, P_{m,eq} = \sum_{i=1}^{n} P_{m,i} \qquad (27)$$

where S_i, C_i, and $P_{m,i}$ represent individual rated power, compensating capacitor and mechanical power of the *ith* wind turbine respectively.

The more detailed model was proposed by Muljadi et al by taking into consideration the wind farm layout where each wind turbine is connected to the step-up transformer which connects to the string of other wind turbines, then the group of strings connected to point of interconnection (POI) [107]. Muljadi and Ellis further performed the validation of the developed model against the real field measurements based on Type III wind turbines [108]. From the validation results, they found that Type III adequately represented the wind farm except for the wind farm constructed from 2 wind turbines. Figure 2.27 and Figure 2.28 displays the modern wind farm configuration and its equivalent single–machine representation.
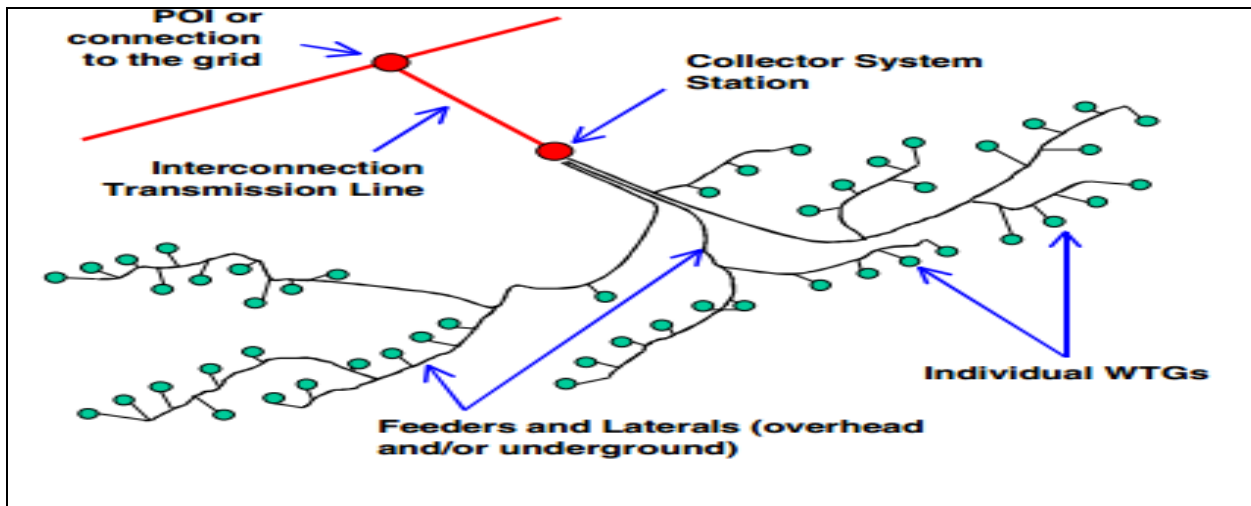
Figure 2.27 Modern wind farm configuration
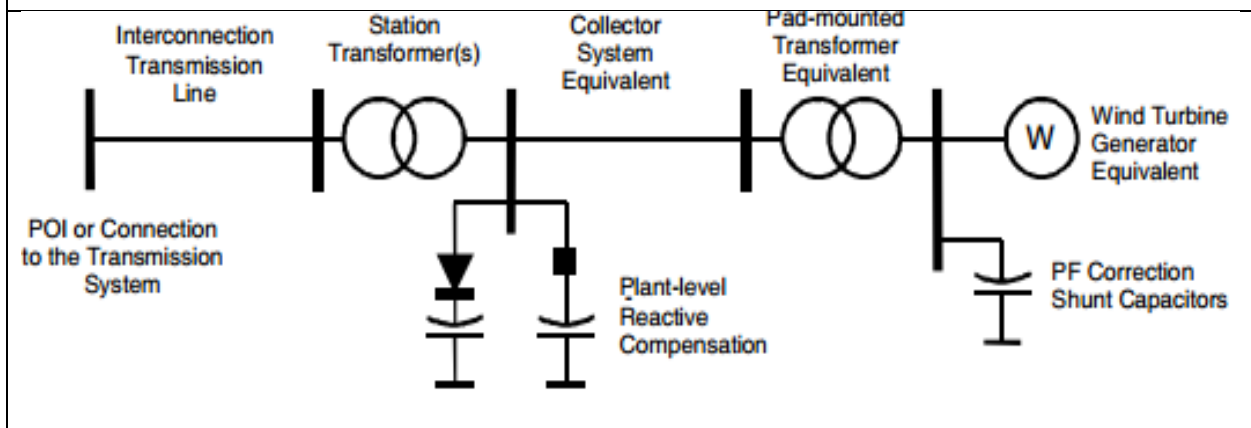
Figure 2.28 Single line equivalence of the wind farm

43

Due the increased need of standardized wind, farm models Western Electricity Commission Council (WECC) in corporation with the IEEE Working Group on Dynamic Performance of Wind Power Generation launched the task force to develop generic models for wind farms based on all types of wind turbines. Ellis et al developed the models and their technical specifications [109]. The models developed by WECC are widely used in commercial softwares such as DigSILENT Power, Powerworld, and Positive Sequence Load Flow (PSLF). Pourbeik et al presented the recent development and the limitations of the models developed by WECC [110].

3 Methodology

The increased large renewable power plant integration to the utility grid affect the power dynamics of the power systems. As the IREGs penetration increases the grid stability may improve or be compromised, hence careful assessment of the impact of IREGs on the utility grid must be performed. The study evaluates the impact of the IREGs (Wind and Solar PV) integration on the stability of Lesotho electric network. The study focuses on the voltage, frequency and rotor angle stability. In addition, the maximum allowable penetration of the IREGs was determined. The study considered both the dynamic and the steady state performance of LEC network. The dynamic analysis was performed by applying the 3-phase short circuit faults to suitable bus bar (stressed) of the electrical network such that the chosen location results in the maximum electrical system instability. The stressed point was chosen based on the critical clearing time (CCT) criterion. The critical clearing time defines the longest time the generator remains synchronized after being disturbed [39]. After the fault was applied, the time-domain responses of voltage, frequency and rotor angle were evaluated against the grid code of Lesotho to ensure that grid code is observed before and after the fault conditions. The steady state performance was evaluated by analyzing the hourly voltage performance against the grid code of Lesotho. The steady state analysis was based on the hourly load from 2018. The load flow and stability simulations were performed using the DigSILENT software.

3.1 System Modelling and Configuration

The study was carried out based on the computer model of the Lesotho Electricity Network, which was supplied by the Lesotho Electricity Company (LEC) and then modelled using the DigSILENT software. LEC is the sole transmission and distribution operator in Lesotho. LEC electrical network consists of hydropower generating unit with capacity of 72 MW, 2 MW of the hybrid system of diesel and mini-hydro at Mantsonyane and the external grid from the neighboring South-African power grid. The electrical transmission network is built from interconnected substations with the voltage levels of 132 kV, 88 kV, 66 kV and 33 kV. The

distribution network is built from 22 kV and 11 kV voltage levels. The end-user voltage levels are constituted by 380 V and 240 V. Figure 3.1 shows the electrical network model over which the impact of the intermittent renewables sources will be integrated and evaluated. The model was built using DigSILENT software. DigSILENT is the computer-aided software suitable for analyzing electrical transmission, distribution and industrial networks. In addition, DigSILENT can model and analyze electrical networks with variable renewable energy generators.
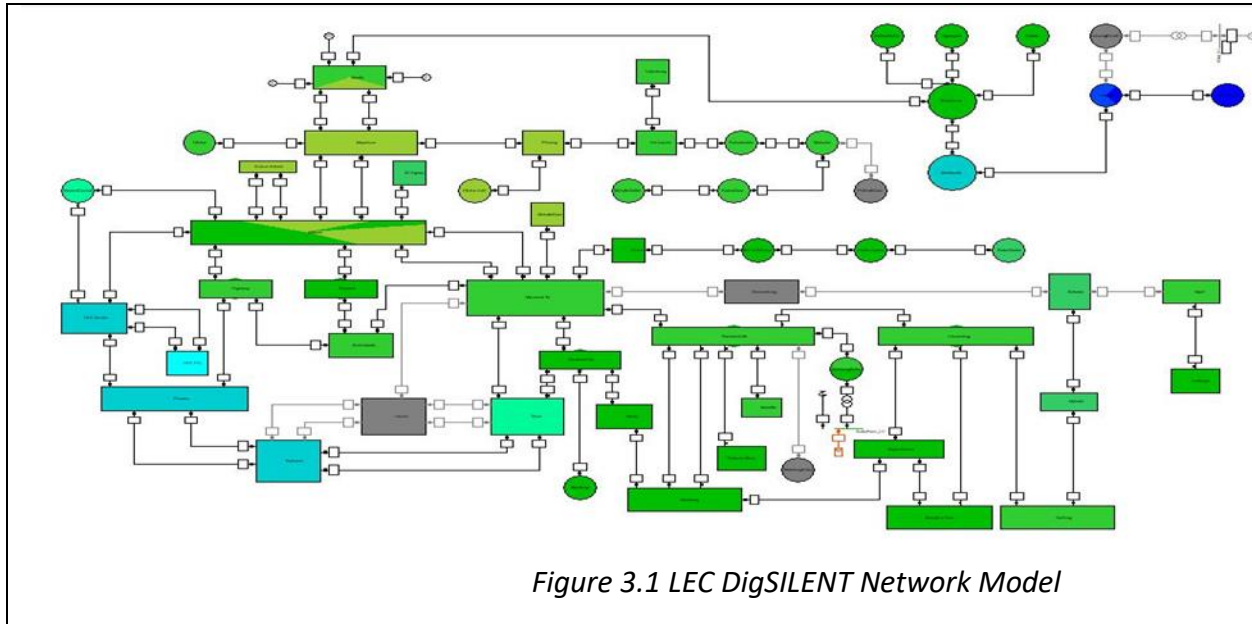
Figure 3.1 LEC DigSILENT Network Model

The external grid acts as the reference machine and balances the load deficit not supplied by hydro power plants in Lesotho. The study considers the integration of wind and solar farm power plants at Letseng and Ha-Ramarothole respectively. The places were identified to have good wind and solar resources. The transient and penetration studies were performed for three different cases namely:

i.   Solar PV Generation only

ii.   Wind Generation only and

iii.   Hybrid (Solar and Wind Generation)

3.1.1 Transformer modelling

The transformers were modelled from the real data provided by LEC and the transformer parameters were captured into DigSILENT as shown in Figure 3.2.

Figure 3.2 Transformer Modelling in DigSILENT
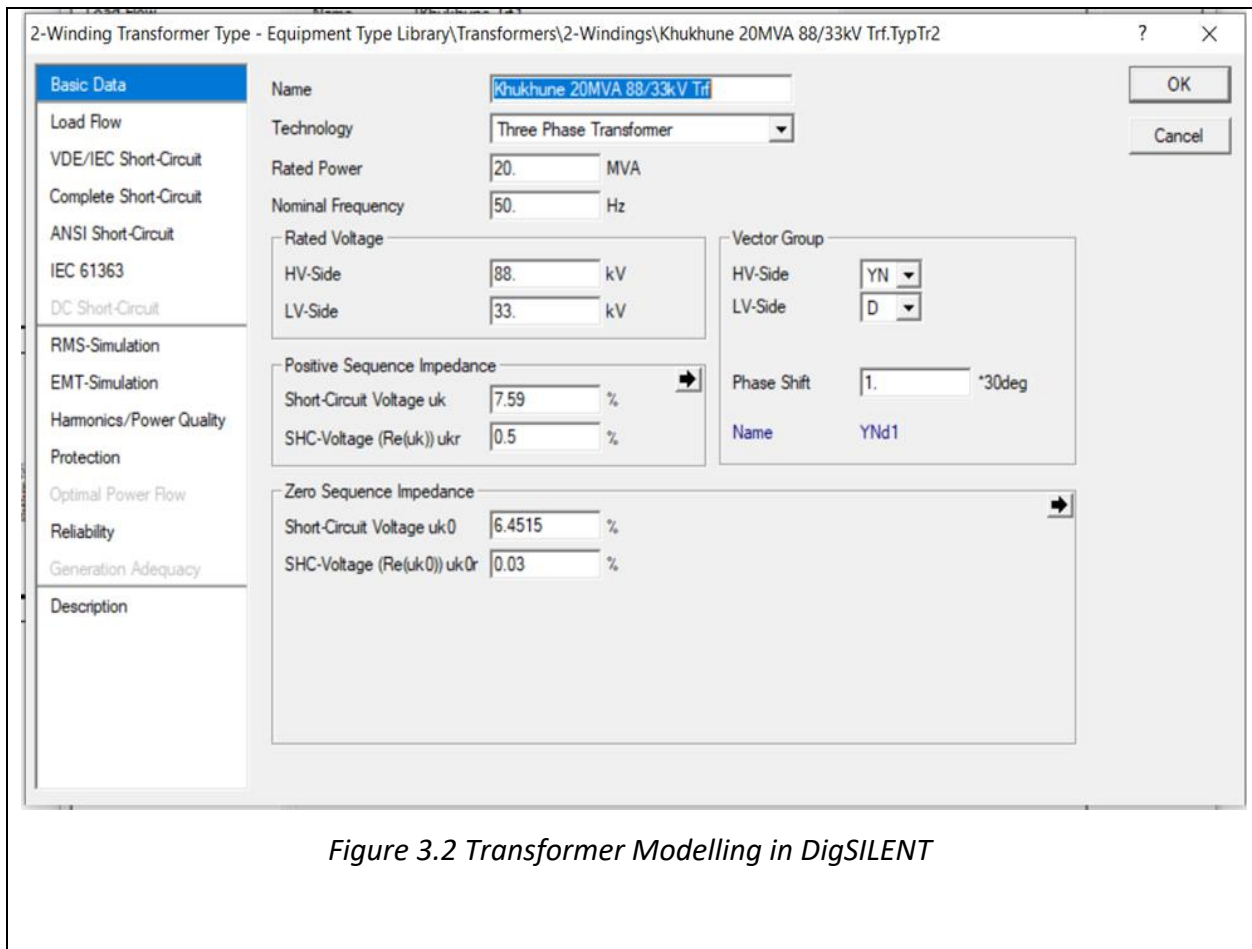
The transformers were modelled using the 3-phase winding transformer model. The transformer data such as the transformer rating, vector group, voltage tap and the zero crossing sequence short circuit settings were captured into DigSILENT LEC model.

3.1.2 Load Modelling

The load was modelled using the static load model which does not model the voltage dependency of the load. The voltage dependent load is modelled as:

$$P = P_o \left(\frac{V}{V_o}\right)^a \tag{28}$$

$$Q = Q_o \left(\frac{V}{V_o}\right)^b \tag{29}$$

where P and Q represent the active and the reactive power respectively. P_0 and Q_0 represent reference active and reactive power respectively.

The voltage V_0 represent the nominal voltage at the load terminals while V represent the instantaneous voltage. The exponent a and b hold values 0, 1, 2 representing the constant power, current and impedance respectively [54]. For the study the constant power model which assumes 0 for exponent a and b was used. Figure 3.3 shows how the load parameters were captured into DigSILENT.
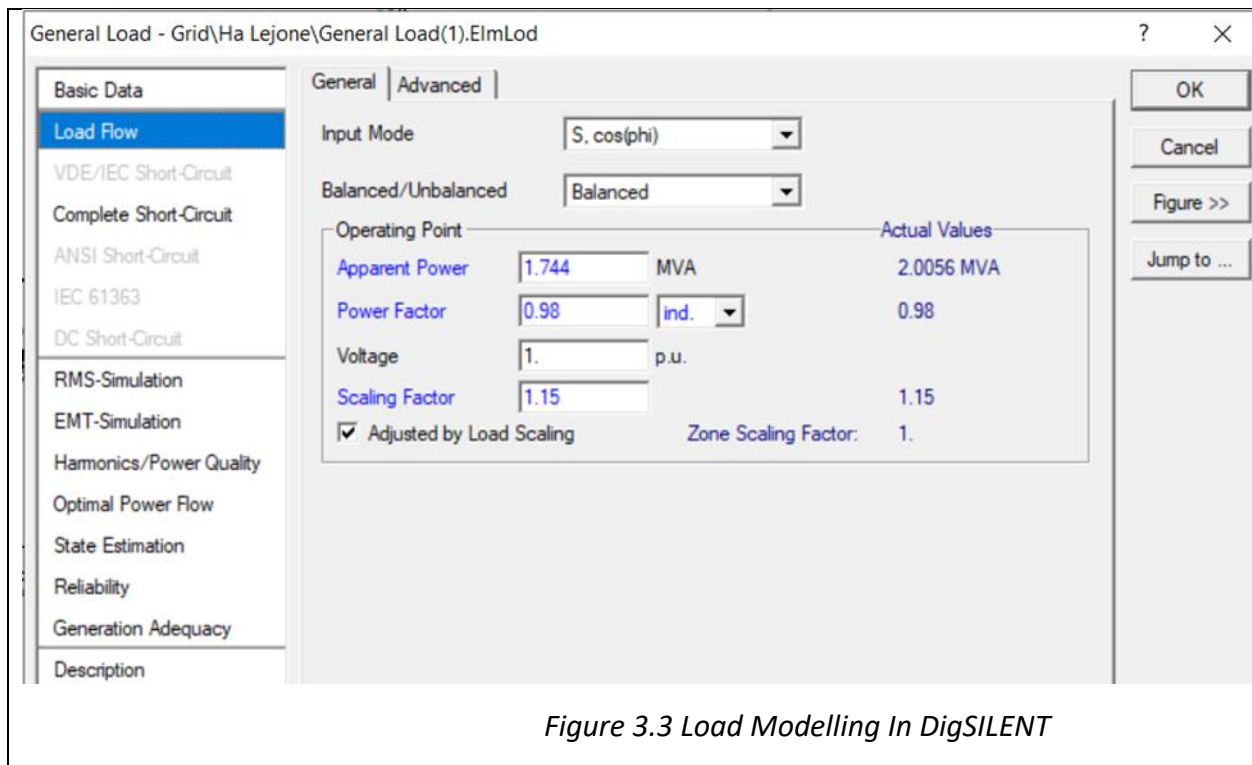
Figure 3.3 Load Modelling In DigSILENT

3.1.3 Transmission Line Modelling

The transmission lines were modelled based on the lumped parameter line model. Basic data such as the number of parallel lines, line length and voltage rating of the lines were inputted into LEC DigSILENT model. The data for the transmission parameters were provided by LEC. Figure 3.4 indicate how the transmission line parameters were captured into LEC electrical DigSILENT model.

Figure 3.4 Transmission Line Modelling in DigSILENT

3.1.4 Hydro Power Generator Modelling
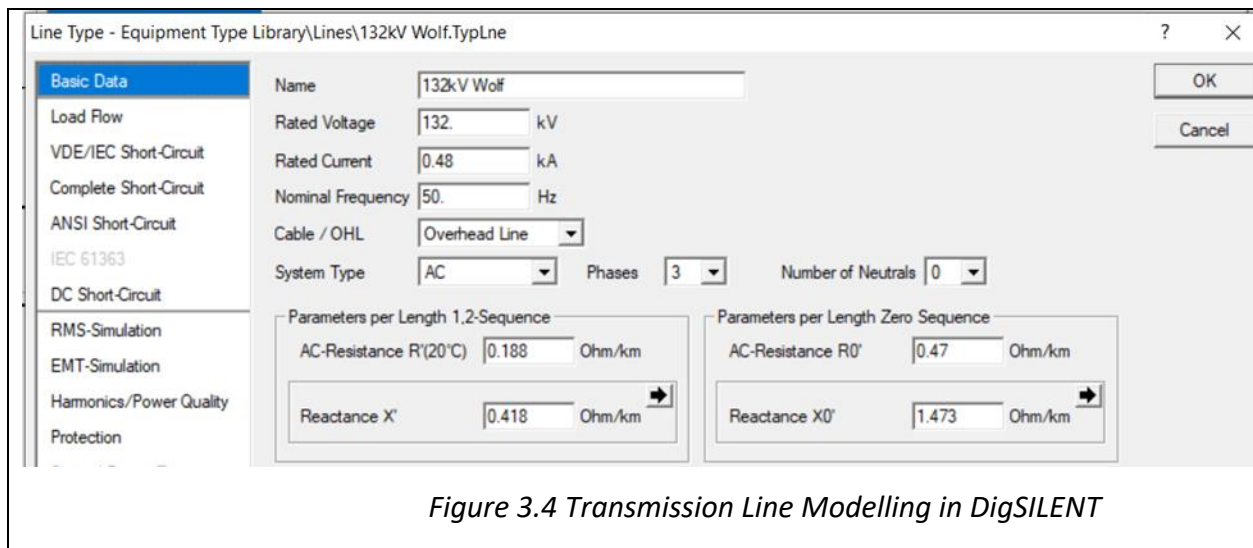
Figure 3.5 Hydro Power Generator Modelling in DigSILENT
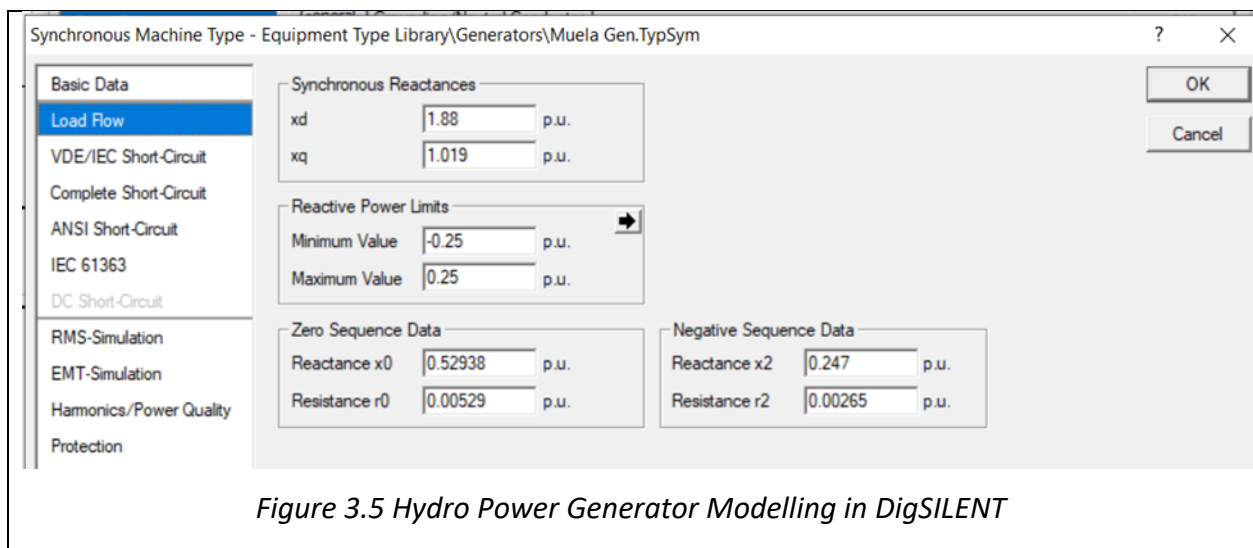
The hydro power station was modelled using the synchronous generator. The machine parameters such the power rating, stator resistance, synchronous reactance and sub-transient reactance were captured as shown in Figure 3.5.

3.1.5 Intermittent Renewable Energy Generators (IREGs)

Solar PV farm was modeled using the DigSILENT aggregated model with the capacity of 0.5 MW and the power factor of 0.95. The 0.5 MW solar PV system were connected in parallel to model the required solar PV capacity under consideration. Figure 3.6 depicts the main block diagram showing how the PV panel model is constructed.
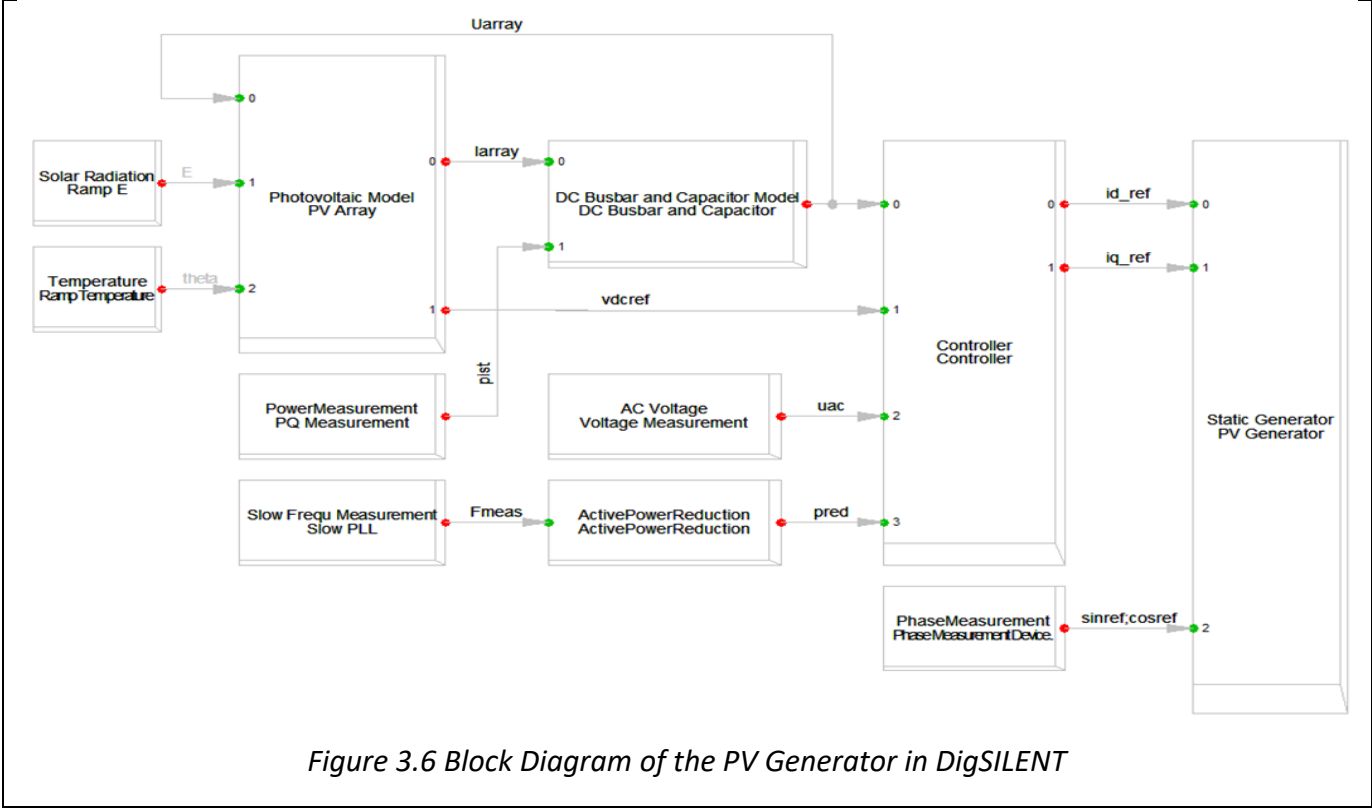
Figure 3.6 Block Diagram of the PV Generator in DigSILENT

The model consists of four main blocks namely the photovoltaic, DC-link, controller and the inverter blocks. The inverter is modelled as the static generator and interfaces with the grid. The photovoltaic model represent the number PV modules connected in parallel and in series to form the solar PV array. The DC-link implements the maximum power point tracking (MPPT) algorithm.

The controller maintains the control for the PV system ensuring that the voltage and power at the point of interconnect is maintained.

The wind farm was modelled from the 2MW DFIG DigSILENT model with the power factor of 0.9. The 2 MW DFIG were connected in parallel to model the desired wind farm capacity. Figure 3.7 depicts the wind model with its functional block diagram.

Figure 3.7 Block Diagram of the DFIG in DigSILENT
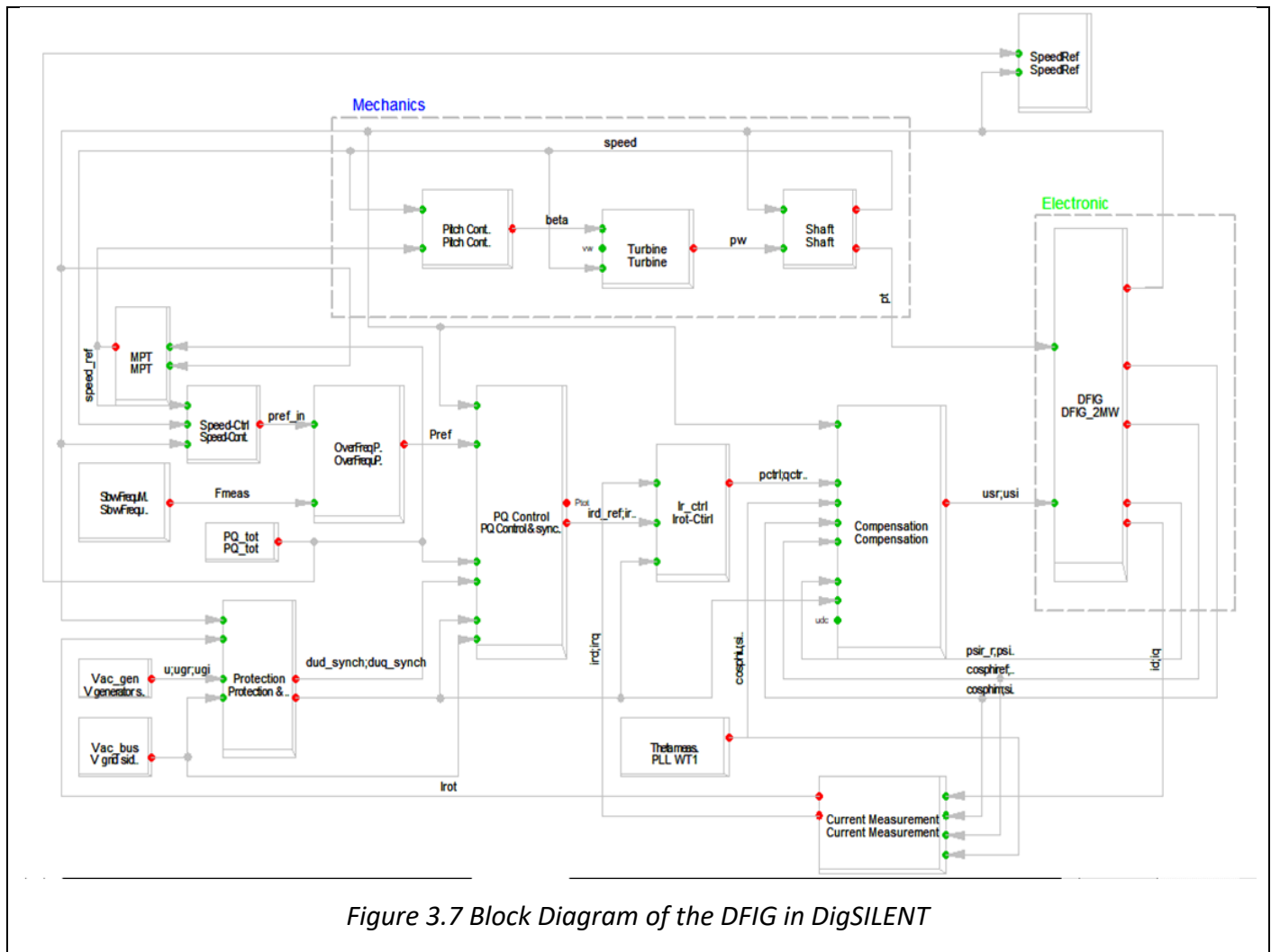
The wind turbine generator model comprises of the wind model, mechanical model (rotor, shaft and gear box)), the generator model and the controls (PQ control, frequency control, ect). The rotor blades transform wind speed to the mechanical power that drives the shaft which is connected to the generator via the gear box. The generator is modelled as the doubly feed

induction generator (DFIG) while the controls ensure that the wind turbine operates within safety limits.

Figure 3.8 and Figure 3.9 present the simplified grid for the proposed sites where the solar PV farm and the wind farm will be integrated to the grid and with the neighboring substations. The proposed site for the solar farm and wind farm are Ramarothole and Letseng respectively. The neighboring substations serve as the important points to consider as they are closed to the IREGs hence affected more by the IREGs integration. The other point that was considered is the hydropower substation as it is the main synchronous generator for the electrical network.

Figure 3.8 Simplified Grid for PV Integration

Figure 3.9 Simplified Grid for Wind Integration
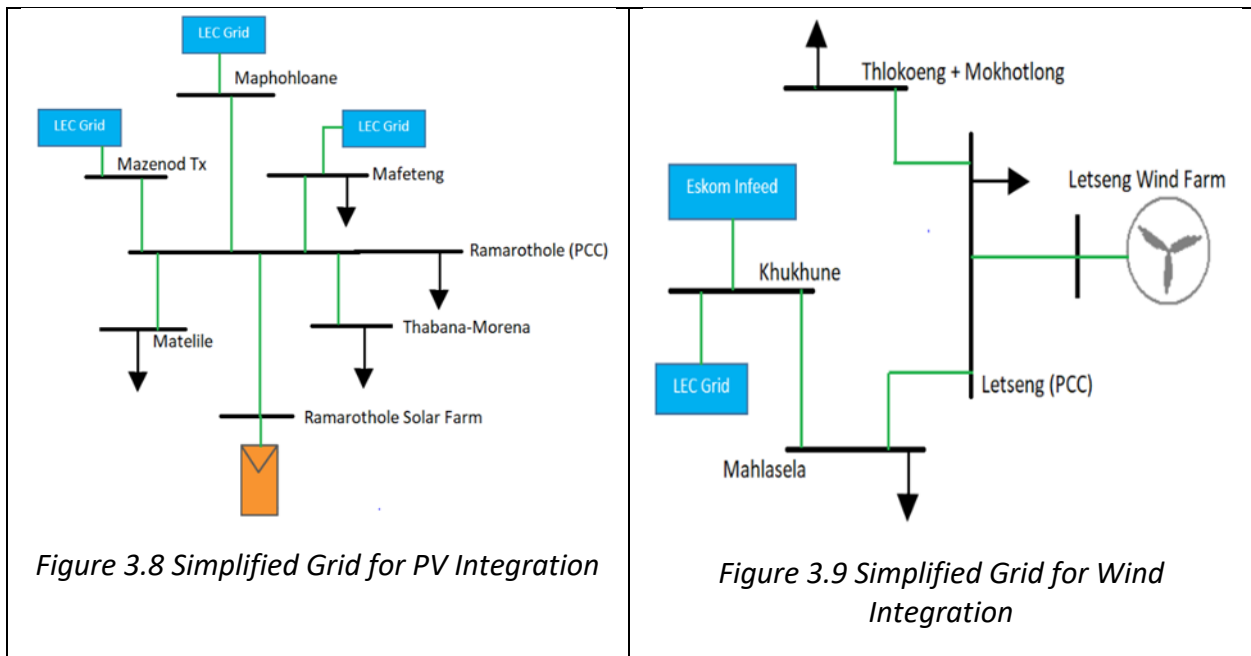
3.2 Dynamic Stability Studies

The stability studies were conducted by performing the load flow under different penetration levels of the scenarios presented in section 3.1. For each case, the penetration levels were increased until grid code was violated. In addition to the load flow analysis, the network was scanned for most stressed point with the least critical clearing time since it results in the worst system stability after the fault 3-phase short circuit was applied to it. Critical clearing time mainly

evaluates the electrical network based on the rotor angle stability, but the transient voltage and frequency could also be evaluated too. The CCT had been used to evaluate the impact of the renewable generators in the following references [56], [58], [111]. The stability studies were performed on the electrical network with the total load of 185.71 MW. The penetration levels for three different scenarios are presented in Table 4. Table 5 and Table 6 show the voltage and frequency limits for Lesotho grid code.

Table 4 Penetrations level for different scenarios

Solar PV (MW)	Wind (MW)	Hybrid (Solar PV (MW) + Wind (MW))	
		Solar + Wind	Solar +Wind
20	30	35 + 30	20 + 50
30	40	35 + 40	30 + 50
36	52	35 + 52	36 +50

Table 5 Grid code voltage levels limits

Normal Conditions			Emergency Conditions	
Normal Voltage (kV)	Maximum (kV)	Minimum (kV)	Maximum (kV)	Minimum (kV)
132	138.6	125.4	145	118.8
88	92.6	83.6	96.8	79.2
66	69.3	59.4	72.5	56.1
33	34.7	31.4	36.3	29.7

Table 6 Grid code frequency limits

Nominal	50
Upper Limit	50.5
Lower Limit	49.5

3.3 Steady State (Quasi-Dynamic) Simulation

The steady state was considered so that impact of the hourly variations of the IREGs is considered. To model the steady performance of the LEC network, the hourly voltage performance of the network was considered. The steady state was performed according to Figure 3.10 based on the yearly load of 2018 and the hydro generation of 2018.

Figure 3.10 Flow chart for the steady state analysis
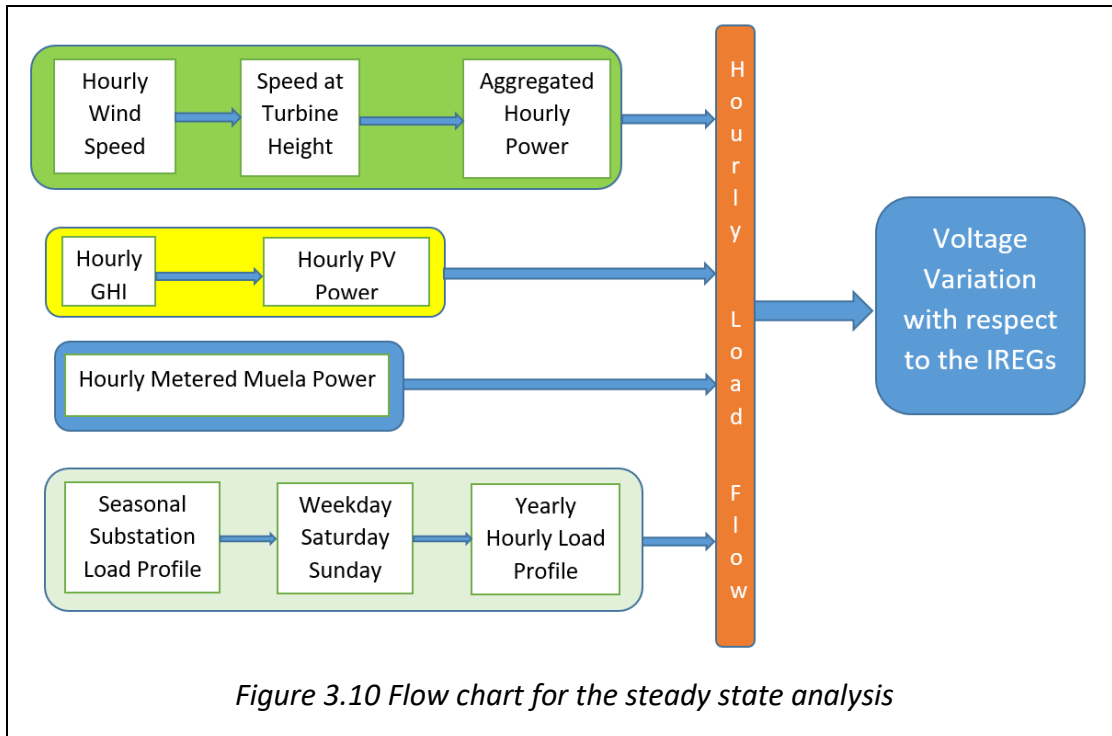
The 30-minute load from the substations was transformed into the hourly load for the week day, Sunday and Saturday. In addition, the load from the substations were categorized into seasonal loads where summer1 represent the load from January to April, winter loads represent the load from May to August and summer2 was represented by the loads September to December. Figure 3.10 represent the scaled load from different substations. From Figure 3.11 it can be seen that the hourly load varies differently for each substation, hence necessary to consider each substation load. Then the yearly load profile for each substation was constructed on the hourly bases.
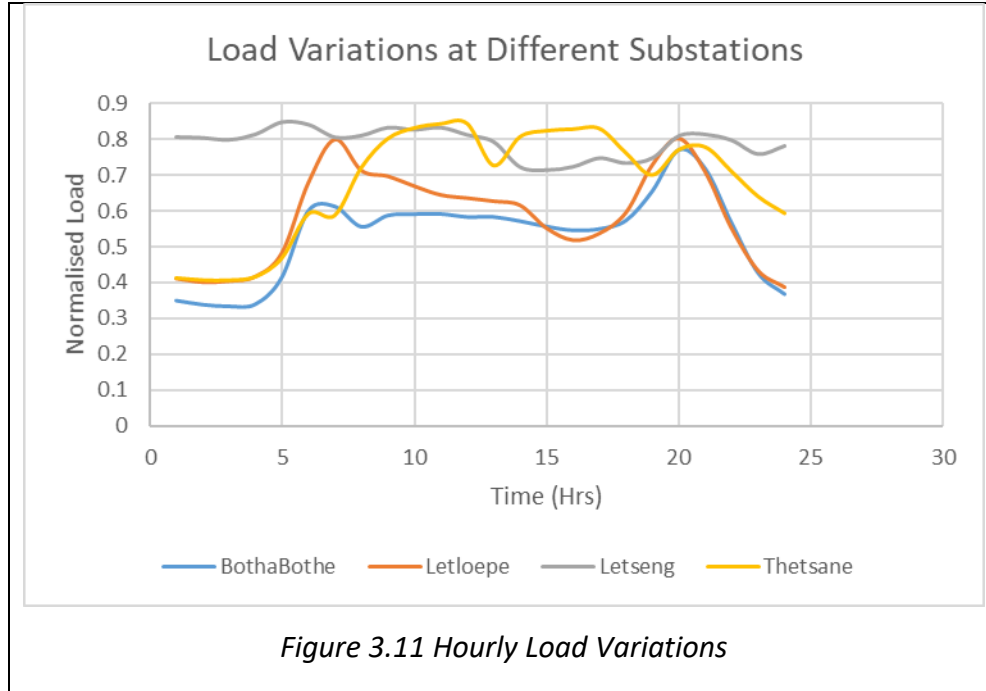
Figure 3.11 Hourly Load Variations

The hourly power from the wind turbine was obtained by using the power curve of the Vestas V80 DFIG wind turbine. The hourly wind speeds at Letseng were obtained from the measured wind speed at the interval of 10 minutes at hub height of 50 m. The power from the wind turbine (P_t) was found from equation 30

$$P_t = \begin{cases} 0: & V_w < V_{cutin}; \ and \ V_w > V_{cutoff} \\ P_{out:} & V_{cutin} < V_w < V_{rated} \\ P_{rated:} & V_{rated} < V_w < V_{cutoff} \end{cases} \tag{30}$$

where P_{out} is the power of the turbine between cut-in wind speed (V_{cutin}) and the rated wind speed (V_{rated}) of the wind turbine. V_w and V_{cutoff} represent the wind speed at the turbine height (H) and the cutoff wind speed of the turbine. The wind speed at the turbine height was obtained using the power rule equation such that:

$$V_w = V_{wr} \left(\frac{H}{H_r}\right)^{1/7} \tag{31}$$

55

where V_{wr} represent the wind speed at the reference height (50 m). The height H and H_r represent turbine height and the reference height at which the wind speed was measured respectively. The total power ($P_{windfarm}$) from the wind farm was obtained as

$$P_{windfarm} = \sum_{n=1}^{N} P_{t\_n} \tag{32}$$

where N represent total number of the wind turbines connected in parallel.

The hourly output power for hourly PV output was calculated based on the solar radiation downloaded from PVGIS website [112]. The hourly output from the solar farm was calculated as

$$P_{pv} = \frac{\eta_{pv}}{\eta_{STC}} \frac{G_t}{G_{STC}} P_{rated} \tag{33}$$

where η_{pv} and η_{STC} are the solar PV array efficiency under operation conditions and standard test conditions (STC) respectively. Incident radiation on the solar array at operating conditions and at standard test conditions is represented as G_t and G_{STC} respectively. Capacity of the solar farm is represented as P_{rated}. The array efficiency and the incident radiation on are calculated based on the model developed by Hove et al [113].

4 Results and Discussions

4.1 Critical Clearing Time Results

Table 7 shows the how critical clearing time varies as the penetration level of the wind and solar vary after the fault is applied to the different buses. The clearing times considered were the least from different bus categories. The comparative outlook of the results shows that the rotor angle stability was compromised as the penetration of the solar PV farm generation increases while wind farm does not affect the rotor angle stability, as the critical clearing time remains constant as the wind generation increases.

Table 7 Critical Clearing Times for solar PV and wind generation with different penetrations

Substation	No RE	Solar Generation CCT (sec)			Wind Generation CCT (sec)		
		20MW	30MW	36MW	30MW	40MW	50MW
Mabote 132kV	0.18	0.13	0.08	0.02	0.18	0.18	0.18
Muela 132kV	0.19	0.17	0.14	0.04	0.19	0.19	0.19
Mazenod Tx 132kV	0.19	0.14	0.09	0.03	0.19	0.19	0.19
Ramarothole 132kV	0.71	0.4	0.24	0.05	0.71	0.71	0.71
Khukhune 88kV	6.9	2.41	1.27	0.24	6.9	6.9	6.9
Letseng 88kV	>20	>20	>20	>20	>20	>20	>20
Katse Intake 66kV	3.82	1.9	1.05	0.2	3.82	3.82	3.82
Matsoku 66kV	4.81	2.56	1.38	0.26	4.81	4.81	4.81
Botshabelo 33kV	0.78	0.44	0.26	0.08	0.78	0.78	0.78
Mazenod Dx 33kV	0.49	0.28	0.16	0.04	0.49	0.49	0.49

Interestingly the results indicate that the high voltage bus bars (132kV) have the least critical clearing times. This suggest that the fault at these buses destabilizes the grid most when subjected to the fault. Based on the observation the Mabote bus bar was considered the most stressed point, the 3-phase short circuit was applied at it as the frequency, and voltage responses for other critical points were observed. The other points of consideration were point of common coupling (where the wind and solar are connected to the grid) and the neighbouring buses as they are affected more due to their proximity wind and solar farms. To further investigate the impact of increased penetration of IREGs time based simulations were performed.

4.2 Solar PV Case

4.2.1 Voltage Stability for the solar PV Case

Figure 4.1 Voltage response at the critical bus bars after the fault is applied at Mabote with different penetration levels of solar PV

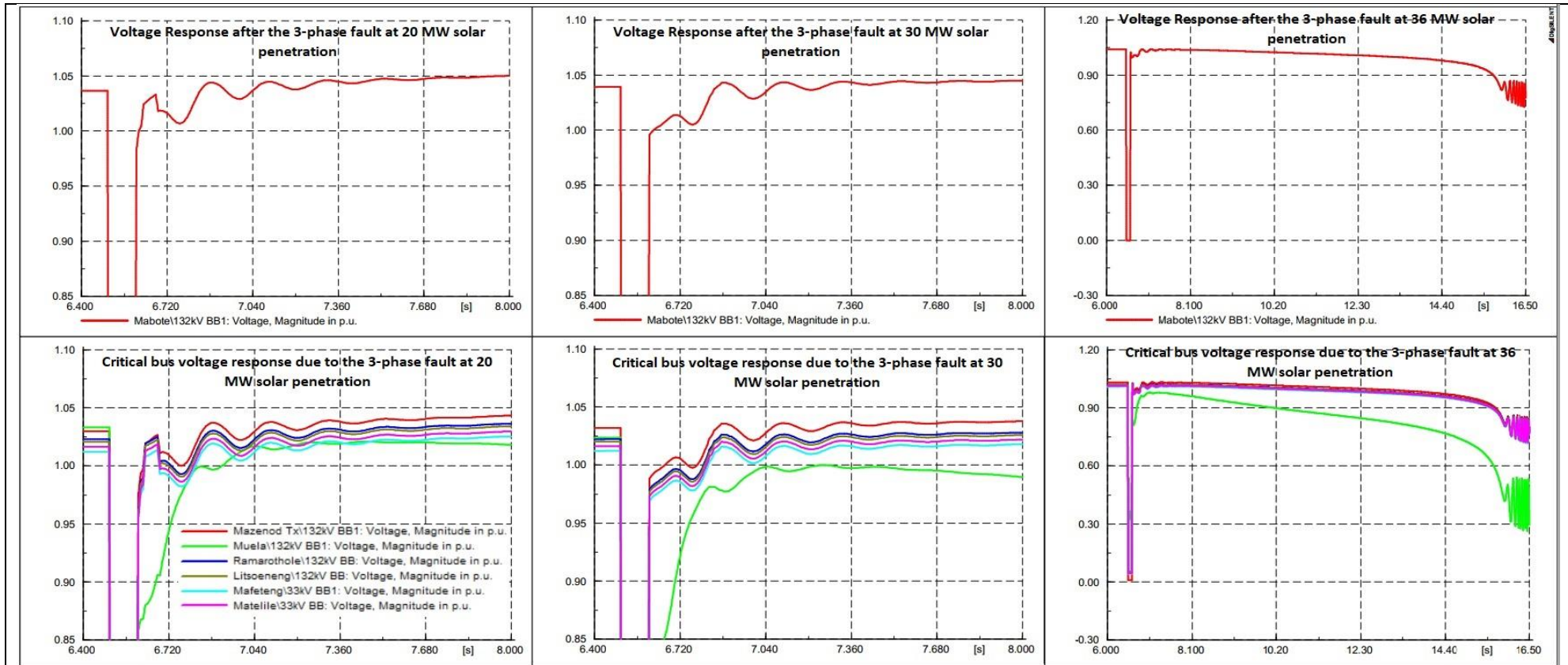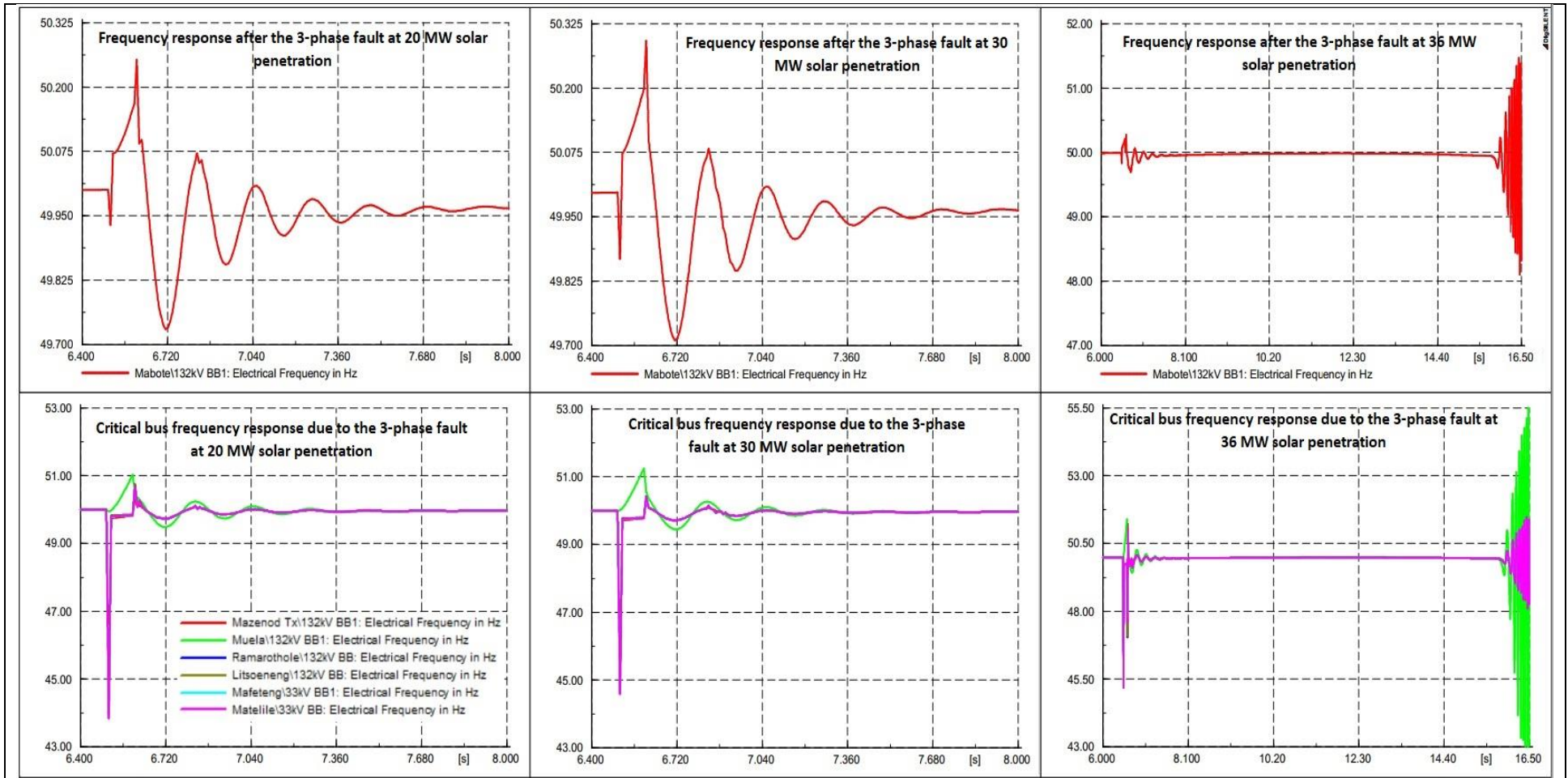### 4.2.2 Frequency Stability for the solar PV case

Figure 4.2 Frequency response at critical bus bars after the fault is applied at Mabote with different penetration levels of solar PV

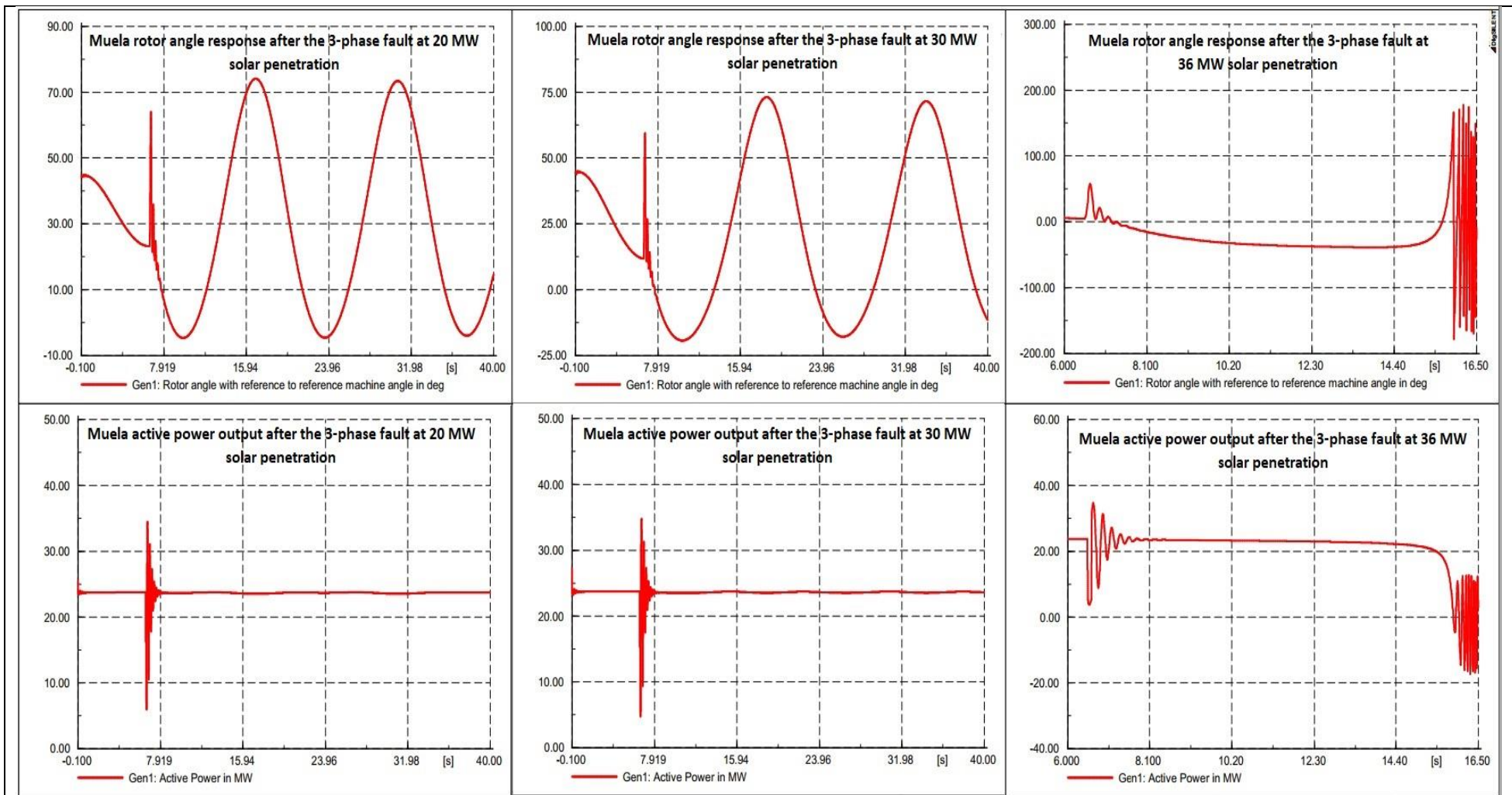### 4.2.3 Rotor Angle Stability for the Solar PV Case

Figure 4.3 Rotor angle and real power response of synchronous generator at Muela due to the fault at Mabote with solar PV at different penetration levels

Figure 4.1 to Figure 4.3 show how the voltage, frequency and rotor angle varies after the 0.1 seconds 3-phase short circuit was applied at bus with the lowest critical clearing time (Mabote) at different penetration levels. From Figure 4.1, it is observed that at penetration levels of 20 MW and 30 MW, the voltage were within the allowed limits and the network was able to recover from the fault as the voltages were damped to the stable limits. Comparing the voltage steady state voltages before and after the fault it is seen that the Muela voltage has reduced to 1.017 p.u. compared to that of 1.03 p.u. before the fault at penetration level of 20 MW. At penetration of 30 MW it is observed that the voltage has dropped further to 0.98 p.u. This suggest that increased penetration of solar PV farm results in the worsening voltage stability as the voltage at Muela is reduced. The rest of the nearby substations oscillations were within the required voltage limits. However, at the penetration level of 36 MW the voltage limit was violated, as the voltage at the critical buses did not return to the allowable steady state limits. The most affected substation was Muela, which shows the worst deviation from the nominal voltage limits.

Figure 4.2 indicates how the frequency at the faulted bus bar and critical bus bars varies as the penetration of the solar PV integration is increased. As the solar PV penetration increased, the oscillations for the first swing were almost equal with the magnitude of 51.027 Hz and 49.486 Hz for the penetration of 20 MW and 51.244 Hz and 49.445 Hz for the 30 MW penetration at Muela. The other critical points had the same response with the highest frequency of 50.749 Hz and 43.837 Hz at 20 MW and 50.416 Hz and 44.586 Hz. In both 20 MW and 30 MW penetrations the oscillations were quickly dumped to the nominal frequency indicating that increased penetrations are not the main contributors to frequency instability. For both 20 MW and 30 MW penetrations, frequency stability was observed. At the penetration, level of 36 MW the frequency stability was violated, as the frequency was initially almost constant but went out of permissible limits after about 15 seconds with Muela exhibiting the highest oscillations.

Figure 4.3 depicts how the rotor angle and the active power at the synchronous generator varies with varying penetrations levels for the solar PV integration. At penetration levels of 20 MW and 30 MW the rotor angle stability was observed, as the output power was constant after the fault even though rotor angle was oscillatory. Comparing the oscillations at 20 MW and 30 MW penetration, it is observed that the oscillations were increasing as the solar PV integration was

increased from 20 MW to 30 MW. The oscillations were between -4.65^0 to 74.05^0 at 20 MW penetration and -19.27^0 to 73.06^0 at 30 MW penetration. At 36 MW the rotor angle stability was violated and the active power at Muela hydropower collapsed. From Figure 4.1 to Figure 4.3, it could be concluded that the penetration level of 36 MW leads to voltage, frequency and rotor angle instability hence the maximum allowable limit for solar PV at Ramarothole must be less than 36 MW. Furthermore, the rotor angle was varying most as the penetration levels increased and this suggest the high penetrations of PV affect rotor angle more than frequency and voltage stability.

4.3 Wind Case

4.3.1 Voltage Stability for the Wind Case

Figure 4.4 Voltage response at critical bus bars after the fault is applied at Mabote with different penetration levels of wind power
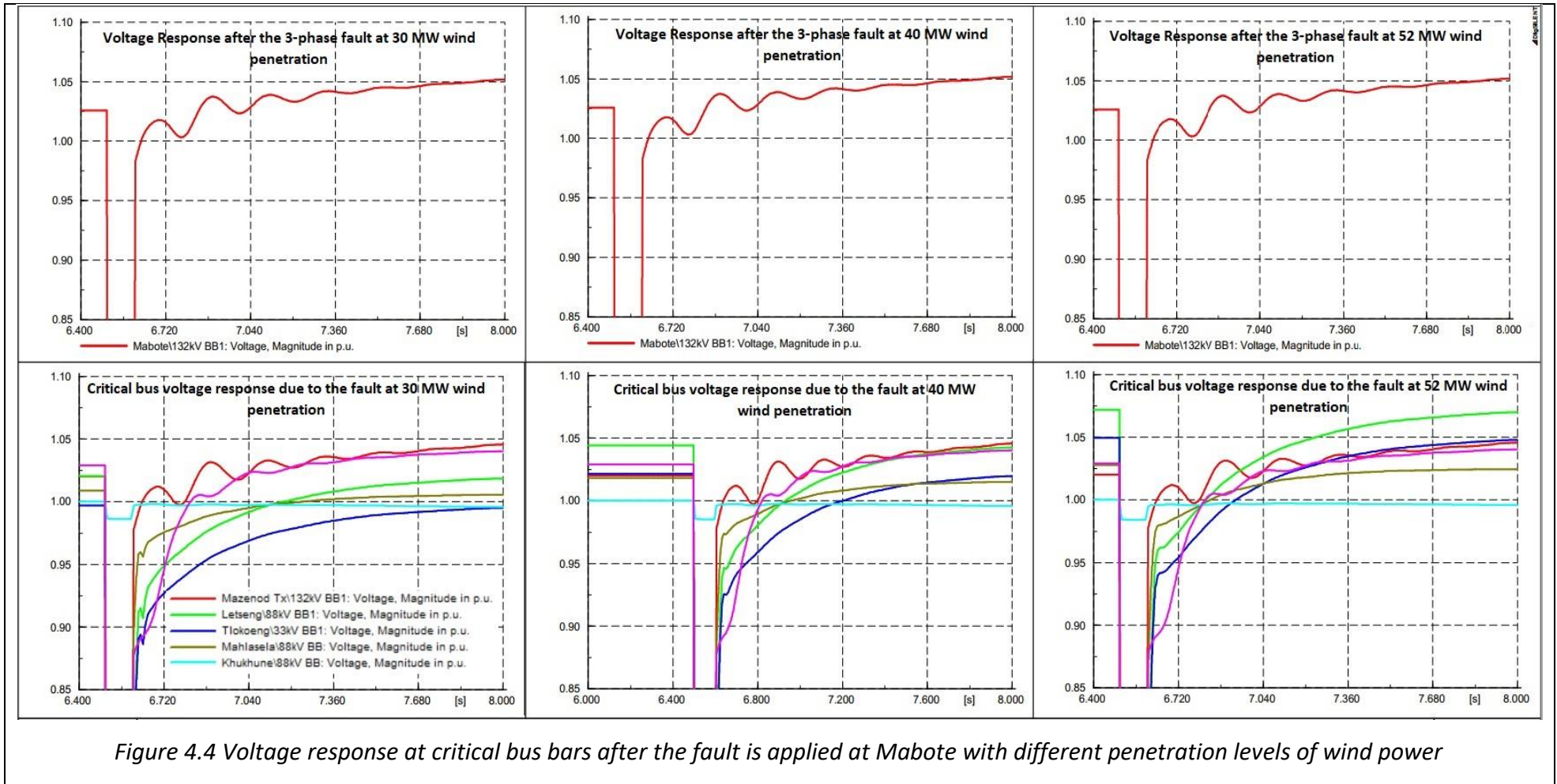
4.3.2 Frequency Stability for the Wind Case

Figure 4.5 Frequency response at critical bus bars after the fault is applied at Mabote with different penetration levels of wind power

4.3.3 Rotor Angle Stability for the Wind Case

Figure 4.6 Rotor angle and real power response of synchronous generator at Muela due to the fault at Mabote with wind farm at different penetration levels

Figure 4.4 to Figure 4.6 depicts how voltage, frequency and the rotor angle varies after the 0.1 seconds 3-phase short circuit is applied to the Mabote substation under different wind power generation penetrations levels. From Figure 4.4, it is seen that after the fault the voltage quickly settles to the constant voltage levels without overshooting. In addition, the only nearby substations (Letseng, Tlokoeng and Mahlasela) were affected by the fault while Khukhune was less affected by the fault. Taking a closer look at Table 8 the voltage levels of the affected substations keeps on increasing as the penetration level of the wind generators increase.

Table 8 Voltage levels as penetration increases at Letseng

Penetration (MW)	Letseng p.u	Tlokoeng p.u.	Mahlasela p.u.
30	1.02	0.99	1
40	1.045	1.021	1.02
52	1.07	1.051	1.02

At the penetration level of 52 MW the steady state voltage at the Tlokoeng substation, was greater than 1.05 p.u. which is stipulated as the limit under the grid code of Lesotho. From this, it is concluded that under the current operating conditions the 52 MW penetration cannot be exceeded as it violates the grid code.

The frequency response due the fault is shown in Figure 4.5. As the penetrations levels were increased, frequency undershoot also increased showing some small oscillations. The frequency undershot was 49.644 Hz, 48.498 Hz and 48.358 Hz at the penetration levels of 30 MW, 40 MW and 52 MW respectively for Letseng and Tlokoeng. The frequency perturbations were severe at the nearby substations (Letseng, Tlokoeng and Mahlasela) while Khukhune experienced very small frequency disturbance. This suggest that the increasing penetration of the wind generation does not result in severe frequency instability as the oscillations were quickly dumped to the allowable frequency limits.

Figure 4.6 displays the rotor angle response of the Muela synchronous generator before and after the fault was applied at Mabote substation. From all different penetrations levels of wind farm, the rotor angle stability was observed as the output power from the generators remained constant. The oscillations had the highest overshoot of 84.69^0 and the lowest undershoot of 9.04^0. Contrary to the solar farm generation the where increased penetration results in worsened rotor angle stability the wind farm generation does not lead to increased rotor angle instability as the penetrations increase.

4.4 Hybrid Case (Wind and Solar)

4.4.1 Voltage Stability Hybrid Case Wind Variations

Figure 4.7 Voltage response at critical bus bars after the fault is applied at Mabote with different penetration levels for hybrid case (wind variation)
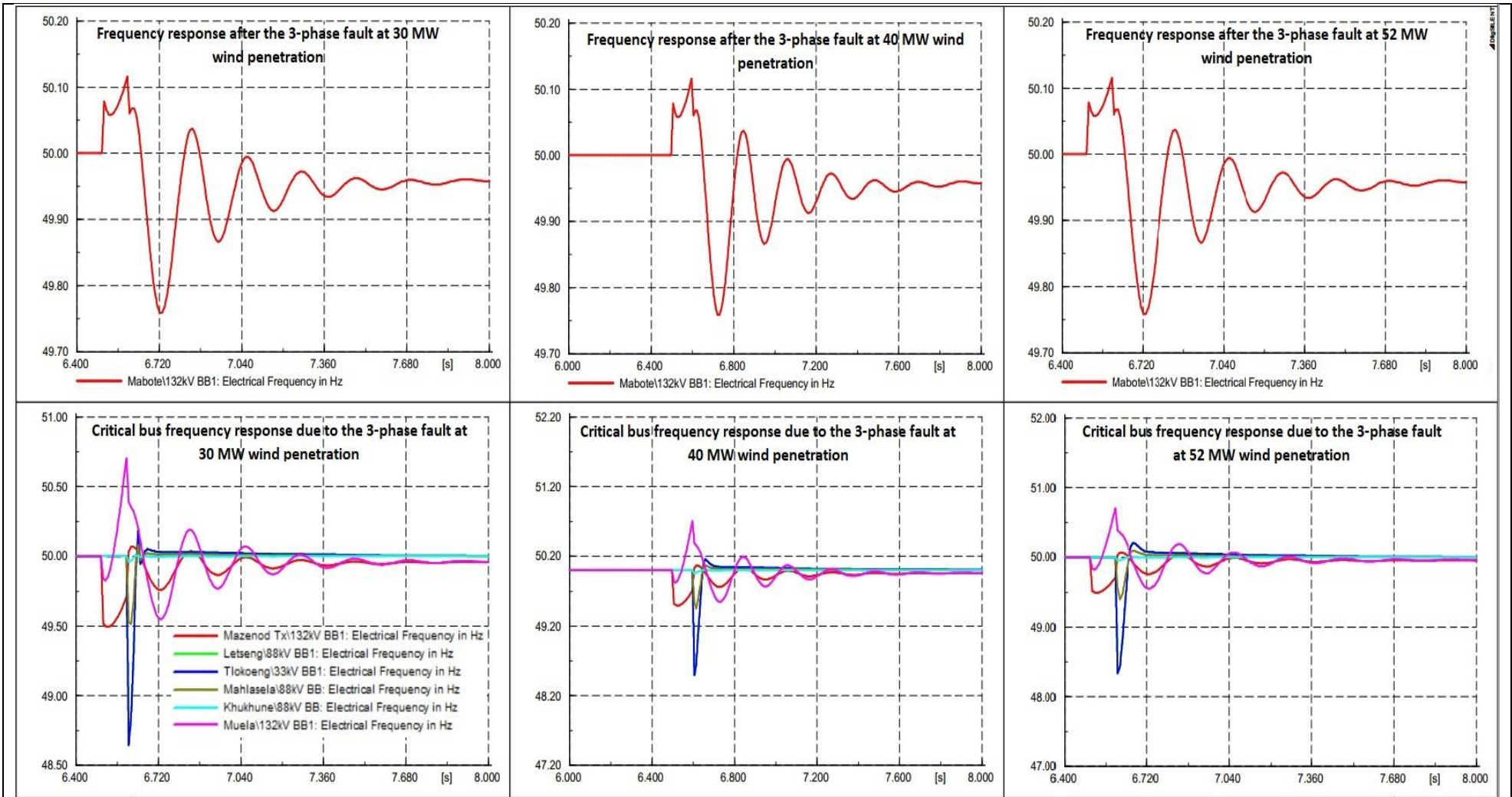
4.4.2 Frequency Stability Hybrid Case Wind Variations

Figure 4.8 Frequency response at critical bus bars after the fault is applied at Mabote with different penetration levels for hybrid case (wind variation)
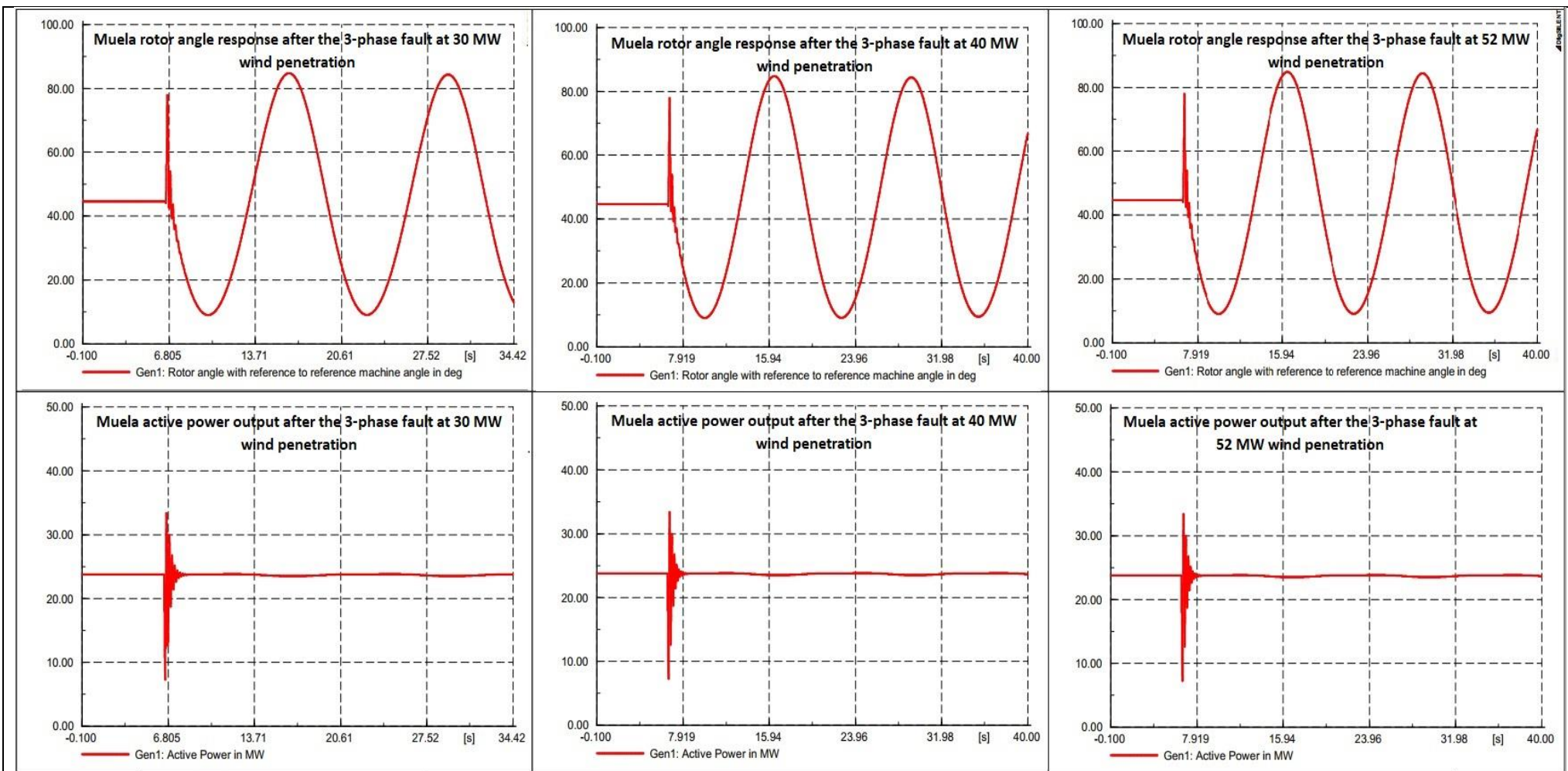
4.4.3   Rotor Angle Stability Hybrid Case Wind Variations

Figure 4.9 Rotor angle and real power response of synchronous generator at Muela due to the fault at Mabote with different penetration levels for hybrid case (wind variations)

Figure 4.7 through Figure 4.9 represents the response of the voltage, frequency and the rotor angle due to the 0.1 seconds 3-phase short circuit faults applied at Mabote substation for the hybrid system build from 35 MW solar farm and the wind farm for different penetration levels. The wind generation capacity was varied from 30 MW to 52 MW. For the hybrid system, both critical points for wind farm and solar PV were considered. Figure 4.7 shows the voltage response after the faults is applied. The voltage levels for the point of common coupling (Letseng) and the Tlokoeng substation remain almost unchanged before, during and after the fault. As in the case for the wind generation, the substations closest to the wind farm experienced increased steady state voltage levels as the wind generation increased. Comparative outlook between the wind only results and the hybrid system (wind variation) indicates that the voltage levels were the same for both cases as in Table 8 but for the hybrid they were maintained during and after the fault. This suggest that the 52 MW wind generation penetration remains the limit for both wind only and hybrid configurations. The voltage levels were as in Table 8 indicating that the solar PV does not contribute to voltage instability at Letseng or increased levels of wind penetrations.

Frequency response of the hybrid system when the fault is applied at the Mabote is shown in Figure 4.8. For the hybrid system with varying wind penetration the frequency at Letseng and Tlokoeng was not perturbed by the fault. The frequency at the Ramarothole (solar farm PCC) and other critical points (except Muela) had the same frequency response with the undershoot of 45.037 Hz for all wind penetration. The frequency at Muela had an overshoot of 51.363 Hz for all penetrations. These observation reveals that under hybrid systems with increasing wind penetration does not result in main frequency instability as the oscillations were always dumped and within allowable limits.

Figure 4.9 displays the rotor angle response after the fault at Mabote substation. In all the penetrations levels of the hybrid system the rotor angle oscillating between -32.299^0 and 70.52^0 while the active power of the synchronous generator was almost constant. Comparing the rotor angle variations with the wind only case, the results show that for the hybrid system the oscillations amplitude was increased. The increased oscillations are attributed the presence of the solar PV farm generation.

71

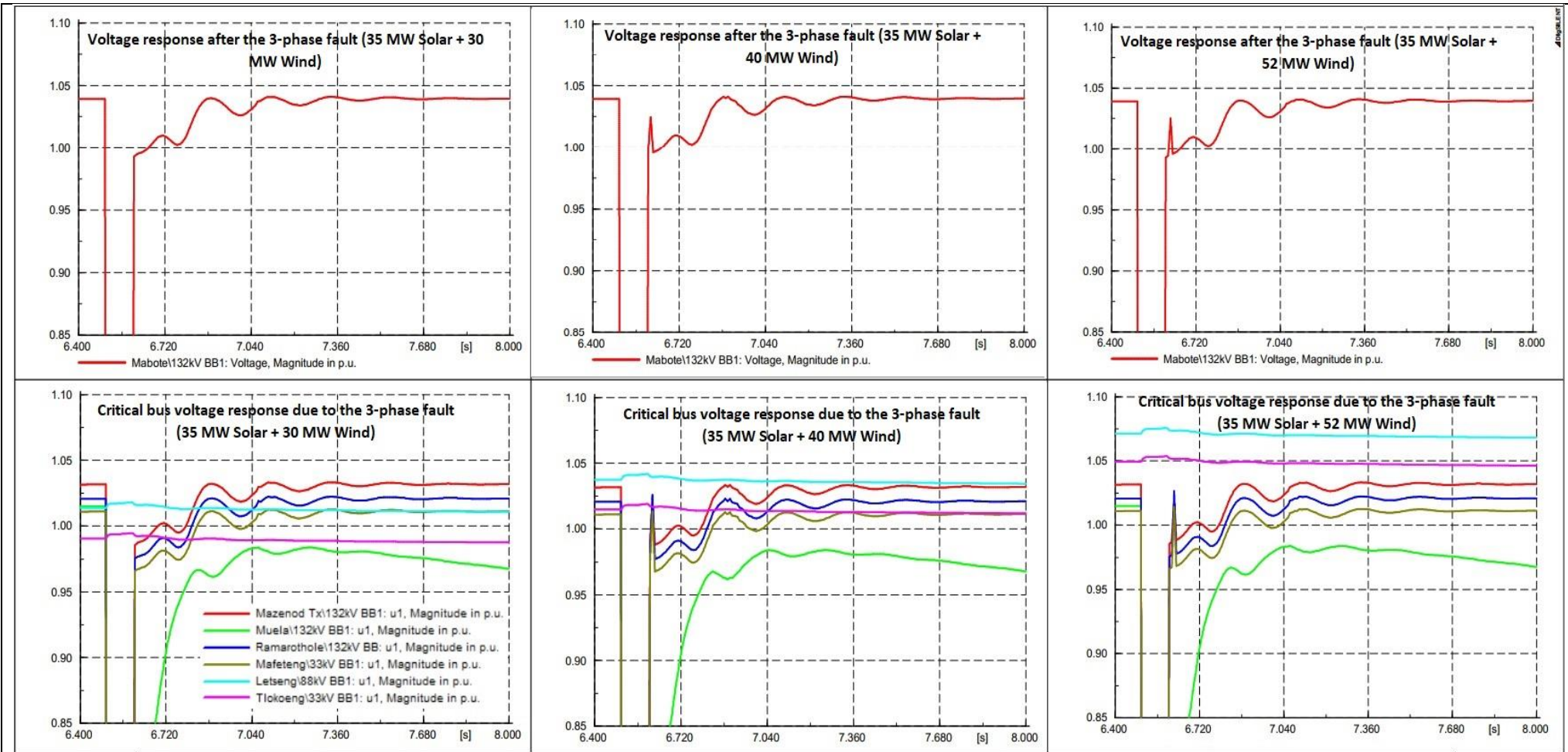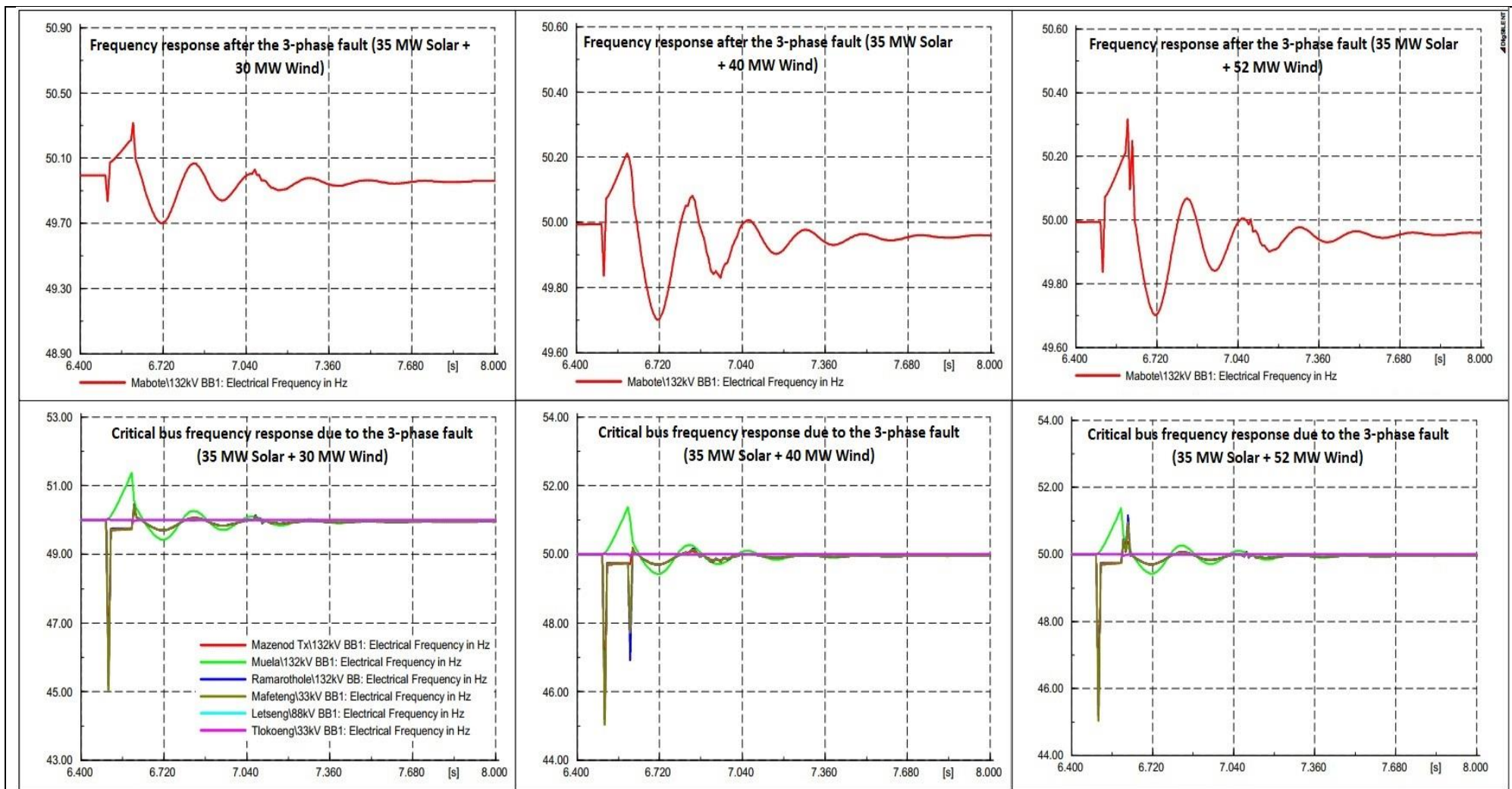### 4.4.4 Voltage Stability Hybrid Case Solar Variations

Figure 4.10 Voltage response at critical bus bars after the fault is applied at Mabote with different penetration levels for hybrid case (solar variation)

4.4.5   Frequency Stability Hybrid Case Solar Variation

Figure 4.11 Frequency response at critical bus bars after the fault is applied at Mabote with different penetration levels for hybrid case (solar variation)

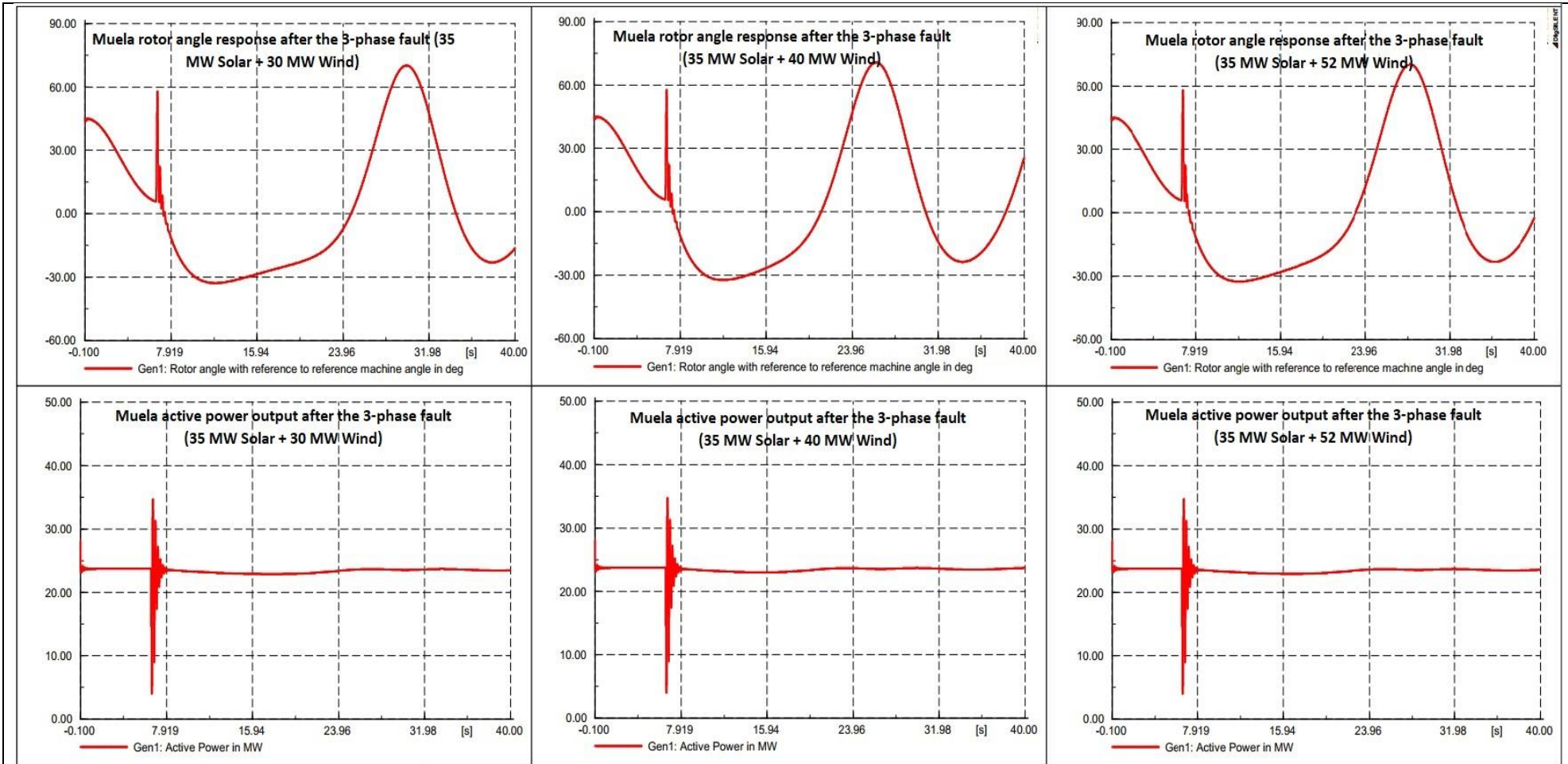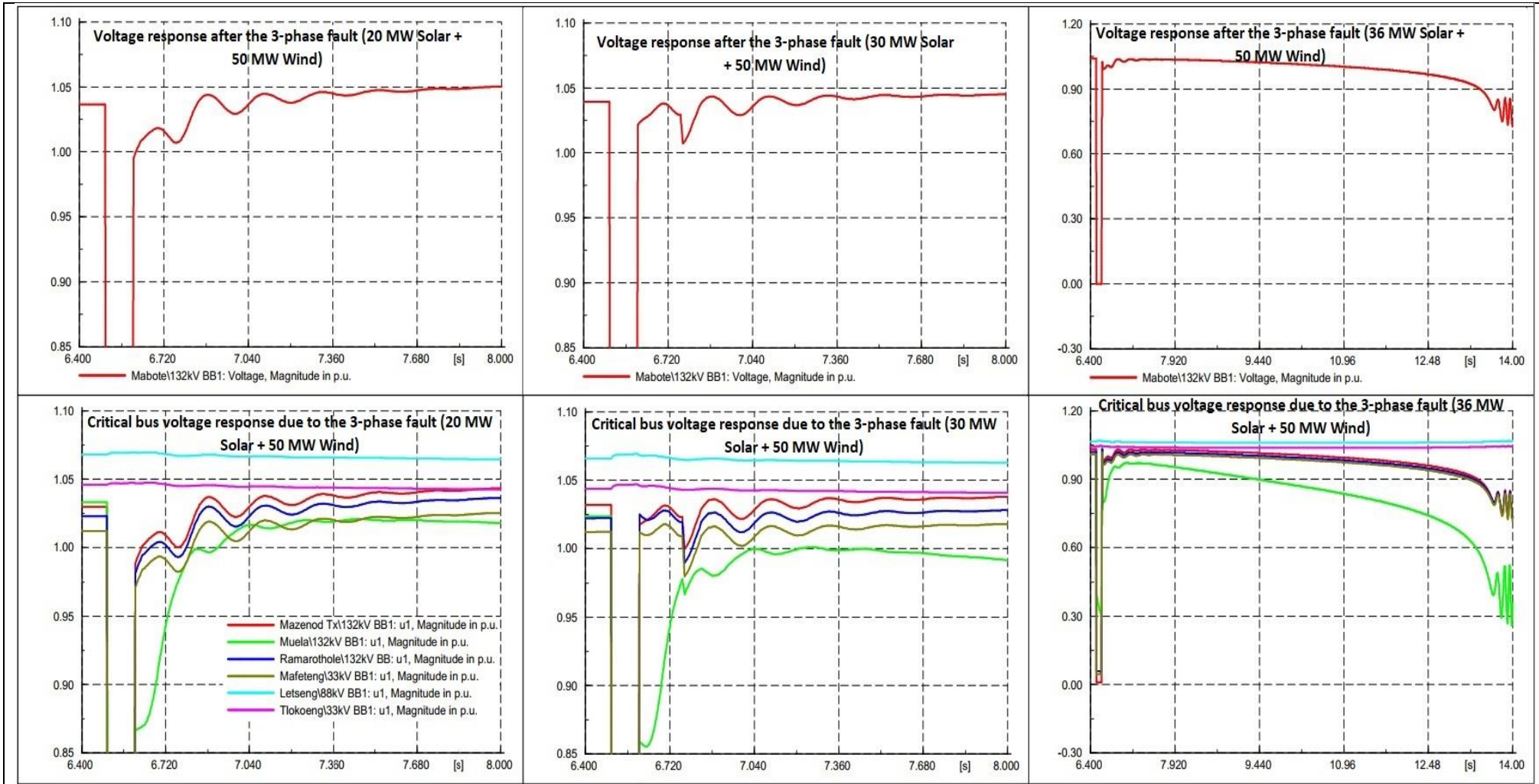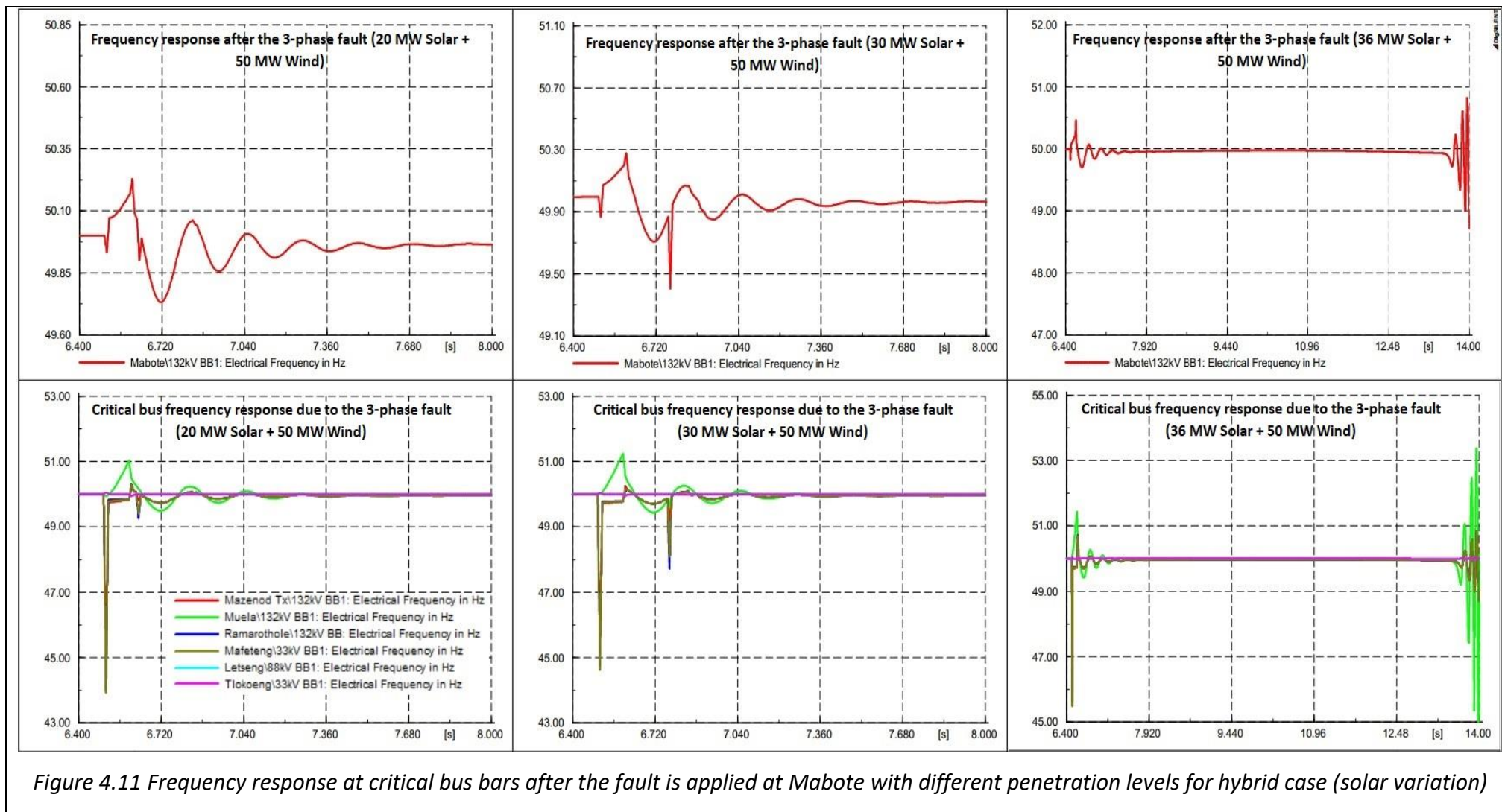### 4.4.6   Rotor Angle Stability Hybrid Case Solar Variation
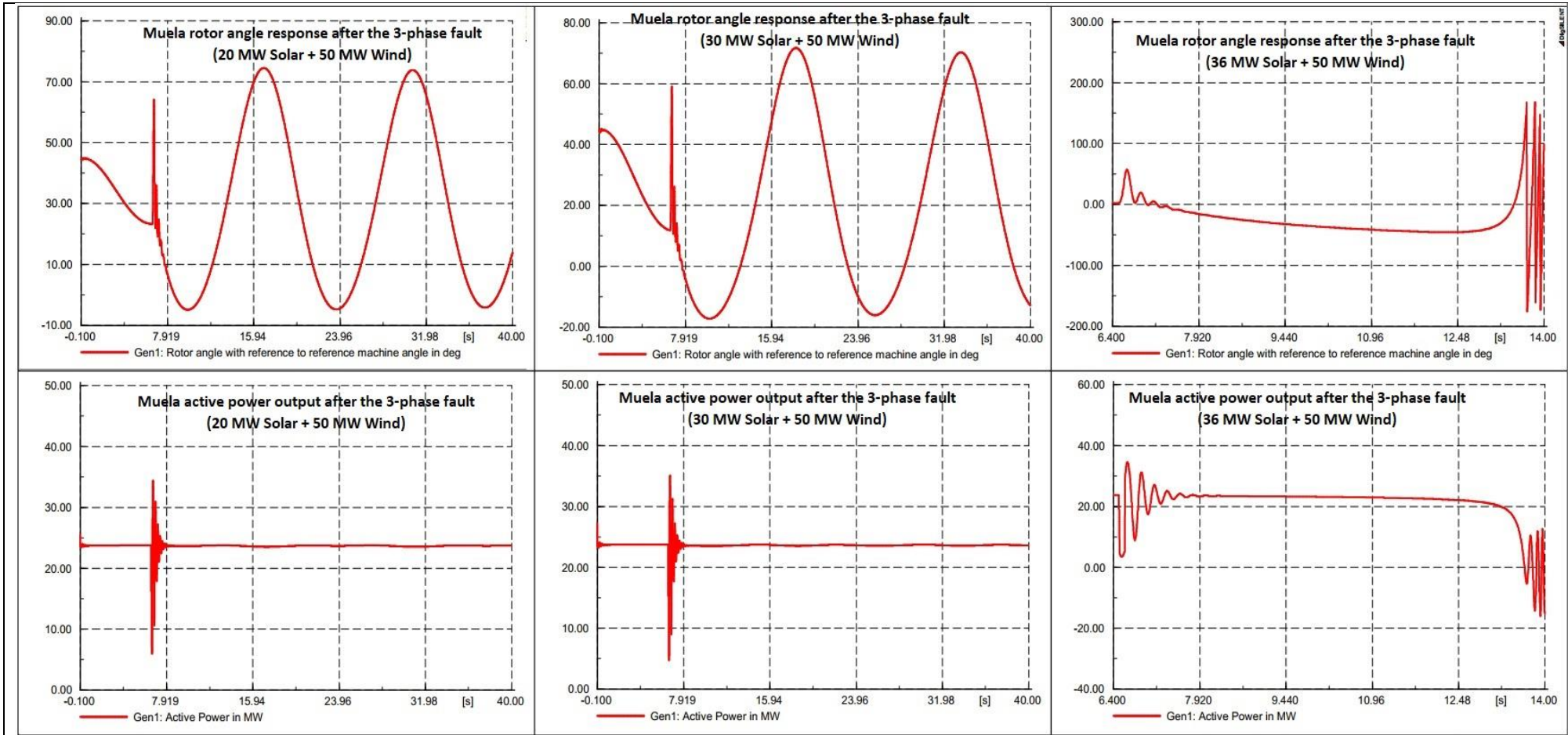
Figure 4.12 Rotor angle and real power response of synchronous generator at Muela due to the fault at Mabote with different penetration levels for hybrid case (solar variation)

Voltage, frequency and rotor angle responses after the 0.1 seconds 3-phase short circuit is applied at Mabote substation is depicted in Figure 4.10, Figure 4.11 and Figure 4.12 respectively under the different penetrations levels. From Figure 4.10 the voltage responses at different substations are presented. The penetration at the wind farm was maintained at 50 MW while the penetration from the solar farm was increased from 20 MW to 36 MW. The voltage at substation near to the wind farm remained almost constant after the fault while other substations voltages oscillated as they stabilized to the allowable voltage ranges. As in the previous case for the solar only case the 36 MW penetration acted as the limiting capacity for the PV. This suggest that the penetrations at the solar farm are independent to those at the wind farm as the hybrid system did not result in increased penetration for the solar PV generation.

Figure 4.11 presents the frequency response after the fault is applied at Mabote substation. The frequency at critical buses near the wind farm maintained the nominal frequency during and after the fault at Mabote substation. The frequency response at other critical points was almost the same for the penetration levels of 20 MW and 30 MW with the exception of Muela. The frequency response at the other critical buses had the overshoot of 50.313 Hz and the undershoot of 43.92 Hz for the penetration of 20 MW. At the penetration level of 30 MW of solar PV the overshoot and undershoot of frequency response were 50.255 Hz and 44.618 Hz respectively. In both cases the oscillations were damped to allowable frequency limits, indicating that the increased solar penetration does not lead to severe frequency instability. In addition, the Muela substation frequency had the overshoot of 51.028 Hz and the undershoot of 49.493 Hz for the 20 MW penetrations. At 36 MW penetration the frequency was violated as the frequency had an increasing frequency oscillations beyond allowable limits.

Figure 4.12 depicts how the rotor angle of the synchronous machines vary due to the fault from the Mabote substation. The results indicate that the rotor angle kept on increasing as the penetrations increased. At the penetration level of 20 MW the rotor angle oscillated between -4.598^0 and 73.67^0 while at the penetration level of 30 MW the it oscillated between -17.136^0 and 71.595^0. The rotor angle exhibit large changes as solar PV penetrations increase relative to the voltage and frequency responses suggesting that rotor angle is the main contributor to the system instability. As in the case of solar only results the 36 MW was the limiting capacity, again suggesting that the wind penetration does not lead to increased solar penetration for the hybrid system.

4.5 Steady State Simulation results

For the steady state analysis, the penetration level of 50 MW for wind and 35 MW for solar are considered. The results indicate the voltage performance LEC electrical networks under both wind and solar integration.
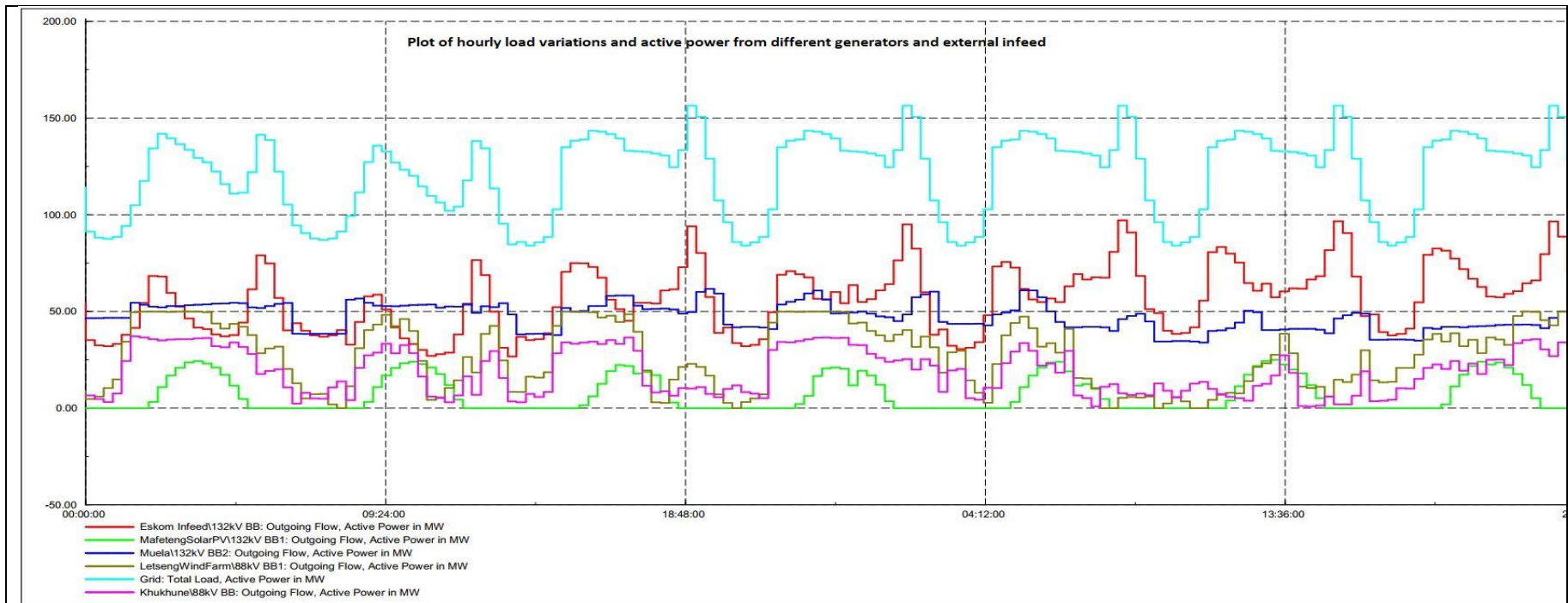
Figure 4.13 IREGs, Muela and Eskom active power variations as the load varies

Figure 4.13 illustrates typical power output from the intermittent renewables energy, Eskom infeed and Muela hydropower station. As shown when the intermittent sources are high Eskom reduces its power output. The same is true when the renewables are low Eskom kicks

to balance the load deficit. In addition, the variations from the solar power plant are rather slow and follow the same pattern, while wind power changes abruptly and does lead to voltage violations at Tlokoeng under high wind generation operations.

Figure 4.14 Voltage variations at PCC for Letseng and Ramarothole and at Eskom infeed and Muela Hydro Power
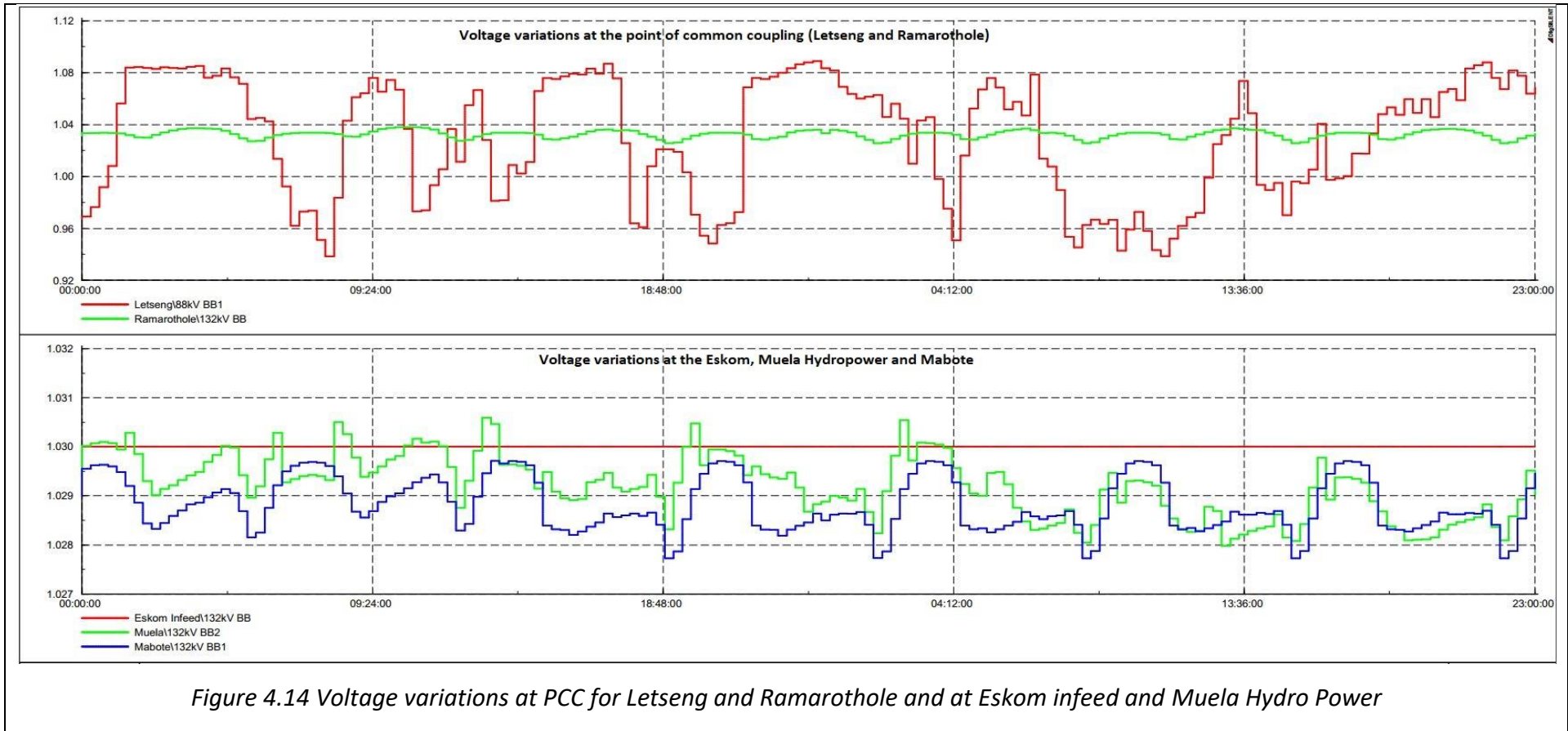
Figure 4.14 present how the voltage at the point of common coupling (Letseng and Ramarothole) changes as the load and the renewable energy resources (RER) vary. It also displays how the voltage at Muela and Eskom infeed vary due to RER. As Eskom acts the reference, machine to the LEC network, its voltage remains constant and it is not affected by load and RER fluctuations. On the other hand, Muela

voltage varied within allowable limits as the limits as the RER and the load vary. The voltage the wind farm varied more while that at the solar farm varied slightly.

Figure 4.15 displays the voltage at the neighboring substations and the power output from the renewable energy generators. The voltage variations at the substations near the solar farm were within limits, and Mafeteng substation showed the lowest voltage while Matelile showed the highest variations. The voltage variations near the wind farm varied randomly as load and wind power varied. Also, the voltage at the Tlokoeng substation sometimes exceeded the required voltage limit of 1.05 p.u. to 1.08 p.u. during high wind power generation. This suggest that the mitigation strategies such as wind power curtailment have to be employed to ensure that the voltage is within limits at all times. Table 9 displays the minimum and the maximum voltage limits for the period of 2018. Most of the voltage limits at the substations were observed except Tlokoeng which experienced the over voltage (1.08 p.u.) and the under voltage (0.88 p.u.) at times. Also at Letseng the under voltage limits were experienced with the minimum voltage of 0.91 p.u. but this does not result from wind penetrations as that voltage level was maintained when there are no renewables.

Figure 4.15 Voltage variations at the neighboring for solar and wind farms substations. Active power injected from solar and wind farms

Table 9 Maximum and minimum voltage variations at various substations

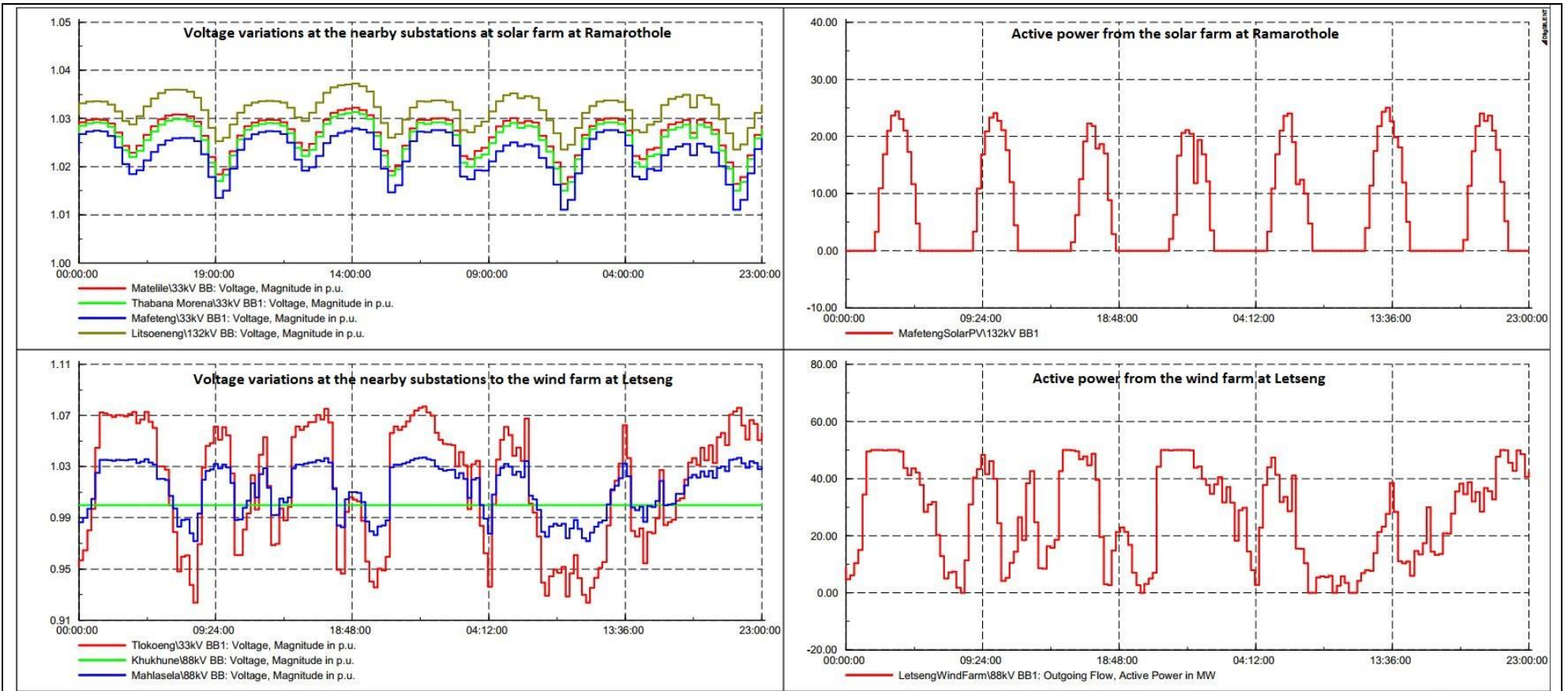| Bus	No RE		Solar case (50 MW)		Wind Case (36 MW)		Wind 50 MW+ Solar 36 MW	
	Min (p.u)	Max (p.u)	Min (p.u)	Max (p.u)	Min (p.u)	Max (p.u)	Min (p.u)	Max (p.u)
Tlokoeng	0.88	0.95	0.88	0.95	0.88	1.08	0.88	1.08
Khukhune	1.00	1.00	1.00	1.00	1.00	1.00	1.00	1.00
Mahlasela	0.96	0.98	0.96	0.98	0.96	1.04	0.96	1.04
ThabaneMorena	1.00	1.03	1.00	1.03	1.00	1.03	1.00	1.03
Matelile	1.01	1.03	1.01	1.03	1.01	1.03	1.01	1.03
Mafeteng	1.00	1.03	1.00	1.03	1.00	1.03	1.00	1.03
Letseng	0.91	0.96	0.91	0.96	0.91	1.09	0.91	1.09
Ramarothole	1.02	1.03	1.02	1.04	1.02	1.04	1.02	1.04
Muela	1.02	1.03	1.02	1.03	1.02	1.03	1.02	1.03
Mabote	1.03	1.03	1.03	1.03	1.03	1.03	1.03	1.03
Mazenod Tx	1.02	1.03	1.02	1.03	1.02	1.03	1.02	1.03

In this research work the DigSILENT software was used to model and analyze the load flow results. DigSILENT is widely used for the modeling generation, transmission, distribution systems and their interactions in the power flow studies. DigSILENT has further been used the industrial networks for more than 25 years. DigSILENT has also been used to analyze the power flow studies and assess the power system stability in [56], [57], [114]. For the grid impact studies, dynamic models for wind generation, photovoltaic generation and the battery storage system are modelled by the IEC TC88 WG27 in conjunction with the Western Electricity Coordinating Council (WECC) Renewable Energy Modelling Task Force (REMTF) [115]. The wind turbines models in DigSILENT are validated against the real measurement data and both compliant industry standards defined in IEC TC88 WG27 and the WECC [115]. Equally so the PV power plants from DigSILENT have been validated against Renewable Energy Model Validation (REMV) tool developed by WECC [116]. REMV tool has been validated against the real world measured data.

To investigate the Lesotho grid response to the increased levels of the IREGs the critical Clearing Time (CCT) matric has been used for the transient voltage, frequency and rotor angle stability studies. CCT has been used in the evaluation of the impact wind interaction for the U.S. Eastern Interconnection [111], the Danish wind integration [56], and in the Canadian solar-PV integration [58]. For the case of Lesotho transmission network, the grid code specifies that the network must be able to withstand any fault that last less than 190 *ms* [117]. For this study, the 3-phase short circuit fault of 100 *ms* was

applied to the most critical bus (Mabote) of which the grid must recover from as the renewable penetrations were increased. The 3-phase short was chosen as it represents the worst fault the electrical network can experience.

The results obtained reveal that higher penetrations of the both solar and wind results in grid instability. However, the integration study reveals that certain penetrations levels of renewables (wind and solar) can be successfully be integrated to the network without compromising the grid stability. For the solar-PV, the penetration of about 10 % (20 MW) at Ha-Ramarothole the CCT of the network in reduced indicating the worsening transient stability. At solar penetrations, increase to about 19 % (36 MW) the network fails to recover to the stable operation after the fault. This penetration is comparative to the study performed by Eftekharnejad et al on the Western U.S. Interconnection on assessing the impact of solar-PV. Eftekharnejad et al found that increased penetrations of solar-PV compromise the rotor angle stability with the penetration limit of 20 % after the fault [59]. For the case of wind integration the penetrations of 16 % (30 MW), 22 % (MW) and 28 % (52 MW) were considered, where the penetration level of around 28 % was the limiting capacity as it steady state voltage at Thlokoeng substation exceeded the recommended limit of 1.05 p.u. This was in line with the study performed by Naser et al where it was found that increased wind penetration level of 30 % resulted in the voltage collapse [62]. However, it is argued that acceptable penetration level of the renewables is highly dependent on the grid infrastructure and its robustness. For the case of Lesotho high penetrations of both solar and wind were experienced because Lesotho network is integrated to the South African distribution network (132 kV and 88 kV) which provide synchronizing and balancing functionality to Lesotho network.

International Energy Agency (IEA) Technology Collaboration Programme (TCP) for wind (Task 25) and solar (Task 14) suggest that for the penetrations levels of 15 % to 25 % (Phase Three) the variability of the renewables become a challenge and flexibility measures must be employed and at penetrations levels of 25 % to 50 % (Phase Four) power system stability is a challenge and the network must be reinforced [118], [119]. For Phase One (less than 3 % penetration) the grid problems are local hence no noticeable grid problems and for Phase Two (4% to 15 % penetration) the network capacity problems become noticeable and congestion management strategies must be employed [118]. The steady state results for the solar-PV show that the PV output varies continually and does not leads to steady state voltage instability under maximum penetration. From this, it can be concluded solar-PV

generation of 35 MW can be integrated to the grid without compromising the grid stability. On the other hand wind output changes abruptly and my lead to steady state voltage instability. This suggest that there is need from extra voltage control for the wind farm under maximum penetration. As such for Lesotho, it is recommended the deployed of the renewable start at Phase Two to avoid greater challenges of flexibility and stability, then the network be gradually fortified to accommodate further penetrations.

5   Conclusions and Recommendations

The performance of Lesotho national Lesotho electricity grid due to the integration of both solar PV and wind generation was conducted. The study considered three operation scenarios namely solar PV generation only, wind generation only and the hybrid of both solar PV and wind generation. The load flow and transient analysis were performed for varying penetrations levels for three scenarios. For the three scenarios the voltage, frequency and rotor angle stability were considered and evaluated against the Lesotho grid code. The penetration for the wind and solar were found by increasing their capacity until the either voltage, frequency and rotor angle stability was violated. To ensure that the network will be resilient at all times the 3-phase short circuit was applied at the point with least critical clearing time (CCT) terminals and ensuring that the system stability was observed before and after the fault.

For the solar PV only scenario the maximum allowable solar PV, capacity was found to be less than 36 MW while for the wind generation scenario it was found to be less than 52 MW. The 50 MW and 35 MW penetrations were chosen to be the maximum allowable penetrations for wind farm and solar farm respectively. Under the hybrid case it was found that the simultaneous for integration of wind and solar PV does not results in either the wind or solar PV penetrations increase. From the observation it is concluded that 85 MW remains as the maximum allowable penetration resulting from 35 MW of solar PV at Ramarothole and 50 MW from Letseng respectively. For all the scenarios considered, the results showed that solar PV generation results in increased rotor angle instability relative to the wind generation option. Furthermore, for both solar PV and wind generation the frequency stability was not severely affected as the penetrations levels increased. Increased solar PV integration did not result in major voltage violations as the penetration increases. On the other hand, increased wind integration resulted in increase of the steady state voltage for the neighbouring substations. At steady state wind resulted in more voltage fluctuations than the solar generating case. This suggest that for the wind case there is the need to employ some voltage control strategies to ensure that the voltage limits are always observed.

In running the simulations, the rotor angle always oscillated after the fault indicating insufficient dumping. Sustained oscillations may spread over the electrical network thus leading to the oscillations at the tie-lines and destabilizing the network. Furthermore, the protection simulations for the LEC network were not considered in the study. It is highly recommended for further studies to consider the protection setting of the network as the integration of renewables alters the short circuit level of the power system. The power quality and harmonics due the integration of intermittent renewable sources also remains a concern as the sustained power variations may compromise system stability.

References

[1] REN21`, "Renewables Global Status Report," Renewable Energy Policy Network, 2018. [Online]. Available: https://www.ren21.net/wp-content/uploads/2019/08/Full-Report-2018.pdf.

[2] IEA, "IEA - IEA Renewables 2018-IEA (2018).pdf," International Energy Agency. [Online]. Available: www.iea.org.

[3] L. Bird and M. Milligan, "Lessons from Large-Scale Renewable Energy Integration Studies: Preprint," Denver, Colorado, May 2012, p. 9.

[4] P. Du, R. Baldick, and A. Tuohy, Eds., *Integration of Large-Scale Renewable Energy into Bulk Power Systems*. Cham: Springer International Publishing, 2017.

[5] Anonymous, "2020 climate & energy package," *Climate Action - European Commission*, Nov. 23, 2016. https://ec.europa.eu/clima/policies/strategies/2020_en (accessed Sep. 19, 2019).

[6] Anonymous, "2030 climate & energy framework," *Climate Action - European Commission*, Nov. 23, 2016. https://ec.europa.eu/clima/policies/strategies/2030_en (accessed Sep. 19, 2019).

[7] "The European Semester," *European Commission - European Commission*. https://ec.europa.eu/info/business-economy-euro/economic-and-fiscal-policy-coordination/eu-economic-governance-monitoring-prevention-correction/european-semester_en (accessed Sep. 19, 2019).

[8] "Updated renewable portfolio standards will lead to more renewable electricity generation - Today in Energy - U.S. Energy Information Administration (EIA)." https://www.eia.gov/todayinenergy/detail.php?id=38492 (accessed Sep. 19, 2019).

[9] X. Liang, "Emerging Power Quality Challenges Due to Integration of Renewable Energy Sources," *IEEE Transactions on Industry Applications*, vol. 53, no. 2, pp. 855–866, Mar. 2017, doi: 10.1109/TIA.2016.2626253.

[10] A. Moreno-Muñoz, Ed., *Large scale grid integration of renewable energy sources*. London, United Kingdom: The Institution of Engineering and Technology, 2017.

[11] J. MacCormack, A. Hollis, H. Zareipour, and W. Rosehart, "The large-scale integration of wind generation: Impacts on price, reliability and dispatchable conventional suppliers," *Energy Policy*, vol. 38, no. 7, pp. 3837–3846, Jul. 2010, doi: 10.1016/j.enpol.2010.03.004.

[12] LEWA, "LEWA Annual Report 2016/17," Lesotho Electricity and Water Authority, Maseru, 2016. [Online]. Available: http://www.lewa.org.ls/library/2016_17LEWAAnnualReport.pdf.

[13] LEWA, "LEWA Annual Report 2017/18," Lesotho Electricity and Water Authority, Maseru, 2017. [Online]. Available: http://www.lewa.org.ls/library/annual_report_17-18.pdf.

[14] LEWA, "Annual Report 2017/18," Lesotho Electricity and Water Authority, 2018.

[15] B. M. Taele, L. Mokhutšoane, and I. Hapazari, "An overview of small hydropower development in Lesotho: Challenges and prospects," *Renewable Energy*, vol. 44, pp. 448–452, Aug. 2012, doi: 10.1016/j.renene.2012.01.086.

[16] W. J. Klunne, "Small hydropower in Southern Africa – an overview of five countries in the region," *Journal of Energy in Southern Africa*, vol. 24, no. 3, p. 12, 2013.

[17] IRENA, "Biogas for domestic cooking: Technology brief," International Renewable Energy Agency, Abu Dhabi, 2017.

[18] M. Mpholo *et al.*, "Rural Household Electrification in Lesotho," in *Africa-EU Renewable Energy Research and Innovation Symposium 2018 (RERIS 2018)*, M. Mpholo, D. Steuerwald, and T. Kukeera, Eds. Cham: Springer International Publishing, 2018, pp. 97–103.

[19] LEC, "Lesotho Generation Master Plan (pre-feasibility study)," Lesotho Electricity Company, Maseru, 2010.

[20] T. Mathaba, M. Mpholo, and M. Letuma, "Velocity and power density analysis of the wind at Letšeng-la-terae in Lesotho," *Renewable Energy*, vol. 46, pp. 210–217, Oct. 2012, doi: 10.1016/j.renene.2012.04.003.

[21] M. Mpholo, T. Mathaba, and M. Letuma, "Wind profile assessment at Masitise and Sani in Lesotho for potential off-grid electricity generation," *Energy Conversion and Management*, vol. 53, no. 1, pp. 118–127, Jan. 2012, doi: 10.1016/j.enconman.2011.07.015.

[22] B M Taele, L Mokhutšoane, and Himanshu Narayan, "Solar energy resources potential and sustainable production of biomass energy in Lesotho." Unpublished, 2010, doi: 10.13140/rg.2.1.2962.0882.

[23] T. Hadjicostas and D. Padayachy, "Lesotho Electrification Master Plan Grid Development Plan," Department of Energy, 2017/387289/1, Jun. 2018.

[24] DoE, "Lesotho Sustainable Energy for All Country Action Agenda," Department of Energy, 2017.

[25] D. Fernandez, "Lesotho Electrification Master Plan Off-Grid Master Plan," Department of Energy, 2017/387289/1, Jun. 2017.

[26] LEC, "Lesotho Services for Renewable Energy Grid Integration Study." 2019, [Online]. Available: https://www.afdb.org/fileadmin/uploads/afdb/Documents/Procurement/Project-related-Procurement/EOI_-_Lesotho_-_Services_for_Renewable_Energy_Grid_Integration_Study.pdf.

[27] "Access to electricity – SDG7: Data and Projections – Analysis," *IEA*. https://www.iea.org/reports/sdg7-data-and-projections/access-to-electricity (accessed Aug. 14, 2020).

[28] LEWA, "Lesotho Electricity and Water Authority Annual Report 2018-19," LEWA, Maseru, 2018.

[29] IEA, "Thailand Grid Renewable Integration Assessment (preliminary report)," International Energy Agency, 2018.

[30] A. T. A. Dyak, E. O. Abu-Lehyeh, and S. Kiwan, "Assessment of Implementing Jordan's Renewable Energy Plan on the Electricity Grid," vol. 11, no. 2, p. 7, 2017.

[31] H.-D. Chiang, *Direct Methods for Stability Analysis of Electric Power Systems: Theoretical Foundation, BCU Methodologies, and Applications*. Hoboken, NJ, USA: John Wiley & Sons, Inc., 2010.

[32] A. R. Bergen and V. Vittal, *Power systems analysis*, 2. ed. Upper Saddle River, NJ: Prentice Hall, 2000.

[33] K. Morison, L. Wang, and P. Kundur, "Power System Security Assessment," *IEEE power & energy magazine*, p. 10, Oct. 2004.

[34] "Definition and Classification of Power System Stability IEEE/CIGRE Joint Task Force on Stability Terms and Definitions," *IEEE Trans. Power Syst.*, vol. 19, no. 3, pp. 1387–1401, Aug. 2004, doi: 10.1109/TPWRS.2004.825981.

[35] K. Prabha, *Power System Stability and Control*. New York: McGraw-Hill, 1994.

[36] M. Eremia and M. Shahidehpour, Eds., *Handbook of electrical power system dynamics: modeling, stability, and control*. Piscataway, NJ: IEEE Press, 2013.

[37] L. L. Grigsby, *Power System Stability and Control*, Third Edition. 6000 Broken Sound Parkway NW, Suite 300; Boca Raton, FL 33487-2742: CRC Press Taylor & Francis Group.

[38] P. W. Sauer and M. A. Pai, *Power System Dynamics and Stability*. Upper Saddle River, New Jersy 07456: Prentice Hall, 1998.

[39] J. Machowski, J. W. Bialek, and J. R. Bumby, *Power System Dynamics*. Jown Wiley &Sons. Ltd, 2008.

[40] N. Amjady and M. R. Ansari, "Small disturbance voltage stability assessment of power systems by modal analysis and dynamic simulation," *Energy Conversion and Management*, vol. 49, no. 10, pp. 2629–2641, Oct. 2008, doi: 10.1016/j.enconman.2008.04.010.

[41] F. Swift and H. F. Wang, "The connection between modal analysis and electric torque analysis in studying the oscillation stability of multi-machine power systems," *Electrical Power & Energy Systems*, vol. 19, no. 5, pp. 321–330, 1997.

[42] V. T. Cutsem and C. Vournas, *Voltage Stability of Electric Power Systems*. Norwell, MA,: Kluwer Academic Publisher, 2001.

[43] J. Deuse and M. Stubbe, "Dynamic Simulation of Voltage Collapses," *IEEE Transactions on Power Systems*, vol. 8, no. 3, pp. 894–904, Aug. 1993.

[44] G. K. Morison, B. Gao, and P. Kundur, "Voltage stability analysis using static and dynamic approaches," *IEEE Trans. Power Syst.*, vol. 8, no. 3, pp. 1159–1171, Aug. 1993, doi: 10.1109/59.260881.

[45] B. Gao, G. K. Morison, and P. Kundur, "Towards the Development of a Systematic Approach for voltage Stability Assessment of Large-Scale Power Systems," *IEEE Transactions on Power Systems*, vol. 11, no. 3, pp. 1314–1324, Aug. 1996.

[46] C. W. Taylor, *Power System Voltage Stability*. Texas: Mcgraw-Hill, 1994.

[47] J. L. Rueda Torres and F. Gonzalez-Longatt, *Dynamic vulnerability assessment and intelligent control for sustainable power systems*, First edition. Hoboken, NJ: Wiley, 2018.

[48] V. Ajjarapu, *Computational Techniques for Voltage Stability Assessment and Control*. Spring Street, New York, NY 10013, USA: Springer, 2006.

[49] S. C. Savulescu, *Real-time Stability Assessment in Modern Power System Control Centers*. Hoboken, New Jersey: John Wiley & Sons, 2009.

[50] J. C. Chow, R. Fiscl, and H. Yan, "On the Evaluation of Voltage Collapse Criteria," *IEEE Transactions on Power Systems,* vol. 5, no. 2, pp. 612–620, May 1990.

[51] S. Abe, Y. Fukunaga, A. Isono, and B. Kondo, "Power System Voltage Stabilty," *IEEE Transactions on Power Apparatus and Systems*, vol. PAS-10l, no. 10, pp. 3830–3840, Oct. 1982.

[52] I. Dobson and H.-D. Chiang, "Towards a theory of voltage collapse in electric power systems," p. 10.

[53] CIGRE Task Force 38-02-14, "Analysis and Modeling Needs of Power Systems Under Major Frequency Disturbances, Final Report. 1999."

[54] K. R. Padiyar, *Power system dynamics: stability and control*. Hyderabad India: BS Publications, 2008.

[55] O. Anaya-Lara, F. M. Hughes, N. Jenkins, and G. Strbac, "Influence of Windfarms on Power System Dynamic and Transient Stability," *Wind Engineering*, vol. 30, no. 2, pp. 107–127, Mar. 2006, doi: 10.1260/030952406778055018.

[56] C. Liu, Z. Chen, C. L. Bak, Z. Liu, P. Lund, and P. Ronne-Hansen, "Transient stability assessment of power system with large amount of wind power penetration: The Danish case study," in *2012 10th International Power & Energy Conference (IPEC)*, Ho Chi Minh City, Nov. 2012, pp. 461–467, doi: 10.1109/ASSCC.2012.6523312.

[57] E. Munkhchuluun, L. Meegahapola, and A. Vahidnia, "Impact on rotor angle stability with high solar-PV generation in power networks," in *2017 IEEE PES Innovative Smart Grid Technologies Conference Europe (ISGT-Europe)*, Torino, Sep. 2017, pp. 1–6, doi: 10.1109/ISGTEurope.2017.8260229.

[58] B. Tamimi, C. Canizares, and K. Bhattacharya, "System Stability Impact of Large-Scale and Distributed Solar Photovoltaic Generation: The Case of Ontario, Canada," *IEEE Trans. Sustain. Energy*, vol. 4, no. 3, pp. 680–688, Jul. 2013, doi: 10.1109/TSTE.2012.2235151.

[59] S. Eftekharnejad, V. Vittal, Heydt, B. Keel, and J. Loehr, "Impact of increased penetration of photovoltaic generation on power systems," *IEEE Trans. Power Syst.*, vol. 28, no. 2, pp. 893–901, May 2013, doi: 10.1109/TPWRS.2012.2216294.

[60] Y. T. Tan and D. S. Kirschen, "Impact on the Power System of a Large Penetration of Photovoltaic Generation," in *2007 IEEE Power Engineering Society General Meeting*, Tampa, FL, USA, Jun. 2007, pp. 1–8, doi: 10.1109/PES.2007.385563.

[61] M. Ndreko, A. A. van der Meer, M. Gibescu, M. A. M. M. van der Meijden, J. A. Bos, and K. P. J. Jansen, "Transient stability analysis of an onshore power system with multi-terminal offshore VSC-HVDC transmission: A case study for the Netherlands," in *2013 IEEE Power & Energy Society General Meeting*, Vancouver, BC, 2013, pp. 1–5, doi: 10.1109/PESMG.2013.6672663.

[62] I. S. Naser, O. Anaya-Lara, and K. L. Lo, "Study of the impact of wind generation on voltage stability in transmission networks," in *2011 4th International Conference on Electric Utility Deregulation and Restructuring and Power Technologies (DRPT)*, Weihai, China, Jul. 2011, pp. 39–44, doi: 10.1109/DRPT.2011.5993859.

[63] E. Vittal, M. O'Malley, and A. Keane, "A Steady-State Voltage Stability Analysis of Power Systems With High Penetrations of Wind," *IEEE Trans. Power Syst.*, vol. 25, no. 1, pp. 433–442, Feb. 2010, doi: 10.1109/TPWRS.2009.2031491.

[64] A. Sajadi, R. M. Kolacinski, and K. A. Loparo, "Transient voltage stability of offshore wind farms following faults on the collector system," in *2016 IEEE Power and Energy Conference at Illinois (PECI)*, Urbana, IL, USA, Feb. 2016, pp. 1–5, doi: 10.1109/PECI.2016.7459227.

[65] N. W. Miller, M. Shao, S. Pajic, and R. D'Aquila, "Western Wind and Solar Integration Study Phase 3 – Frequency Response and Transient Stability," NREL/SR--5D00-62906, 1167065, Dec. 2014. doi: 10.2172/1167065.

[66] N. W. Miller, M. Shao, S. Pajic, and R. D'Aquila, "Eastern Frequency Response Study," NREL/SR-5500-58077, 1083365, May 2013. doi: 10.2172/1083365.

[67] L. Meegahapola and D. Flynn, "Impact on transient and frequency stability for a power system at very high wind penetration," in *IEEE PES General Meeting*, Minneapolis, MN, Jul. 2010, pp. 1–8, doi: 10.1109/PES.2010.5589908.

[68] V. Vittal, J. McCalley, and V. Ajjarapu, "Impact of Increased DFIG Wind Penetration on Power Systems and Markets," Arizona State University, PSERC project S-34.

[69] T. Alquthami, H. Ravindra, M. O. Faruque, M. Steurer, and T. Baldwin, "Study of photovoltaic integration impact on system stability using custom model of PV arrays integrated with PSS/E," in *North American Power Symposium 2010*, Arlington, TX, USA, Sep. 2010, pp. 1–8, doi: 10.1109/NAPS.2010.5619589.

[70] R. Yan, T. K. Saha, N. Modi, N.-A. Masood, and M. Mosadeghy, "The combined effects of high penetration of wind and PV on power system frequency response," *Applied Energy*, vol. 145, pp. 320–330, May 2015, doi: 10.1016/j.apenergy.2015.02.044.

[71] H. Bevrani, A. Ghosh, and G. Ledwich, "Renewable energy sources and frequency regulation: survey and new perspectives," *IET Renew. Power Gener.*, vol. 4, p. 20, 2010.

[72] J. Morren, J. Pierik, and S. W. H. de Haan, "Inertial response of variable speed wind turbines," *Electric Power Systems Research*, vol. 76, no. 11, pp. 980–987, Jul. 2006, doi: 10.1016/j.epsr.2005.12.002.

[73] W. Li, G. Joos, and C. Abbey, "Wind Power Impact on System Frequency Deviation and an ESS based Power Filtering Algorithm Solution," in *2006 IEEE PES Power Systems Conference and Exposition*, Atlanta, Georgia, USA, 2006, pp. 2077–2084, doi: 10.1109/PSCE.2006.296265.

[74] K. Abe, S. Ohba, and S. Iwamoto, "New load frequency control method suitable for large penetration of wind power generations," in *2006 IEEE Power Engineering Society General Meeting*, Montreal, Que., Canada, 2006, p. 6 pp., doi: 10.1109/PES.2006.1709177.

[75] J. P. Barton and D. G. Infield, "Energy Storage and Its Use With Intermittent Renewable Energy," *IEEE Trans. On Energy Conversion*, vol. 19, no. 2, pp. 441–448, Jun. 2004, doi: 10.1109/TEC.2003.822305.

[76] B. M. Taele, K. K. Gopinathan, and L. Mokhuts'oane, "The potential of renewable energy technologies for rural development in Lesotho," *Renewable Energy*, vol. 32, no. 4, pp. 609–622, Apr. 2007, doi: 10.1016/j.renene.2006.02.014.

[77] L. El Chaar, L. A. lamont, and N. El Zein, "Review of photovoltaic technologies," *Renewable and Sustainable Energy Reviews*, vol. 15, no. 5, pp. 2165–2175, Jun. 2011, doi: 10.1016/j.rser.2011.01.004.

[78] Q. Ai, X. Wang, and X. He, "The impact of large-scale distributed generation on power grid and microgrids," *Renewable Energy*, vol. 62, pp. 417–423, Feb. 2014, doi: 10.1016/j.renene.2013.07.032.

[79] M. G. Molina and E. J. Espejo, "Modeling and simulation of grid-connected photovoltaic energy conversion systems," *International Journal of Hydrogen Energy*, vol. 39, no. 16, pp. 8702–8707, May 2014, doi: 10.1016/j.ijhydene.2013.12.048.

[80] S. A. Rahman, T. Vanderheide, and R. K. Varma, "Generalised model of a photovoltaic panel," *IET Renewable Power Generation*, vol. 8, no. 3, pp. 217–229, Apr. 2014, doi: 10.1049/iet-rpg.2013.0094.

[81] P.-H. Huang, W. Xiao, J. C.-H. Peng, and J. L. Kirtley, "Comprehensive Parameterization of Solar Cell: Improved Accuracy With Simulation Efficiency," *IEEE Trans. Ind. Electron.*, vol. 63, no. 3, pp. 1549–1560, Mar. 2016, doi: 10.1109/TIE.2015.2498139.

[82] M. Hejri, H. Mokhtari, M. R. Azizian, M. Ghandhari, and L. Soder, "On the Parameter Extraction of a Five-Parameter Double-Diode Model of Photovoltaic Cells and Modules,"

IEEE J. Photovoltaics, vol. 4, no. 3, pp. 915–923, May 2014, doi: 10.1109/JPHOTOV.2014.2307161.

[83] J. A. Duffie and W. A. Beckman, *Solar Engineering of Thermal Processes*, Forth Edition. Hoboken, New Jersey: John Wiley & Sons, Inc, 2013.

[84] M. Iqbāl, *An introduction to solar radiation*. Toronto: Academic Press, 1983.

[85] S. A. Kalogirou, *Solar energy engineering: processes and systems*, 2. ed. Amsterdam: AP, Academic Press/Elsevier, 2014.

[86] W. Xiao, *Photovoltaic power system: modelling, design and control*. Hoboken, NJ: Wiley, 2017.

[87] W. Cao and Y. Hu, *Renewable energy: utilisation and system integration*. 2016.

[88] J. M. Pacas, M. G. Molina, and E. C. dos Santos, "Design of a robust and efficient power electronic interface for the grid integration of solar photovoltaic generation systems," *International Journal of Hydrogen Energy*, vol. 37, no. 13, pp. 10076–10082, Jul. 2012, doi: 10.1016/j.ijhydene.2011.12.078.

[89] R. Teodorescu, M. Liserre, and P. Rodríguez, *Grid Converters for Photovoltaic and Wind Power Systems: Teodorescu/Grid Converters for Photovoltaic and Wind Power Systems*. Chichester, UK: John Wiley & Sons, Ltd, 2011.

[90] D. Zhou, Y. Song, and F. Blaabjerg, "Modeling and Control of Three-Phase AC/DC Converter Including Phase-Locked Loop," in *Control of Power Electronic Converters and Systems*, Elsevier, 2018, pp. 117–151.

[91] M. G. Molina and M. Pacas, "Improved power conditioning system of micro-hydro power plant for distributed generation applications," in *2010 IEEE International Conference on Industrial Technology*, Vi a del Mar , Chile, 2010, pp. 1733–1738, doi: 10.1109/ICIT.2010.5472461.

[92] J. F. Manwell, J. G. McGowan, and A. L. Rogers, *Wind Energy Explained*. Chichester, UK: John Wiley & Sons, Ltd, 2002.

[93] T. Ackermann, Ed., *Wind power in power systems*, 2. ed. Chichester: Wiley, 2012.

[94] O. Anaya-Lara, N. Jenkins, J. Ekanayake, P. Cartwright, and M. Hughes, *Wind Energy Generation Modelling and Control*, First Edition. John Wiley & Sons, Ltd.

[95] O. Anaya-Lara, D. Campos-Gaona, E. Moreno-Goytia, and G. Adam, *Offshore Wind Energy Generation: Control, Protection, and Integration to Electrical Systems*. Chichester, UK: John Wiley & Sons, Ltd, 2014.

[96] Z. Lu and S. Zhou, *Integration of Large Scale Wind Energy with Electrical Power Systems in China*. Singapore: John Wiley & Sons Singapore Pte. Ltd, 2018.

[97] *Wind Energy Handbook*. Chichester, UK: John Wiley & Sons, Ltd, 2011.

[98] O. Wasynczuk, D. T. Man, and J. P. Sullivan, "Dynamic Behavior of a Class of Wind Turbine Generators during Random Wind Fluctuations," *IEEE Power Eng. Rev.*, vol. PER-1, no. 6, pp. 47–48, Jun. 1981, doi: 10.1109/MPER.1981.5511593.

[99] P. M. Anderson and A. Bose, "Stability Simulation of Wind Turbine Sytems," *IEEE Transactions on Power Apparatus and Systems*, vol. PAS-102, no. No. 12, p. 5, Dec. 1983.

[100] P. C. Razusi and M. Eremia, "Prediction of wind power by artificial intelligence techniques," in *2011 16th International Conference on Intelligent System Applications to Power Systems*, Hersonissos, Greece, Sep. 2011, pp. 1–6, doi: 10.1109/ISAP.2011.6082239.

[101] B. Fox, Ed., *Wind power integration: connection and system operational aspects*, 2. ed. Stevenage: Inst. of Engineering and Technology, 2014.

[102] J. G. Slootweg, H. Polinder, and W. L. Kling, "Dynamic modelling of a wind turbine with doubly fed induction generator," in *2001 Power Engineering Society Summer Meeting. Conference Proceedings (Cat. No.01CH37262)*, Vancouver, BC, Canada, 2001, pp. 644–649 vol.1, doi: 10.1109/PESS.2001.970114.

[103] L. Holdsworth, X. G. Wu, J. B. Ekanayake, and N. Jenkins, "Comparison of fixed speed and doubly-fed induction wind turbines during power system disturbances," *IEE Proc., Gener. Transm. Distrib.*, vol. 150, no. 3, p. 343, 2003, doi: 10.1049/ip-gtd:20030251.

[104] R. M. G. Castro and J. M. F. Jesus, "A wind park reduced-order model using singular perturbations theory," *IEEE Transactions on Energy Conversion*, vol. 11, no. no 4, pp. 735–741, Dec. 1996.

[105] R. M. G. Castro and J. M. F. Jesus, "An aggregated wind park model," *13th PSCC Power Systems Computation Conference Proceedings*, vol. 2, pp. 1302–1307, June 28-July 2.

[106] V. Akhmatov and H. Knudsen, "An aggregate model of a grid-connected, large-scale, offshore wind farm for power stability investigationsÐimportance of windmill mechanical system," p. 9, 2002.

[107] E. Muljadi *et al.*, "Equivalencing the collector system of a large wind power plant," in *2006 IEEE Power Engineering Society General Meeting*, Montreal, Que., Canada, 2006, p. 9 pp., doi: 10.1109/PES.2006.1708945.

[108] E. Muljadi and A. Ellis, "Validation of wind power plant models," in *2008 IEEE Power and Energy Society General Meeting - Conversion and Delivery of Electrical Energy in the 21st Century*, Pittsburgh, PA, USA, Jul. 2008, pp. 1–7, doi: 10.1109/PES.2008.4596053.

[109] A. Ellis, Y. Kazachkov, E. Muljadi, P. Pourbeik, and J. J. Sanchez-Gasca, "Description and technical specifications for generic WTG models — A status report," in *2011 IEEE/PES Power Systems Conference and Exposition*, Phoenix, AZ, USA, Mar. 2011, pp. 1–8, doi: 10.1109/PSCE.2011.5772473.

[110] P. Pourbeik *et al.*, "Generic Dynamic Models for Modeling Wind Power Plants and Other Renewable Technologies in Large-Scale Power System Studies," *IEEE Trans. Energy Convers.*, vol. 32, no. 3, pp. 1108–1116, Sep. 2017, doi: 10.1109/TEC.2016.2639050.

[111] A. Sajadi, R. M. Kolacinski, K. Clark, and K. A. Loparo, "Transient Stability Analysis for Offshore Wind Power Plant Integration Planning Studies – Part I: Short Term Faults," *IEEE Transactions on Industry Applications*, vol. 55, no. 1, pp. 182–192, Feb. 2019.

[112] B. CATTANEO, "Photovoltaic Geographical Information System (PVGIS)," *EU Science Hub - European Commission*, Jun. 15, 2018. https://ec.europa.eu/jrc/en/pvgis (accessed Mar. 03, 2020).

[113] T. Hove, "A method for predicting long-term average performance of photovoltaic systems," *Renewable Energy*, vol. 21, no. 2, pp. 207–229, Oct. 2000, doi: 10.1016/S0960-1481(99)00131-7.

[114] O. E. Oni, I. E. Davidson, and N. Parus, "Static Voltage Stability Analysis of Eskom Eastern Grid," Birmingham UK, Nov. 2016.

[115] Ö. Göksu, P. Sørensen, J. Fortmann, A. Morales, S. Weigel, and P. Pourbeik, "Compatibility of IEC 61400-27-1 Ed 1 and WECC 2nd Generation Wind Turbine Models," p. 8.

[116]   G. Lammert, L. D. P. Ospina, P. Pourbeik, D. Fetzer, and M. Braun, "Implementation and validation of WECC generic photovoltaic system models in DIgSILENT PowerFactory," in *2016 IEEE Power and Energy Society General Meeting (PESGM)*, Boston, MA, USA, Jul. 2016, pp. 1–5, doi: 10.1109/PESGM.2016.7741608.

[117]   LEWA, "Lesotho Grid Code," Lesotho Electricity and Water Authority, 2015.

[118]   H. Holttinen *et al.*, "Design and operation of power systems with large amounts of wind power."

[119]   K. Ogimoto, "Power system operation planning with PV integration," International Energy Agency, IEA-PVPS T14-04, Nov. 2014.